Contribution de l'éclairage et de la réalité mixte pour l'assistance des personnes malvoyantes

Sofiane Vernet

▶ **To cite this version:**

Sofiane Vernet. Contribution de l'éclairage et de la réalité mixte pour l'assistance des personnes malvoyantes. Traitement du signal et de l'image [eess.SP]. Université Jean Monnet (EPSCPE), 2025. Français. NNT : 2025UJMO0080 . tel-05545907

HAL Id: tel-05545907

https://theses.hal.science/tel-05545907v1

Submitted on 10 Mar 2026

HAL is a multi-disciplinary open access archive for the deposit and dissemination of scientific research documents, whether they are published or not. The documents may come from teaching and research institutions in France or abroad, or from public or private research centers.

L'archive ouverte pluridisciplinaire **HAL**, est destinée au dépôt et à la diffusion de documents scientifiques de niveau recherche, publiés ou non, émanant des établissements d'enseignement et de recherche français ou étrangers, des laboratoires publics ou privés.

HAL Authorization

N° d'ordre NNT : 2025UJMO0080

THÈSE de DOCTORAT
DE L'UNIVERSITÉ JEAN MONNET SAINT-ÉTIENNE

Membre de l'Université de Lyon

Ecole Doctorale N°488
SIS - Sciences Ingénierie Santé

Spécialité de doctorat : Image, vision, signal

Soutenue publiquement le 18 décembre 2025, par :

Sofiane VERNET

Contribution de l'éclairage et de la réalité mixte pour l'assistance des personnes malvoyantes

---

Devant le jury composé de :

Rafael HUERTAS, Full professor, Université de Grenade - Espagne	Rapporteur - Président
Yoko MIZOKAMI, Full professor, Université de Chiba - Japon	Rapporteure
Pichayada KATEMAKE, Docteure, Université de Chulalongkorn - Thaïlande	Examinatrice
Alain TRÉMEAU, Professeur des universités, Université Jean Monnet Saint-Etienne	Directeur de thèse
Éric DINET, Maître de conférences, Université Jean Monnet Saint-Etienne	Co-encadrant de thèse
Philippe COLANTONI, Maître de conférences, Université Jean Monnet Saint-Etienne	Co-encadrant de thèse

Contribution of lighting and mixed reality for the assistance of low-vision people

Résumé

Ce travail de thèse explore comment léclairage peut constituer une aide visuelle pour les personnes souffrant de basse vision plus particulièrement en permettant daméliorer leur capacité de discrimination des couleurs. Les contraintes liées au coût, au confort ou encore à la complexité d'utilisation des aides visuelles existantes freinent considérablement leur adoption. Par ailleurs, les recommandations et les recherches dans le domaine de léclairage sont majoritairement centrées sur les observateurs bénéficiant d'une vision normale tandis que les métriques couramment utilisées en colorimétrie négligent les spécificités de la basse vision.

Afin de pallier ce manque, les recherches développées ici proposent dexaminer comment la composition spectrale de la lumière peut être optimisée pour faciliter la discrimination des couleurs selon le type de déficience visuelle concerné. Dans ce cadre, plusieurs méthodes de simulation de la basse vision, telles que des lunettes spécifiques ou des dispositifs de réalité mixte, ont été explorées afin de pouvoir déployer des expériences psychophysiques standardisées, étape préliminaire avant l'implication de participants souffrant de troubles visuels. Trois types de troubles de la vision ont été initialement sélectionnés : la vision floue, la vision en tunnel ainsi que la perte de vision centrale. Lenvironnement expérimental quant à lui repose sur un système déclairage LED multicanaux parfaitement caractérisé pour un contrôle précis et reproductible dune très grande diversité de spectres lumineux.

Cette thèse apporte plusieurs contributions majeures :

- Le développement de protocoles expérimentaux adaptés à létude de la discrimination des couleurs en condition de basse vision simulée.
- La conception et la validation de méthodes de calibrage et de stabilisation spectrale pour des systèmes d'éclairage LED multicanaux.
- La mise en évidence de l'importance de la modulation de la composition spectrale de la lumière en fonction du type de déficience visuelle concernée.

Les résultats montrent que la capacité de discrimination des couleurs peut être améliorée par un ajustement approprié de léclairage. Ces résultats ouvrent la voie au développement de spectres lumineux optimisés pour répondre aux besoins spécifiques des personnes dont les capacités visuelles déclinent avec l'âge.

Abstract

This thesis research investigates how lighting can be used as a visual aid for low vision people especially by enhancing their ability to discriminate colors. Existing visual aids are often limited by cost, comfort and usability which restrict their adoption. Furthermore, lighting research and standards are largely based on observers with normal vision while conventional colorimetric metrics fail to consider the specificities of low vision.

To address this gap, the present work explores how the spectral composition of light can be optimized to improve color discrimination for different types of visual impairments. In this context, several low vision simulation techniques including specialized goggles and mixed reality devices, were investigated to enable standardized psychophysical experiments with normally sighted participants prior to testing with visually impaired individuals. Initially, three types of low vision were selected: blurry vision, tunnel vision as well as central vision loss. The experimental setup relied on a fully characterized multichannel LED lighting system, allowing precise and reproducible control over a wide range of light spectra.

This thesis makes several major contributions:

- The development of experimental protocols tailored to the study of color discrimination under simulated low vision conditions.
- The design and validation of calibration and spectral stabilization methods for multichannel LED lighting systems.
- The demonstration of the importance of modulating the spectral composition of light according to the specific type of visual impairment.

The results show that color discrimination ability can be improved through appropriate adjustments of lighting conditions. These findings open the possibility for the development of spectrally optimized lighting solutions designed to meet the specific needs of people experiencing age-related or other forms of visual decline.

Contents

List of Figures

List of Tables

Chapter 1

Introduction

Visual impairments have a significant impact on quality of life, limiting autonomy and independence as well as mobility of millions of people worldwide. While many visual impairments can be corrected with eyeglasses, contact lenses, or surgical procedures, some conditions are too severe to be fully corrected, and others have no available medical treatment at all. Moreover, surgical interventions can be prohibitively expensive, technically complex, or carry risks that discourage patients from pursuing them.

Individuals with moderate to severe visual impairments but not completely blind are commonly referred to as low vision individuals. The World Health Organization (WHO) defines low vision as having a visual acuity between 20/70 and 20/400 or a visual field of 20 degrees or less, with the best possible correction. This definition will be further explained in Chapter 3, where it will be described how low vision can affect visual functions. Low vision results in difficulties performing daily tasks such as reading, recognizing faces, or navigating unfamiliar environments, leading to a significant loss of autonomy and increased dependency on others. These challenges can have important consequences, often contributing to reduced well-being, social isolation, and an increased risk of anxiety and depression.

Globally the WHO estimates that 2.2 billion people live with some form of visual impairment. In addition to refractive errors which can often be corrected, a significant proportion suffer from other eye conditions such as cataract, diabetic retinopathy, glaucoma, or age-related macular degeneration. These conditions are particularly prevalent for older adults, and with the increasing aging of the global population, the number of individuals living with low vision is expected to increase significantly in the coming decades. This is especially true for low-income countries, where poor living conditions, financial constraints and limited access to eye care hinders both prevention and treatment efforts.

A wide variety of low vision aids have been developed to help individuals make better use of their residual vision. These include traditional optical devices such as magnifiers, telescopes, or reading lamps, as well as electronic and digital aids that use image processing to enhance contrast and magnify scenes in real time. Although these devices are effective to assist low vision people in many of their tasks, these devices often have practical limitations that reduce their adoption such as size, price or reliance on battery power.

More recently, various prototypes have been proposed to further support low vision

people in a wider range of situations. Some devices integrate ultrasonic or LIDAR sensors to detect obstacles and provide auditory or tactile feedback to the user. In parallel, the use of mixed reality (MR) headsets and smart glasses has gained increasing attention, using advanced computer vision and artificial intelligence models to highlight visual details and assist with object recognition or navigation. MR headsets were also used to increase color contrast to make scenes more easily distinguishable for individuals with low vision. However, these technologies still face significant limitations, both technical, such as restricted field of view or latency, and practical as they remain expensive, often heavy, and uncomfortable to wear for extended periods which reduces their widespread adoption by low vision people.

1.1 Problem Statement and Research Questions

With the widespread adoption of LED lighting over the past decade, important research efforts from both researchers and industry have focused on improving LED performance and exploring its potential to produce light with specific characteristics, such as enhanced color rendering, higher energy efficiency, and spectral properties aligned with human circadian rhythms. However, most research on lighting have focused only on normal vision, neglecting the specific needs of people with low vision. Given that our perception of the world and the saturation of colors are strongly influenced by our surrounding light, the spectral capabilities of LED technology offer an opportunity to increase color contrast in an interior environment for low vision individuals, which could achieve similar color contrast enhancing capabilities as mixed reality systems, but without their limitations.

The **research goal** of this work is to propose methods that would allow to optimize light to improve the residual vision functions of low vision individuals. To achieve this, a special emphasis has been made on the precise control of the lighting environment during psychophysical experiments, with particular attention given to the use of spectrally tunable LED lighting systems. The experiments conducted during this work were specifically designed to address the research questions under investigation. Since involving participants with low vision would be premature at this exploratory stage, investigation has been done on the simulation of low vision conditions.

The **central hypothesis** of this work is that light can be optimized to enhance color discrimination, and therefore improve the ability of low vision individuals to discern different colored objects in a scene. To investigate this hypothesis, a series of psychophysical experiments were conducted using a spectrally tunable LED system, allowing precise control of lighting spectra.

1.2 Organization of the Thesis

This thesis is organized into five chapters:

- **Chapter 2** introduces the theoretical and technical background necessary to understand colorimetry and the principles necessary to understand this thesis.
- **Chapter 3** reviews current knowledge on low vision, including clinical tests used to assess visual function, and highlights psychophysical methods relevant to color vision

research. Current research on lighting is also presented as well as the gaps that are still present for low vision individuals.

- **Chapter 4** addresses the first research question: What are the potential differences in color discrimination ability across different types of visual impairment? This chapter presents the first psychophysical experiment conducted in this work, investigating the influence of the wavelength of individual LED channels on color discrimination ability for different simulated low vision conditions.

- **Chapter 5** addresses the second research question: How can the diversity of light spectra LED lighting can provide be explored, generated using a tunable LED system, and maintained under rigorously stable lighting conditions? This chapter describes the development and implementation of two algorithms for color matching and light stabilization stabilization for LED lighting. The combined use of both algorithms is also presented and is instrumental for the psychophysical experiments conducted under white light.

- **Chapter 6** addresses the second research question: How can white light be optimized based on the variations in color discrimination ability of individuals with low vision? This chapter builds upon the previous findings to propose a new experimental design for evaluating how specific lighting spectra affect color discrimination. A pilot study is presented to validate the proposed approach, then a the final experiment using the low vision simulation goggles is conducted.

Finally, the Conclusion and Perspectives chapter summarizes the key findings and contributions of this thesis, highlighting their impact on the understanding of experimentation on the influence of lighting in low vision conditions. It also presents potential directions for future research aimed at further improving the applicability and performance of the proposed methodologies.

1.3 Main Contributions

The main contributions of the thesis are:

1. The introduction of a comprehensive procedure for controlling all aspects of the experimental environment, with particular emphasis on the management of a spectrally tunable LED system detailed in Chapter 2.

2. The development of a new psychophysical experiment with the aim of studying the differences between types of visual impairments under monochromatic LED channels experiment based on the FarnsworthMunsell 100 Hue Test, and the implementation of an automated scoring method. This contribution is detailed in 4. This work was presented at the ENVISION conference 2025 and is currently under review for publication.

3. The development of scoring methods and statistical analysis of the proposed psychophysical experiment based on the FarnsworthMunsell 100 Hue Test presented in Chapter 4.

4. The development of a new LED light stabilization method to match and maintain precise lighting conditions over extended periods of time. This contribution is detailed in 5 and in the publication "Stabilization of the spectral power distribution of a tunable multichannel LED lighting system" that was presented at the Computational Color Imaging Conference in 2024 [1].

5. The development of a new psychophysical experiment able to evaluate color discrimination ability under different lighting conditions, while benefiting from a stabilized LED light. This contribution is detailed in 6 and in the publication "Experimental Protocol for Color Difference Evaluation Under Stabilized LED Light" [2].

6. The implementation of dedicated software applications to support the experiments conducted in this study and coordinate all experimental equipment. This automation facilitated the experimental processes, significantly reducing their duration and the strain on the participant, while enhancing the consistency and reproducibility of the results. These contributions are detailed in the two Chapters 4 and 5.

Chapter 2

Theoretical and Technical Background

Conducting experiments in any scientific field requires a carefully controlled environment to minimize external biases and maximize reproducibility. This is particularly true for psychophysical experiments on color perception, which are inherently sensitive to subtle changes in experimental conditions. The human visual system can be influenced by a wide range of factors, including ambient lighting, observer fatigue, age or mood, making unbiased measurements especially challenging.

Moreover, the subjective nature of color perception along with the typically limited number of participants in psychophysical studies underlines the importance of careful control over the experimental setup. To ensure accuracy and reproducibility, particular attention was paid in this work to the calibration of equipment, the reliability of colorimetric computations, and their correct implementation in Python.

Figure 2.1: The light booth used throughout this study.

The experimental environment was fully characterized, with a focus on the light booth used for the experiments (Figure 2.1), and in particular on its LED panel, whose spectral properties were thoroughly defined and analyzed. This enabled precise predictions of the lighting conditions during all experiments conducted in this work.

This chapter begins by presenting the human visual system, alongside an overview of key visual impairments, followed by the theoretical and colorimetric foundations necessary for this study. It then describes the experimental setup, detailing the characterization of the light booth and its components. The final section discusses the methods selected for simulating low vision and presents the specifications of the simulation goggles.

2.1 The Human Visual System

Human vision plays the primary role in our ability to perceive and interact with the world. It is a complex sense that uses a wide range of biological and neural mechanisms (Figure 2.2) to detect, process, and interpret the light reflected from our surroundings, allowing us to perceive and make sense of the world in remarkable detail. Light entering the eyes is converted from a physical stimulus into neural signals, which the brain interprets as perceptual sensations, ultimately resulting in the phenomenon of vision. Understanding the physiological basics underlying human vision is essential in studies involving visual perception, especially when conducting psychophysical experiments with the aim of studying low vision.

This section will present the mechanisms of vision, beginning with the anatomy of the eye, followed by the retina, its photoreceptors and their role in the fundamental processes behind color perception. Finally, an overview of some of the most common visual impairments and their origins in disruptions of specific stages within the visual process will be presented.

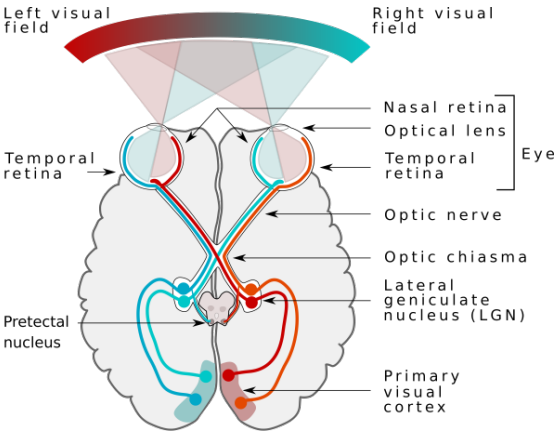

Figure 2.2: Diagram of the human visual pathways. Image from [3].

2.1.1 Anatomy of the eye

The eye functions as an optical system, it is designed to capture and focus incoming light rays onto a surface where the photoreceptors react to the incoming light and produce neural signals that will be processed by the brain. Figure 2.3a shows the structure of the eye. At the front of the eye, the light enters through the cornea which serves both as a barrier against dirt and a lens. The amount of light entering the eye is then regulated in the same way as with a diaphragm by the iris contracting or extending. Light is then focused by the crystalline lens through a process named accommodation in order to produce a sharp projection in the retina. The retina is in the back of the eye, it serves as a screen that is divided in two regions, the fovea which is in the center of the retina and responsible for high-resolution vision while the peripheral retina is more important for low-light conditions and motion detection (see Figure 2.3b).

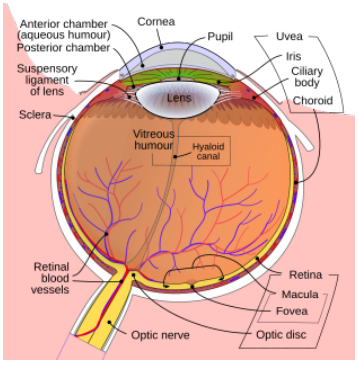

(a) Structure of the human eye. Image from [4].

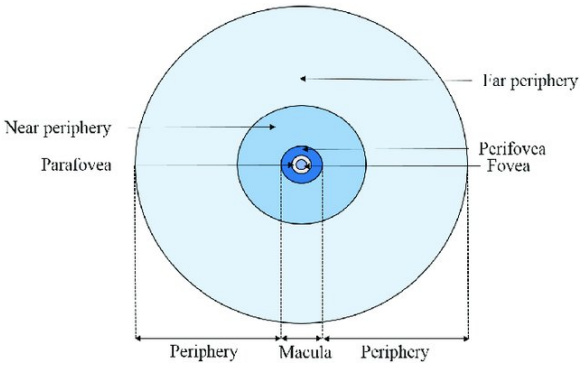

(b) Regions of the retina. Image from [5].

Figure 2.3: The human eye and Retina.

2.1.2 Photoreceptors and retinal processing

There are two types of photodetectors present in the retina, the rods and the cones, which are respectively specialized in low-light condition vision and color vision. Their distribution in the retina is shown in Figure 2.4a. Rods, numbering over 110 million, are mainly distributed in the peripheral retina and are specialized for low-light conditions, offering high sensitivity but low spatial resolution and only monochromatic vision. Cones on the other hand, only amount to about 6 million in total, are concentrated in the fovea and allow for sharp central and color vision. Cones are divided in three subtypes sensitive to long, medium, and short wavelengths [6], known as L-, M-, and S-cones, with S-cones representing only about 2% of the total, while the proportions of L- and M-cones vary significantly between individuals [7]. When light reaches the photoreceptors, it is absorbed by photopigments that trigger an electrical signal transmitted indirectly to the optic nerve [8]. The structure and distribution of rods and cones in the retina are illustrated in Figure 2.4b.

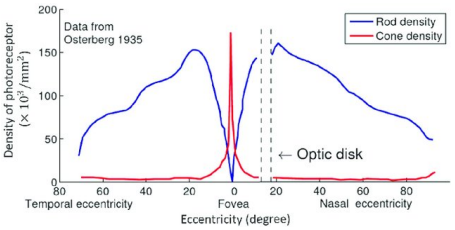

(a) Distribution of cones and rods in the human retina. Image from [9].

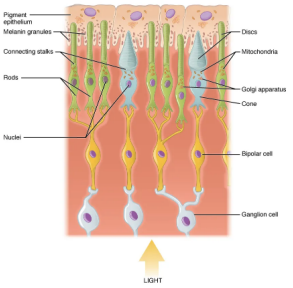

(b) Photoreceptors placement in the Retina. Image from [10].

Figure 2.4: Distribution and Arrangement of the photoreceptors in the human retina.

2.1.3 Mechanisms of color perception

The three types of cones LMS are sensitive to different regions of the visible spectrum, with respective sensitivity peaks of 560, 530 and 420 nm. Their relative stimulation by a light spectrum allows the brain to produce a large variety of colors. These three types of receptor form the basis of the trichromatic system of human color perception as was first theorized with the Young-Helmholtz theory in the 19th century. According to this theory, any perceived color can be described as a weighted combination of the responses from the three cone types. This served as the main hypothesis for development of the CIE 1931 XYZ color space that will be further detailed in Section 2.2.

The human visual system functions across a wide range of illumination levels. This adaptability is partially enabled by the iris, which adjusts the pupil size in response to ambient light. However, the primary mechanisms of light adaptation occur at the level of the retina, particularly within the photoreceptors. These cells regulate their sensitivity through a process known as visual adaptation. When transitioning from a dark to a bright environment, rod photoreceptors gradually deactivate through a phenomenon called photobleaching, allowing cones to take over vision under high luminance. Full adaptation to bright conditions typically occurs within about five minutes. Conversely, when moving from bright to dark settings, cones that are less sensitive in low light, transfer the task of visual processing back to the rods, which gradually resume activity as their photopigments regenerate [8]. The adaptation process affects not only perceived brightness but also color vision. One notable phenomenon is the Purkinje effect, which refers to the shift in peak sensitivity toward shorter wavelengths as the eye adapts to darkness. As rod activity becomes dominant, colors such as red, which lies far from the peak sensitivity of rods, appear significantly darker than other colors.

Another form of adaptation used by the visual system is chromatic adaptation, which refers to the ability to adjust to varying lighting conditions while maintaining a stable perception of object colors, a phenomenon known as color constancy. Although the photobleaching of the most stimulated cones contributes to this process, chromatic adaptation is complex and involves multiple levels of the visual system. Despite this complexity, several mathematical models have been developed to approximate and simulate its effects known

as color adaptation transform (CAT) [11].

2.1.4 Visual impairments

In this subsection, we will present some of the most common visual impairments and how they relate to the underlying physiological conditions. Understanding these connections helps us see the effects of these impairments and the need for appropriate support and solutions.

The most common type of visual impairments are refractive errors which happen when the shape of the eye doesn't allow light to correctly focus on the retina. The most frequent refractive errors include:

- Myopia: The eye is too long making the light focus before the retina and preventing vision from afar.
- Hypermetropia: The eye is too short, making the light focus after the retina and making near vision blurry or forcing the eye to accommodate more.
- Astigmatism: The cornea or lens is incorrectly shaped, making the light focus in abnormal way and blurring vision at any distance.
- Presbyopia: With aging, the eye can't accommodate as much as it used to. In the same way as hypermetropia, it makes near vision blurry.

These conditions mostly induce blurry or slightly deformed vision, and while these conditions are often corrected using glasses or contact lenses, in many cases it remain uncorrected due to impracticality or price.

Cataract is a visual impairment that is often due to ageing, but that can be caused or accelerated by a lot of other factors, such as physical trauma, diabetes or generally poor living conditions. It corresponds to a clouding of the lens of the eye and comes with blurry vision, faded perception of colors and other symptoms, hindering mobility, reading ability and more generally independence in everyday life. Although a surgical procedure exists to replace the opacified lens, it is still the leading cause of blindness in the world, and especially in the developing countries where cost is the most limiting factor.

Macular degeneration, often called age-related macular degeneration (AMD) is another visual impairment linked with ageing. It is caused by the degeneration of the central part of the retina which results either in complete blindness or loss of central vision. It is an incurable and incorrectable low vision condition that affects more than 200 million people worldwide.

The last type of low vision condition developped in this subsection are the ones caused by damage to the optic nerve. This can be caused by many different factors such as trauma, various infections, tumors or specific diseases such as glaucoma, optic neuritis, or ischemic optic neuropathy. The symptoms are also various including blurry vision, blind spots (scotoma) in the visual field or even color vision deficiencies.

The visual impairments described in this section highlight the difficulty to work with low vision. There is a great diversity in existing types of visual impairments and even for one type, a lot of variations can be observed between individuals. This emphasizes the

challenges of conducting psychophysical experiments in this context, as creating a set of observers large enough and representative of the studied condition is difficult.

2.2 Metrology and Colorimetry

Since the early days of modern colorimetry in the 1850s, important advancements have been made to the study of color. From the Young-Helmholtz theory to the latest developments in Color Appearance Models, color has come from an entirely perceptual feeling to quantifiable data.

This section will outline the mathematical background to understand colorimetric computations needed in this thesis. It will first present the steps required to transform a purely physical quantity that is a light spectrum to mathematical models used to represent color and detail some of the existing color spaces, followed by a definition of standard illuminants. Then color rendering index and other light quality metrics will be introduced before giving an overview of the commonly used color measuring devices.

2.2.1 Defining light

Light is a physical phenomenon that can be described both as a self-propagating electromagnetic wave and as a stream of discrete particles called photons. These complementary descriptions form the basis of waveparticle duality. The properties of EMRs differ depending on their frequency, or wavelength, and are classified in different bands as shown in Figure 2.5. In the field of physics, the definition of light can be as broad as to include any types of radiations but it is common to define light as electromagnetic radiations of the UV, visible and infrared, or in some cases even as strictly as only containing the visible radiations. For this work, and in the context of the study of human perception of color, the latter definition will apply whenever light is mentioned. Although the human eye can, in certain condition see part of the UV or near infrared radiations these bands do not influence color perception in any meaningful way, so the visible spectrum will be defined with the CIE standard that restricts the definition of visible light to the 380 to 780 nm band and all measurements or computation will use this range [12].

Radiometry is the science of measuring electromagnetic radiation in terms of its physical energy. It provides techniques and units that make it possible to quantify how radiations are emitted by a source, transmitted through a medium or received by a detector. On the other hand, photometry focuses only on visible light and takes into account the sensitivity of visual system by weighting the radiometric quantities according to the luminous efficiency function. [14, 15]. The base photometric unit is the candela (cd) it corresponds approximately to the luminous intensity of a candle and measures the perceived power of light emitted by a source in a particular direction. Multiple commonly used photometric units were derived from the candela: the Lumen (lm), equivalent to cd·sr and the Lux (lx), equivalent to cd·sr/m^2. They respectively describe the perceived power of a light source and the received light by a surface. Luminance, which is the photometric measure of luminous intensity per unit area in a given direction, is also defined in cd/m^2.

As explained in Section 2.1 the human visual system adapts from low-light conditions to

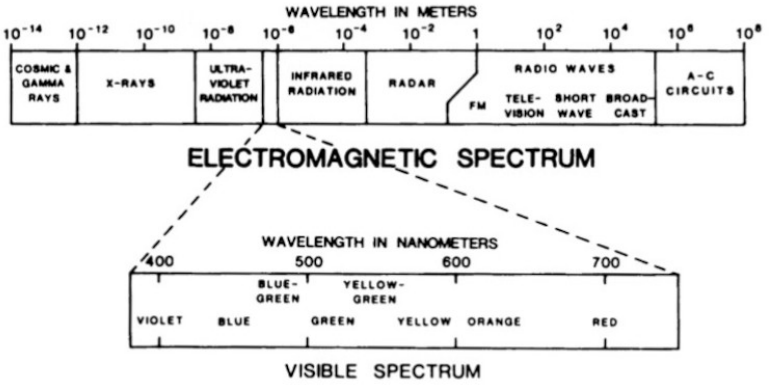

Figure 2.5: The classification of radiations. Image from [13].

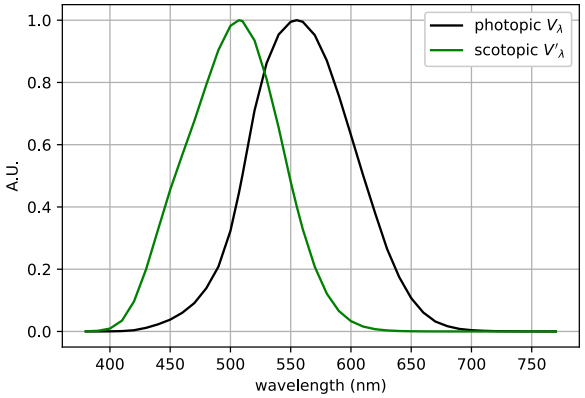

Figure 2.6: Normalized Luminous efficiency functions.

bright conditions. This is formalized by distinguishing three modes of vision of the human visual system, depending on the luminance level it is subject to:

- Photopic vision is active in well-lit environment such as daylight (10 to 10^8 cd/m^2), vision is assured exclusively by the cones,
- Scotopic vision is active under low-light conditions (10^{-3} to 10^{-6} cd/m^2), vision is assured exclusively by the rods,
- Mesopic vision is a combination of photopic and scotopic vision (10^{-3} to $10^{0.5}$ cd/m^2), vision is assured by a combination of cones and rods.

The photopic luminous efficiency as it was defined by the CIE in 1924 is usually named $V(\lambda)$ and is plotted in black while the scotopic function is plotted in green in Figure 2.6.

As shown first by Newton with his dispersive prism experiment, white light coming from the sun is in fact the sum of an infinite amount of light rays with different wavelengths.

Most lights are polychromatic and just a few examples emit light at a specific wavelength (e.g. laser, sodium lamp, ...), which qualifies them as monochromatic. The composition of a light can be viewed by displaying its Spectral Power Distribution (SPD). Figure 2.7 shows an example of SPD, here from a fluorescent lamp.

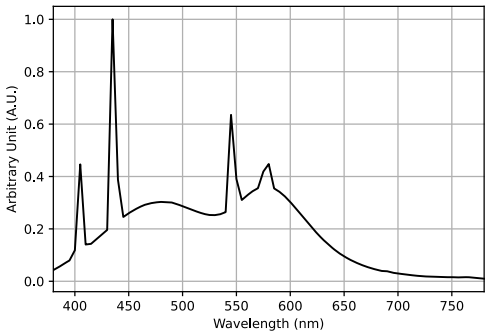

Figure 2.7: SPD of a fluorescent lamp.

If an object does not emit light, it becomes visible to the human eye solely through its interaction with ambient light. This interaction depends on the objects chemical composition and how its material reflects, absorbs or transmits light. The quantities used to describe these interactions are the following: reflectance which represents the proportion of light reflected, absorbance which indicates the proportion of light absorbed at each wavelength, and transmittance which represents the proportion of light transmitted through a given medium. In this work, material-light interactions are characterized using reflectance and transmittance. As an example, Figure 2.8 illustrates the reflectance of wood, showing that wavelengths corresponding to the orange to red regions are predominantly reflected justifying woods characteristic brown appearance.

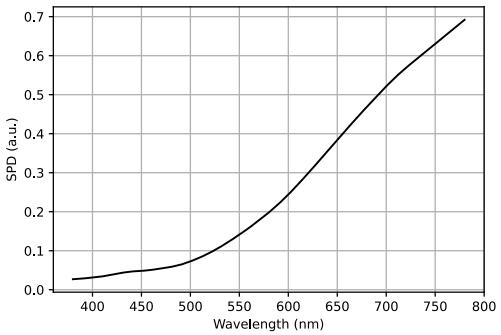

Figure 2.8: Spectral reflectance of wood.

Once the spectrum of the illuminating light and the reflectance of a material are known, the spectrum of the reflected light can be easily calculated. This is done by performing

a wavelength-wise multiplication of the illumination spectrum $E(\lambda)$ with the material's reflectance $R(\lambda)$ as shown in Equation 2.1.

$$S(\lambda) = R(\lambda) \cdot E(\lambda) \tag{2.1}$$

2.2.2 Correlated color temperature (CCT)

In the common language, different types white light are often described as warm or cold light respectively for yellowish light and for blueish light. Unlike color temperature, which applies only to ideal blackbody radiators, CCT extends the concept to real light sources whose spectra do not follow a blackbody curve. It is defined by the CIE as "temperature of a Planckian radiator whose perceived color most closely resembles that of a given stimulus at the same brightness and under specified viewing conditions". Since it represents an equivalent temperature, it is expressed in Kelvin (K), the lower values corresponding to reddish light and conversely higher values to blueish light. Its calculation involves the use of the planckian locus, which corresponds to the colors a black body will emit depending on its temperature. Figure 2.9 shows the Planckian locus plotted in the CIE 1960 UCS color space.

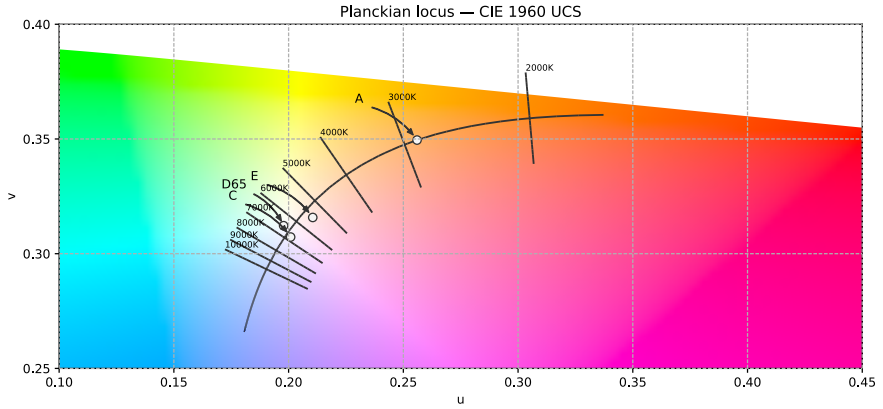

Figure 2.9: Planckian locus in the CIE 1960 UCS chromaticity diagram.

Because incandescent light bulbs behave similarly to a black body, their operating temperature provides a close approximation of their correlated color temperature. In contrast, modern lighting technologies such as fluorescent and LED sources can produce a much broader range of chromaticities, which can deviate significantly from the black body locus. Therefore, although the CCT can be calculated for any light spectrum, the value obtained can only be meaningful if the chromaticity of the light is close enough to the planckian locus. In the CIE 1960 UCS color space, it corresponds to a distance Δ_{uv} lower than 0.05 (Equation 2.2). The calculation of CCT involves computing the isotherm, the perpendicular straight line defining the shortest path from the chromaticity of the light to the planckian locus in the CIE 1960 color space [16].

$$\Delta_{uv} = \sqrt{(u_t - u_p)^2 + (v_t - v_p)^2} \leq 0.05 \tag{2.2}$$

with u_t and v_t the light source coordinates and u_p and v_p the coordinates of the equivalent black body on the planckian locus.

2.2.3 Standard illuminants

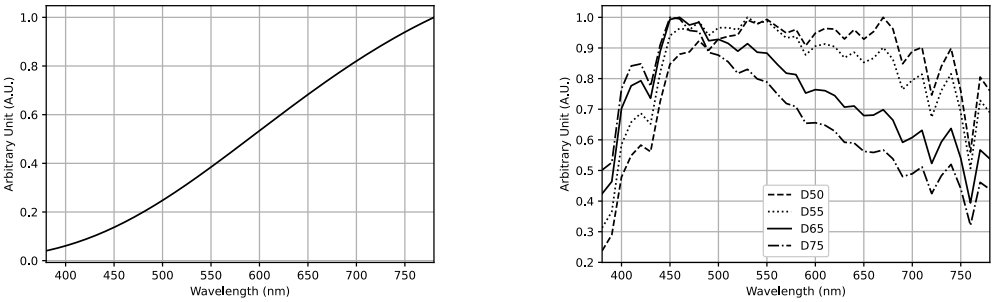

(a) SPD of CIE standard illuminant A. (b) SPD of D-series illuminants D50-55-65-75.

Figure 2.10: SPDs of CIE standards A and D-series.

In order to ensure consistency and reproducibility in colorimetric measurements, the CIE has published a set of standard illuminants that serve as reference lighting conditions. These illuminants are theoretical light sources with specified SPDs designed to simulate various typical lighting scenarios.

The earliest illuminants introduced by the CIE were the illuminants A, B and C in 1931. As shown by Figure 2.10a Illuminant A represents the SPD of an incandescent tungsten light bulb at a color temperature of about 2856K, and is only used today for legacy systems. On the other hand, illuminants B and C used to represent daylight at 4874K and 6774K but were deprecated in favor of the CIE D-series illuminants shown in Figure 2.10b.

In 2004 standard illuminants were issued by the CIE specifically for newer light sources such as fluorescent lamps, high pressure discharge lamps (See Appendix B). Finally, and more importantly in the context of this work, in 2018 standard LED lighting illuminants were added to the list of standard illuminants:

- LED-B1…B5: five different CCT of phosphor-converted blue LEDs (Figure 2.11a).
- LED-BH1: phosphor-converted blue LED and a red LED (Figure 2.11b).
- LED-RGB1: combination of red green and blue LEDs (Figure 2.11b).
- LED-V1/V2: two phosphor-converted violet LEDs (Figure 2.11c).

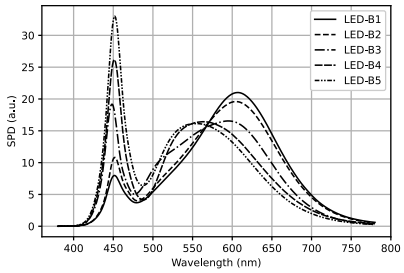

(a) Standard LED-B series (B1 to B5).

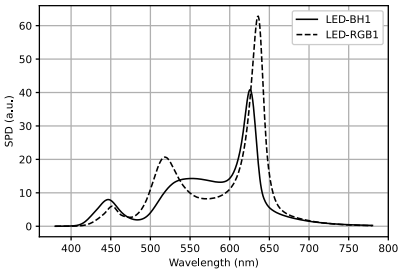

(b) LED-BH1 and LED-RGB1.

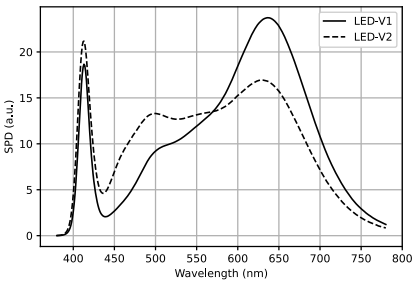

(c) Standard LED-V series (V1 and V2).

Figure 2.11: CIE standards for LED lighting.

2.2.4 Color spaces

Light emitted from different light sources in our environment bounce around on objects with complex interactions. Eyes serve as an optical sensor able to concentrate the incoming light rays into an image on the retina. The human visual system being trichromatic, it is possible to describe all the visible colors by three values and various color spaces were developed based on this property of trichromacy of human color vision. This subsection provides an overview of several commonly used color spaces, beginning with the CIE 1931 XYZ model and introducing more recent color spaces developed to address its limitations. Details are also given to how these spaces were utilized in the context of this work. All colorimetric computations were performed using the Luxpy library [17], ensuring consistency and reliability across all results.

CIE 1931 XYZ:

The first color space created to obtain tristimulus values out of a light spectrum was the CIE 1931 RGB. It was obtained from the results of the Wright-Guild color matching experiment. This experiment consists in asking participants to match with three primaries (red, green and blue) in one 2° hemicircle to the second hemicircle which is a monochromatic color. The results of this experiment allowed to obtain the CIE RGB color-matching functions. Figure 2.13 depicts the Wright-Guild color matching experiment.

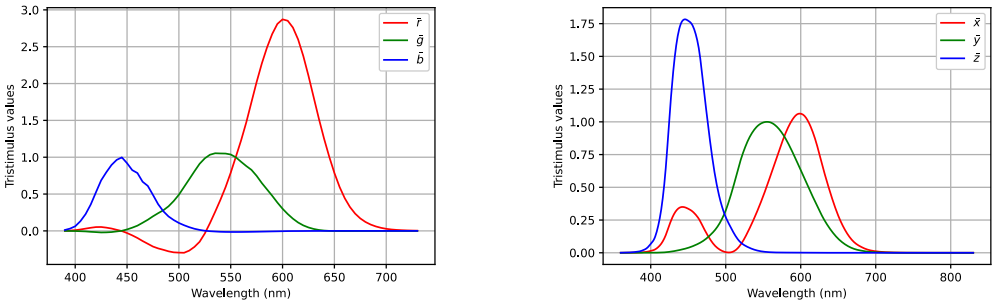

(a) CIE 1931 RGB color matching functions. (b) CIE 1931 XYZ color matching functions.

Figure 2.12: CIE 1931 color matching functions.

As can be observed on Figure 2.12a, the obtained RGB color-matching functions are not strictly positive, therefore in order to facilitate computation, the CIE proposed a linear transformation of the CIE RGB functions, resulting in the CIE XYZ color matching functions, which allowed to obtain three color matching functions always greater or equal to zero, with $\bar{y}(\lambda) = V(\lambda)$. The CIE XYZ color matching functions are displayed in Figure 2.12b and allow to compute the tristimulus values for a given light spectrum.

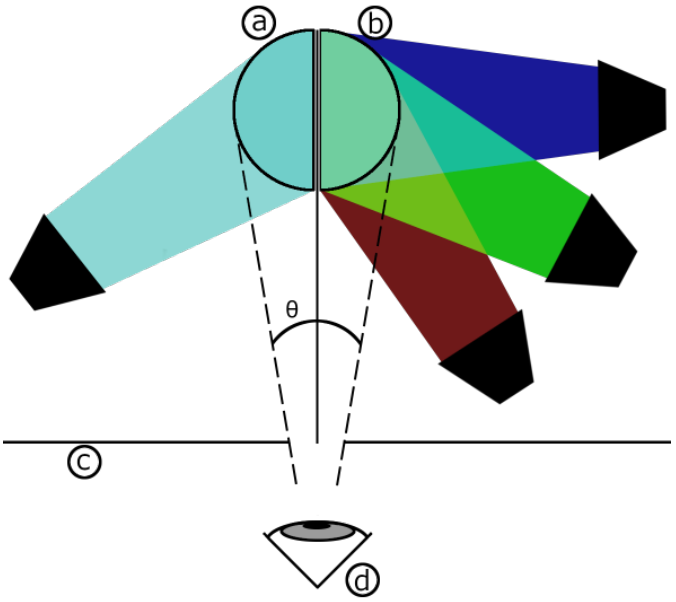

Figure 2.13: Diagram of the Wright-Guild color-matching experiment (θ usually 2° or 10°), (a) Monochromatic field, (b) Tricolor field, (c) Masking screen, (d) Observer position.

Color matching functions are designed to represent an idealized model of normal human color vision. While this model has significant limitations and substantial inter-individual

variability [18], further experiments led to the development of alternative color matching functions. Judd and Vos proposed important corrections [19], and Stiles and Burch extended the approach by developing functions based on a 10° visual field instead of the standard 2° field [20].

When considering an emissive source of light, we can compute its chromaticity as shown in Equation 2.3.

$$\begin{aligned} X &= \int_{380}^{780} E(\lambda)\,\overline{x}(\lambda)\,d\lambda, \\ Y &= \int_{380}^{780} E(\lambda)\,\overline{y}(\lambda)\,d\lambda, \\ Z &= \int_{380}^{780} E(\lambda)\,\overline{z}(\lambda)\,d\lambda. \end{aligned} \tag{2.3}$$

with E the spectrum of the light source and $\{\overline{x}, \overline{y}, \overline{z}\}$ the three color matching functions.

On the other hand, when looking at a colored object, the light is first reflected on the object before reaching the eye. Therefore, the reflected SPD entering the eye is the product of the light and the reflectance of the object, as stated in Equation 2.1. In this case the XYZ tristimulus values are computed with Equation 2.4.

$$\begin{aligned} X &= \frac{K}{N}\int_{380}^{780} R(\lambda)\,E(\lambda)\,\overline{x}(\lambda)\,d\lambda, \\ Y &= \frac{K}{N}\int_{380}^{780} R(\lambda)\,E(\lambda)\,\overline{y}(\lambda)\,d\lambda, \\ Z &= \frac{K}{N}\int_{380}^{780} R(\lambda)\,E(\lambda)\,\overline{z}(\lambda)\,d\lambda, \end{aligned} \tag{2.4}$$

where K is a scaling factor (1 or 100) and

$$N = \int_{380}^{780} E(\lambda)\,\overline{y}(\lambda)\,d\lambda.$$

sRGB:

The majority of color displays are able to produce their full range of colors through the use of additive color mixing with pixels divided in red, green and blue subpixels. To represent colors on such a device the sRGB standard was developed by Microsoft in 1996. It soon became a standard for many computer applications and web pages to provide a rough standardization of color appearance across displays of different technologies and manufacturers. It uses a simple three values color model (R,G,B), each ranging from 0 to 1, and respectively representing red, green and blue contents needed to produce the desired color.

The conversion from XYZ to sRGB is done as follows:

$$\begin{bmatrix} r_{linear} \\ g_{linear} \\ b_{linear} \end{bmatrix} = \begin{bmatrix} +3.2406255 & -1.5372080 & -0.4986286 \\ -0.9689307 & +1.8757561 & +0.0415175 \\ +0.0557101 & -0.2040211 & +1.0569959 \end{bmatrix} \begin{bmatrix} X \\ Y \\ Z \end{bmatrix}$$

The linear rgb values are then made non linear with $V = \{R, G, B\}$ and $v = \{r_{linear}, g_{linear}, b_{linear}\}$:

$$V = \begin{cases} 12.92\, v & \text{if } v \leq 0.0031308, \\ 1.055\, v^{1/2.4} - 0.055 & \text{otherwise} \end{cases}$$

CMYK:

On the other hand, printers use subtractive color mixing in order to produce color with a mix of inks. In order to mimic this idea, the CMYK was developed in the 1890s for newspaper printing and represents colors as an addition of cyan, yellow, magenta and black inks. There is no simple formula to convert from any color space into CMYK since it is device dependant and lookup tables are used instead. In this work, when printing specific colors was needed, images were provided to the printer using sRGB values in conjunction with special calibration methods that will be developed in Section 6.

Uniform Color Spaces: One of the main issue of both CIE XYZ and sRGB is their lack of perceptual uniformity. Perceptually Uniform Color Spaces (UCS) are color spaces that aim at representing colors from a perceptual standpoint and where differences in numerical values are proportional to the perceived difference in color.

CIE 1960 UCS and CIE 1976 $L^*u^*v^*$:

The CIE 1960 color space is the color space used to compute the correlated color temperature. It is simple transformation of the CIE 1931 XYZ color space that attempted percptual uniformity. It uses only two coordinates (u, v) and the conversion from XYZ is done as follows:

$$u = \frac{4X}{X + 15Y + 3Z}$$
$$v = \frac{6Y}{X + 15Y + 3Z}$$

An improved version of this color space was developped and is known as the CIE 1976 $L^*u^*v^*$ or CIELUV color space. For a reference white (X_n, Y_n, Z_n)

$$L^* = \begin{cases} \left(\frac{29}{3}\right)^3 \frac{Y}{Y_n}, & \frac{Y}{Y_n} \leq \left(\frac{6}{29}\right)^3, \\ 116 \sqrt[3]{\frac{Y}{Y_n}} - 16, & \frac{Y}{Y_n} > \left(\frac{6}{29}\right)^3, \end{cases}$$

$$u^* = 13L^* \cdot (u' - u'_n),$$
$$v^* = 13L^* \cdot (v' - v'_n).$$

with

$$u' = \frac{4X}{X + 15Y + 3Z}$$
$$v' = \frac{9Y}{X + 15Y + 3Z}$$

L*a*b* CIE 1976:

The L*a*b* CIE 1976 or CIELAB color space is an improvement over the CIE XYZ color space with the aim of being a perceptually uniform color space and although it does not perfectly achieve this goal, it is an important improvement over CIE XYZ in this regard. Like the CIE XYZ, it encompasses all colors visible to the human eye. Its color model represents color with three values (L^*, a^*, b^*). L^* represents lightness and is a value between 0 (black) and 100 (white) according to a specified reference white. $a*$ represents the green/red ratio with negative values toward the green and positive toward the red. b^* represents the blue/yellow ratio with negative values toward the blue and positive toward the yellow. The a^* and b^* values are unbounded. The conversion from XYZ is done as follows:

$$L^* = \begin{cases} 116 \times \sqrt[3]{\frac{Y}{Y_W}} - 16, & \text{if } \frac{Y}{Y_W} > 0.008856, \\ 903.3 \times \frac{Y}{Y_W}, & \text{if } \frac{Y}{Y_W} \leq 0.008856. \end{cases}$$

$$a^* = 500 \times \left(f\left(\frac{X}{X_W}\right) - f\left(\frac{Y}{Y_W}\right) \right)$$

$$b^* = 200 \times \left(f\left(\frac{Y}{Y_W}\right) - f\left(\frac{Z}{Z_W}\right) \right)$$

$$\text{where} \quad f(x) = \begin{cases} \sqrt[3]{x}, & \text{if } x > 0.008856, \\ 7.787x + \frac{16}{116}, & \text{if } x \leq 0.008856. \end{cases}$$

where t is $\frac{X}{X_n}$, $\frac{Y}{Y_n}$, or $\frac{Z}{Z_n}$ and (X_n, Y_n, Z_n) are the XYZ values of the reference white.

CIELCh:

Based on the CIELAB, the CIELCh is a useful colorspace that trades the a^* and b^* of CIELAB for polar coordinates C^* and h°. C^* represents the chroma, which is defined by the CIE as "colorfulness of an area judged as a proportion of the brightness of a similarly illuminated area that appears white or highly transmitting". h° represents the hue angle as a value between 0° and 359° with 0°, 90°, 180° and 270° respectively representing approximately unique red, yellow, green and blue. CIELCh has the advantage of being both perceptually uniform and intuitive to use with its lightness/chroma/hue representation of colors. The conversion of a^* and b^* to C^* and h° is done as follows:

$$C^* = \sqrt{a^{*2} + b^{*2}},$$

$$h^\circ = \begin{cases} \arctan(b^*/a^*) & \text{if } a^* > 0,\ b^* \geq 0 \\ \arctan(b^*/a^*) + 180 & \text{if } a^* < 0 \\ \arctan(b^*/a^*) + 360 & \text{if } a^* > 0,\ b* \leq 0 \end{cases}, a^* \neq 0$$

Physical swatches color systems:

The color spaces previously described are based on the CIE 1931 XYZ color space, however some color spaces were developed in parallel with the idea of using physical colored samples to standardize colors. These are often used to standardize colors in various industries such as design, textile or manufacturing for example.

Pantone Matching System:

Although it is not a color space, the Pantone Matching System remains the most widely used standardized color collection. The most widely used of these color spaces is the Pantone Matching system. It consists in 2161 uniquely named colors in no particular order, for example Figure 2.14 shows the color named 534c.

Figure 2.14: Pantone 534c.

In this work, two physical swatches-based color systems were considered for the design of psychophysical experiments: the Munsell Color System (MCS) and the Natural Color System (NCS). Contrary to the Pantone Matching system, both of these color spaces use an organized naming scheme for their colors based on their perceptual aspect.

Munsell Color System (MCS):

The Munsell Color System or MCS is a color space created in the early 20th century. It was based on measurements of human perception and represents colors on three aspects: hue, lightness and chroma. Hue is described using 5 principal hues (red, yellow, green, blue and purple) and 5 intermediate hues (YR, GY, BG, PB and RP). Lightness describes how white a color is, 0 being black and 10 white. Finally, chroma describes the vividness of the colors and has no upper limit since the chroma is hue specific.

For example, Figure 2.15 shows the MCS color 5GY 8/4 corresponding to a color halfway between green and yellow, with a lightness of 8 and a chroma of 4. Standard Munsell charts typically include 40 hues, though some extended versions, such as those used in the Farnsworth-Munsell 100 Hue Test, subdivide hues further, offering up to 100 distinct hue steps.

Natural Color System (NCS):

The Natural Color System or NCS that uses Hering's opponency theory and postulates the existence of six elementary colors, complementary two by two: white-black, red-green and yellow-blue. The latest iteration of the NCS contains 1950 colors that are all designated

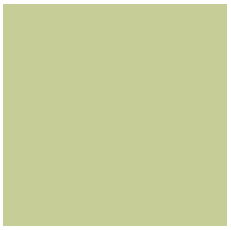

Figure 2.15: MCS 5GY 8/4.

using the same format by their blackness, chromaticness and hue. For example color S 4040 Y30R shown in Figure 2.16 corresponds to 40% blackness, 40% chromaticness and a hue with 70% yellow and 30% red [21].

Figure 2.16: NCS color S 4040 Y30R.

2.2.5 Color distance metrics

The development of uniform color spaces allowed to represent colors mathematically while taking into account human perception of colors. More precisely it made meaningful the notion of distance in a color space.

The first metric presented in this chapter to quantify color differences is the Δ_{uv}, introduced in Subsection 2.2.2. Its main use it to compute the distance of the chromaticity of a light to the planckian locus. Since then, the concept of color distances was generalized by the CIE with the different iterations of ΔE metrics.

ΔE^*_{ab}:

When the CIELAB color space was proposed, it was considered to be perceptually uniform. This meant that a simple euclidean distance in this color space was a valid perceptual measure of color distance. For two colors with coordinates (L^*_1, a^*_1, b^*_1) and (L^*_2, a^*_2, b^*_2), we have:

$$\Delta E^*_{ab} = \sqrt{(L^*_2 - L^*_1)^2 + (a^*_2 - a^*_1)^2 + (b^*_2 - b^*_1)^2}$$

ΔE^*_{94}:

It was found later that the asumption of uniformity of the CIELAB color space was not

actually true. In order to fix this issue, a new color distance was developped as the ΔE^*_{94}. The formula uses CIELCh instead of CIELAB, for two colors with coordinates $(L^*_1, C^*_1, h^\circ_1)$ and $(L^*_2, C^*_2, h^\circ_2)$, we have:

$$\Delta E^*_{94} = \sqrt{\left(\frac{\Delta L^*}{k_L S_L}\right)^2 + \left(\frac{\Delta C^*}{k_C S_C}\right)^2 + \left(\frac{\Delta H^*}{k_H S_H}\right)^2},$$

where

$$\begin{aligned}
\Delta L^* &= L^*_1 - L^*_2, \\
C^*_1 &= \sqrt{a^*_1 + b^*_1}, \\
C^*_2 &= \sqrt{a^*_2 + b^*_2}, \\
\Delta C^* &= C^*_1 - C^*_2, \\
\Delta H^* &= \sqrt{\Delta E^2_{76} - \Delta L^{*2} - \Delta C^{*2}} \\
S_L &= 1, \\
S_C &= 1 + K_1 C^*_1, \\
S_H &= 1 + K_2 C^*_1,
\end{aligned}$$

$K_1 = 0.045$, $K_2 = 0.015$ and k_L, k_C, k_H depend on the application.

ΔE^*_{00}:

Since the ΔE^*_{94} did not solve all the non-uniformity issues, the CIE proposed the CIEDE2000 noted as ΔE^*_{00}. The formula is much more complex and is as follows for two colors (L^*_1, a^*_1, b^*_1) and (L^*_2, a^*_2, b^*_2) [22]:

$$\Delta E^*_{00} = \sqrt{\left(\frac{\Delta L'}{k_L S_L}\right)^2 + \left(\frac{\Delta C'}{k_C S_C}\right)^2 + \left(\frac{\Delta H'}{k_H S_H}\right)^2 + R_T \left(\frac{\Delta C'}{k_C S_C}\right)\left(\frac{\Delta H'}{k_H S_H}\right)}$$

with the different components of the formula detailed in Appendix C

2.2.6 Light quality metrics

With the number of artificial light sources increasing on the market, lighting quality metrics were developed to compare their performance for different aspects of human vision such as color fidelity, color discrimination or visual comfort.

Color rendering index (CRI):

The most common one and readily adopted by lamp manufacturers is the Color Rendering index (CRI). It aims at describing how natural or faithful colors appear under a given light source, compared to ideal or natural light used as a reference. The CRI score is named the

CIE R_a and has a maximum value of 100, with the reference light itself reaching a perfect score. The score however doesn't have a lower bound and can be in the negative for certain light sources. The calculation of the CIE R_a uses 8 colored samples, shown in Figure 2.17, that are measured under the test light and under a reference light. The choice of reference light depends on the correlated color temperature of the test light, if it is under 5000K, then the reference illuminant is the black body at the same CCT. Else, it is selected as the standard illuminant of the D series with the same CCT. The chromaticity in the CIE 1960 UCS color space of the 8 samples is measured under the test light, then chromatically adapted using the Von Kries transform [23]. The same is done for the samples under the reference illuminants and the euclidean distance ΔE_i is calculated for each pairs between the two lighting conditions. For each colored samples, the particular CRI is calculated using the formula $R_i = 100 - 4.6\Delta E_i$. Finally, the CIE R_a is defined as the arithmetical mean of the eight particular scores.

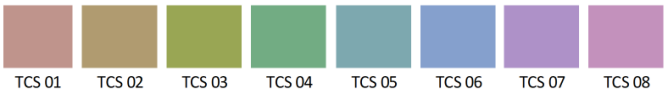

Figure 2.17: Test Color Samples (TCS) used for the calculation of the CRI R_a.

Many critics have been made to the CIE R_a such as the use of an outdated color space and Von Kries chromatic adaptation, the reduced number of colored samples that isn't able to represent all the diversity of colors in everyday life or its inability to correctly assess modern lighting such as LEDs [24]. This lead to the development of many alternative light quality metrics.

Color quality scale (CQS):

The color quality scale (CQS) aims at solving some of the issues of the CIE R_a while keeping the same fundamental principle. The CIELAB is used instead of the CIE 1960 UCS, the Von Kries chromatic adaptation is replaced by the CMCCAT2000 [25] and the colored samples used are more numerous and more diverse in saturation than for the CRI. Furthermore, a root mean square is used instead of an arithmetic mean to compute the score from the particular scores in order to penalize small numbers of poorly rendered samples. The score of the CQS is named the Q_a and contrary to CIE R_a, is bounded to a value between 0 and 100 for improved user readability [26]. Although it has not become a standard, some manufacturer have started specifying it on some of their products.

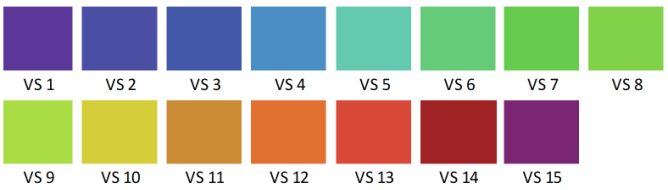

Figure 2.18: Color samples used for the calculation of the CQS Q_a.

Gamut area index (GAI):

One of the critics of the CRI is that it is only a measure of difference of color rendering compared to a reference illuminant, and although it quantifies well the naturalness of color rendering under a given light, it was often used inadequately to quantify other quality of a light source. However, especially for the study of color discrimination this might not be a good metric. The main hypothesis behind the CRI is that natural daylight is the best possible light to achieve, however if an artificial light were to have a better color discrimination capability due to increased saturation, shift of certain hues for example, it would still score a low CIE R_a. In an effort to solve this contradiction, Thornton [27] proposed to use of the eight samples in the original CRI to calculate the gamut of the test light and compare it to the gamut of a reference illuminant. The Gamut Area Index (GAI) was developed in 2008 by Rea and Freyssinier-Nova [28] following this idea. The chromaticities of the eight TCS samples are calculated in the CIE 1964 color space and the area of the polygon it forms is compared to the gamut area of a reference illuminant. The score is written R_g and compares the gamut of the test light to a reference light: if R_g<100 the test light renders color less saturated than the reference, on the opposite, if R_g>100 the test light renders colors more saturated than the reference.

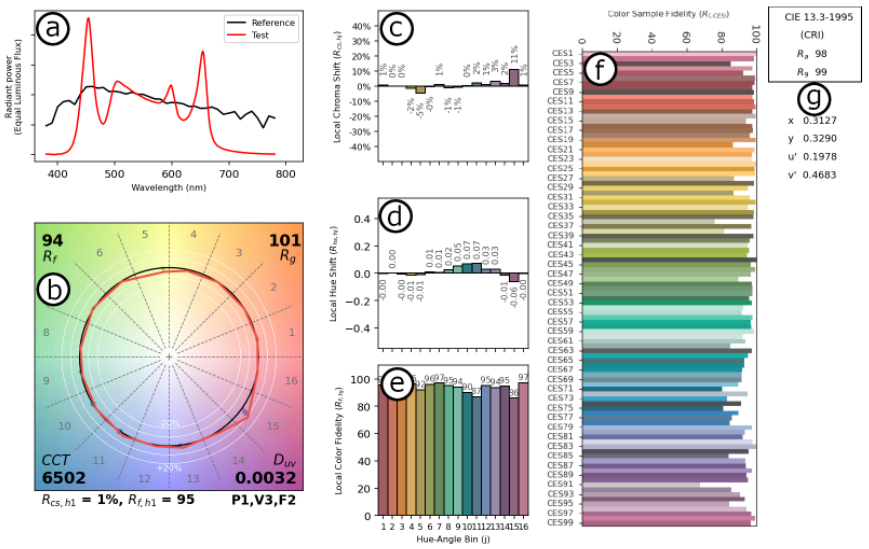

Figure 2.19: IES TM-30 report. (a) light source SPD and comparison to D65, (b) Color Vector Graphic, (c) Local Chroma Shifts, (d) Local Hue Shifts, (e) 16 Local Color Fidelity Bins, (f) 99 Color Sample Fidelity Values, (g) CRI and Chromaticity of the light.

IES TM30:

The TM-30-20, often simply called TM-30 is a measure for color rendering developed by the Illumination Engineering Society (IES). The calculation of TM-30 like previous metrics is based on the comparison of color rendering of samples under a test light and a reference light. The color sample set used is made of 99 samples selected from a set

of 100 000 object spectral reflectances in order to be representative and even sampling of all commonly found colors. The TM-30 returns a collection of values which describe different aspects of color rendering. Figure 2.19 shows an example of a full TM-30 report and details the values it returns. The most important value returned by the TM-30 is the Fidelity index noted R_f and was adopted by the CIE as the CIE R_f, it corresponds to a value between 0 and 100 calculated in the same way as the CRI but with the 99 colored samples. The second value is the Gamut Index noted R_g. It is calculated like the Gamut Area Index as a ratio of gamut between the text light and the reference light. The TM-30 also features local indexes that allow to quantify the color rendering specifically for different hues. The three local indexes are the local chroma shift, the local hue shift and the local color fidelity. Finally, the 99 samples are divided into 16 bins depending on their hue angle giving an average color rendering ability per hue region. This also allows to display the Color Vector Graphic which can be used to intuitively present the shape of the gamut and where the rendering differences are [29].

2.2.7 Instrumentation and measurement tools

In this work, to minimize potential errors arising from inconsistent measurement conditions, all data was collected using the same instruments and a standardized procedure. Moreover, all colorimetric computations were systematically based on the measured spectral power distribution (SPD). To do so, two different devices were used, a spectroradiometer to measure light sources and their properties and a spectrophotometer used to measure the reflectance and color of surfaces.

JETI spectraval 1511:

The spectroradiometer used in this study is the Spectraval 1511 manufactured by JETI (Figure 2.20). A spectroradiometer typically operates by dispersing light into its spectral components using a monochromator, either consisting of a prism or a grating. The different wavelengths are then diffracted onto an array of sensors. The spectraval 1511 uses a grating in order to measure light and near infrared from 360 nm to 1000 nm with a spectral resolution of 1 nm. Two modes are available depending on the type of head installed, either radiance or luminance mode and is therefore able to measure radiometric and photometric units. The specifications of the Spectraval 1511 are listed in Table 2.1.

Spectral range	350...1000 nm
Spectral resolution	5 nm (interpolated to 1nm)
Measuring range	0.2...140000cd/m^2

Table 2.1: Specifications of the JETI Spectraval 1511 spectrometer.

X-Rite i1Pro 3:

The spectrophotometer used in this work is the i1Pro 3 manufactured by X-Rite (Figure 2.21). A spectrophotometer operates on the same principle as a spectroradiometer, with a combination of a monochromator and a light sensor. The difference lies in the ability

Figure 2.20: JETI Spectraval 1511.

of spectrophotometer to measure non emissive surfaces by shining an integrated light on the colored sample. The i1Pro 3 uses a diffraction grating with a 128 pixel diode array to measure surfaces between 380nm and 730nm with a spectral resolution of 10nm with an integrated light producing the D50 illuminant. This spectrophotometer also features a screen calibration mode, which was used to calibrate screens during psychophysical experiments. The characteristics of the i1Pro 3 are listed in Table 2.2.

Spectral range	380...730 nm
Spectral resolution	10 nm
Measuring aperture	4.5mm
Measurement condition	D50

Table 2.2: Specifications of the X-Rite I1pro 3.

Figure 2.21: X-Rite i1Pro 3.

X-Rite Farnsworth-Munsell 100 Hue test:
This work centers on the evaluation of color discrimination under varying light conditions.

One of the useful tool, able to give insight on color discrimination capability on the full hue circle is the Farnsworth-Munsell 100 Hue Test. This test was used in previous psychophysical experiments with the goal of studying color discrimination under different light spectra [30, 31]. This test was used extensively during this work to quantify color discrimination. The test and its procedure will be further detailed in Subsection 3.1.2, however, it is useful to present here its characteristics. The test is composed of 85 color caps. The caps are made of a black shell allowing for ease of manipulation as well as protecting the color samples enclosed in the middle. The 85 caps are uniquely numbered. The colored caps are divided in 4 trays: red to green, green to blue, blue to purple, purple to red. The reflectance of the 85 samples is shown in Figure 2.22a and their chromaticity is displayed on Figure 2.22b.

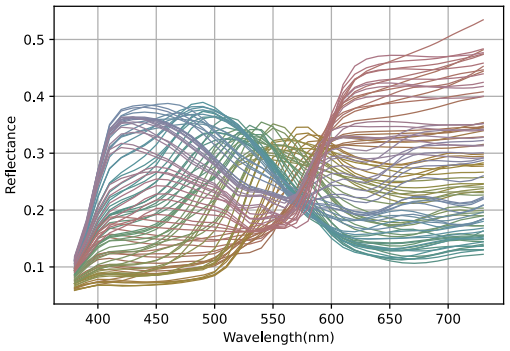

(a) Spectral reflectance of the 85 colored caps of the Farnsworth-Munsell 100 Hue Test

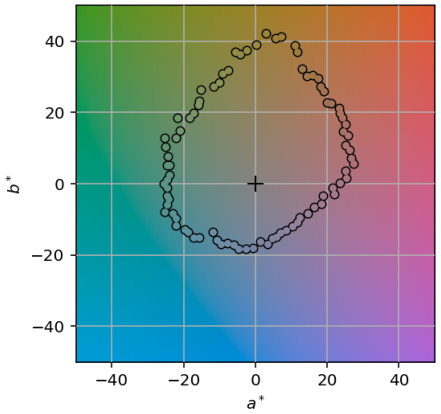

(b) Chromaticity of the 85 FM100 caps in the a^* b^* plane.

Figure 2.22: Characteristics of the Farnsworth-Munsell 100 Hue Test.

2.3 Experimental Environment Setup

To ensure complete control over the experimental conditions in the upcoming psychophysical experiments, the light booth used in this work was thoroughly characterized. This section will present the detailed documentation of its physical dimensions, the reflectance properties of its interior surfaces as well as the full spectral capabilities of the integrated LED panel. A special attention was given to the LED panel, which is central in this work and was subjected to a full characterization of its light output, taking into account temperature of the device and mapping the spatial distribution of the light. Finally, the attempt to produce a digital twin to the experimental environment will be explored.

Figure 2.23: The light booth used in this work.

2.3.1 Description of the light booth

Size	602 x 602 mm
Power consumption	$\sim$ 100 W
N° of channels	24 (365-940nm)
Max luminous output	$\sim$ 5000 lumen
Precision	250:1

Table 2.3: Specifications of the Telelumen Dittosizer Light Player.

The light booth is situated in the Imaging and eXtended Reality (IXR) platform in University Jean Monnet. It consists in a small room enclosed in 4 white rolling blinds with dimensions 2.5x2.5x2.5m (Figure 2.23). During the experiment the three walls facing the participant were closed, only the back one remained open for ease of access but was still covered with a black curtain to prevent light from the outside to interfere. The floor is light gray concrete and the ceiling is white painted wood. The chair used in every experiment is black and completely adjustable to any body sizes. The experiment table is placed exactly in the center of the booth just under the LED device. This allowed maximum illumination of the table as well as preventing any shadow cast by the participant on the experimentation area. The spectrally tunable LED system is a Dittosizer 24 light player produced by Telelumen (Figure 2.24). It features 24 individual channels from UV to infrared radiations, that can be individually varied in order to produce an immense variety of light spectra in the power limit of the power supply of the panel with a maximal

output of around 5000 Lumen with max input power of about 100W. The characteristics of the panel are listed in Table 2.3.

Figure 2.24: pThe Telelumen Dittosizer 24 light player.

2.3.2 Spectrally tunable LED system characterization

The light output of the spectrally tunable LED system can be precisely controlled by sending to the unit an array containing the desired drive level of each of the channels as a 10 bit float between 0 and 1, 1 representing the maximum output of the channel. This allowed us to measure the spectral output of the tunable LED system in various configurations in order to propose prediction models of the light output.

One of the main advantage of tunable LED light sources is that the total spectral output of a tunable LED panel $S(\lambda)$ is equal to the sum of the spectral output of the individual channels $S_i(\lambda)$. This means that in order to measure the full spectral range of the device, we can measure each channels independently. Equation 2.5 shows how to calculate the full spectrum of a tunable LED system from the measurement of a number L of individual channels.

$$S(\lambda) = \sum_{i=1}^{L} S_i(\lambda) \tag{2.5}$$

Measurement of the channels:

The first step of the characterization procedure was to measure all the channels at their maximum drive level. Out of 24 channels, only 19 were in the range of the JETI spectraval 1511, for this reason the 2 ultraviolet (UV) and 3 near-infrared (NIR) channels were excluded from the rest of this work. The results of these measures are shown on Figure 2.25. This allowed us to obtain the peak wavelength of the 19 channels, which are reported in Table 2.4. This first measurement allowed us to select the channels to use in psychophysical experiments. It was decided to only use 13 of the channels based on two

criteria: being completely inside the visible range and have a sufficient luminous flux. The final selection is marked in bold in Table 2.4.

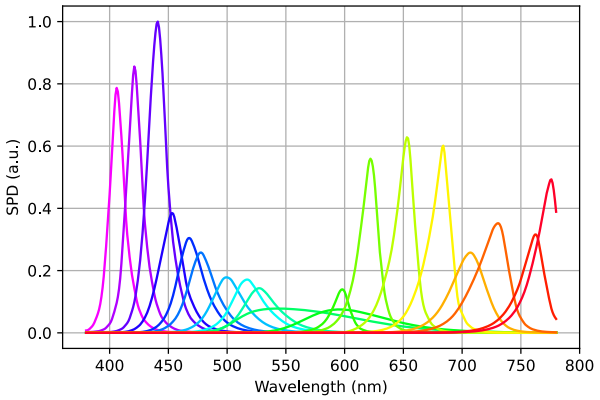

Figure 2.25: Spectral power distribution of the 19 LED channels close to the visible range of the Telelumen Dittosizer 24 lights player.

	V1	V2	**RB1**	**RB2**	**B1**	**B2**	**C**	**G1**	**G2**	**L**
Peak wavelength (nm)	406	421	**441**	**454**	**468**	**478**	**500**	**517**	**528**	**544**

	PC-A	**OR**	**R1**	**R2**	**DR1**	DR2	FR1	FR2	FR3
Peak wavelength (nm)	**594**	**624**	**636**	**654**	**686**	708	732	765	777

Table 2.4: Peak wavelengths of the 19 visible range channels with the 13 selected for the experiment highlighted in bold.

Taking temperature into consideration:

After measuring each channel at maximum power, it was attempted to measure the channels at different drive levels. However, after doing so, discrepancies were noticed in the measurements. This is due to the fact that LED devices exhibit fluctuations in output due to heat buildup during operation [32, 33, 34]. LEDs have been studied in order to model their behaviour as a function of their junction temperature. Chhajed et al. [35] measured the junction temperature of 4 types of LEDs and reviewed their optical properties at different temperatures. They showed that increasing the temperature of LEDs induced a noticeable difference in light rendering. However, with a device such as the one in this study, there is no way to measure the junction temperature of the individual LEDs. However, the Telelumen LED system is equipped with 4 temperature sensors placed at different position in the package. The readings of one of the sensors on the heat sink

of the panel will be used, not as a measurement of the junction temperature but a value correlated to it. The 13 channels were measured one by one at every percent of drive level while having the temperature sensor stabilized at readings from 30°C to 45°C. Figure 2.26 shows the flowchart for the procedure to measure at a stabilized temperature.

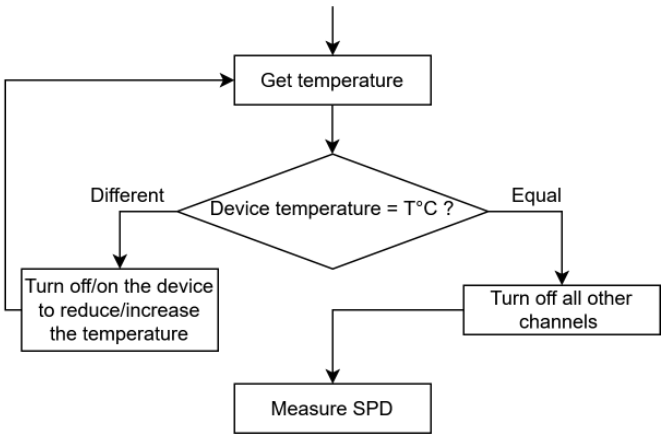

Figure 2.26: Flowchart of the characterization procedure. Image from Vernet et al. [2].

There are two major effects due to temperature on the light output of LEDs: a reduction of the amplitude of the peak of the SPD and a shift of the SPD toward the longer wavelengths. Moreover these effects are not as pronounced for every channels, increasing the color deviation of the light produced. Figure 2.27 shows the difference of SPD for the 13 channels when the device is cold and when it is at its maximum registered temperature, after one hour. The mitigation techniques developed to stabilize the LED light output will be described in Chapter 5.

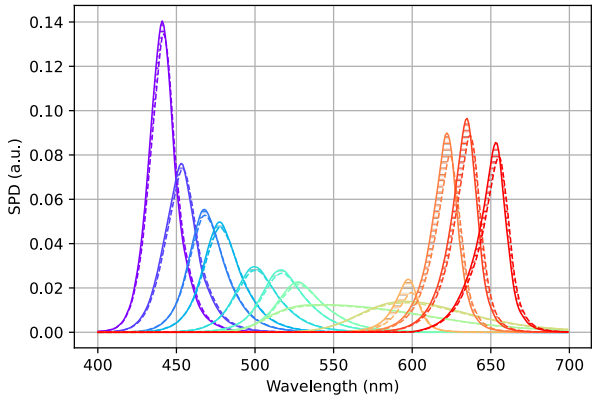

Figure 2.27: Difference of SPD after an hour.

Spatial characterization:

Finally, the last characterization step needed is the spatial distribution of light inside the light booth. The 13 channels were measured at their maximum power at different points in space under the LED system while being maintained at constant temperature. The main goal of this part is to check the maximum area where the light can be considered uniform. The light was measured in a 120×120cm grid with a regular spacing of 30cm between adjacent points along both axes at a height of about 1m over the ground, centered in the middle of the light booth as shown on Figure 2.28.

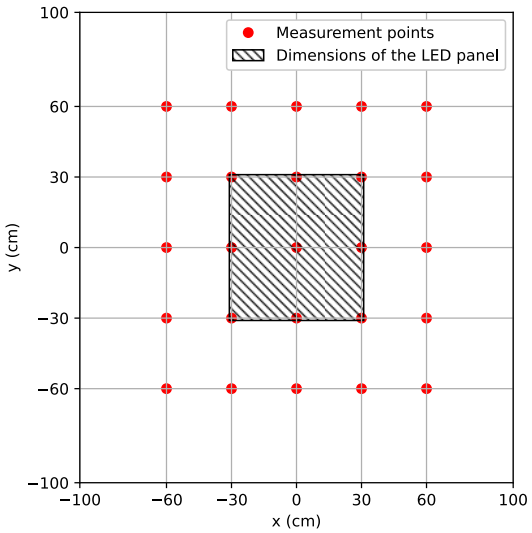

Figure 2.28: Measurement point locations inside the light booth.

Each one of the 13 channels were measured 3 times on each point of the grid and the average SPD was calculated. The center point of the grid served as a reference and the Mean Absolute Error (see Equation 2.6) between the SPDs measured at the other point of the grid compared to the reference was plotted.

$$MAE = \frac{1}{401} \sum_{\lambda=380}^{780} |ref(\lambda) - M(\lambda)| \tag{2.6}$$

with $ref(\lambda)$ the reference SPD measured in the center of the booth and $M(\lambda)$ the SPD measured at a different point in space.

Figure 2.29 shows such plots for channels 1 and 5 and the rest of the plots are available in Appendix A. These measures allow us to observe that there is a noticeable difference in light distribution between the channels: those with broader spectral bands distribute light more evenly, while narrower bands show a steeper decrease. Interestingly, we can also see that the light distribution forms a plateau in the center with a diameter of about 40 centimeter where the light can be considered uniform. This supports the idea that if psychophysical experiments are held right under the LED panel, the light can be considered

uniform and this gives a wide area to position the spectroradiometer to monitor the lighting condition on the experimental table.

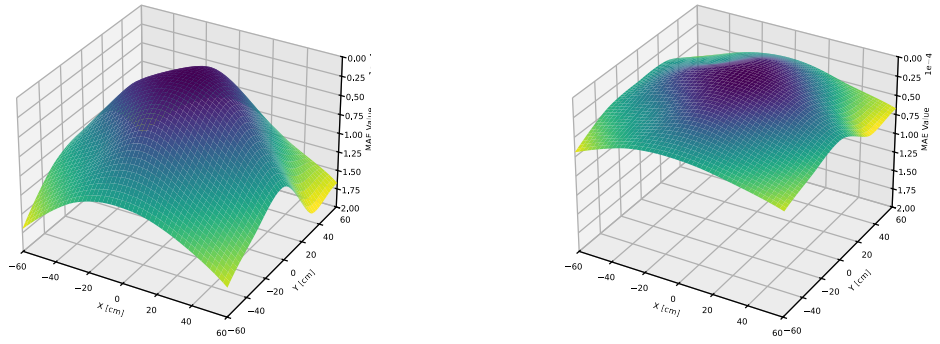

(a) Channel 1. (b) Channel 5.

Figure 2.29: Mean Average Error of the SPD compared to the center of the booth for channel 1 and 5.

2.3.3 Physically based simulation of the light booth

The detailed characterization of the light booth in all its aspects led us to develop a simulation of its environment in an effort to evaluate the possibility of creating a digital twin of possible psychophysical experiments and derive potential findings from simulation.

This was carried out using Mitsuba 3 [36], a research-oriented light simulation engine that uses ray tracing to render physically accurate 3D scenes. Unlike many other rendering engines, Mitsuba 3 supports not only RGB-based rendering but also full multispectral light simulation.

The light booth was faithfully recreated in Blender by modeling the environment to its exact dimensions as well as the various materials used for experiments (see Figure 2.30). In addition, the reflectance of each surface was measured with an i1Pro spectrophotometer to provide accurate data for simulating light interactions with the environment. Finally, the spectrally tunable LED system's behavior was faithfully simulated, and its output was precisely modeled using the previously described measurement data.

Mitsuba 3 allows for precise customization of the camera used to render images. While traditional rendering relies on three sensors (red, green, and blue) our goal of spectral imaging required to carefully configure parameters to ensure the most faithful image reconstruction. The spectral camera can be configured in terms of both spatial and wavelength resolution. For this work, an image resolution of 1920×1080 was selected to produce a high-quality representation of the booth interior. Through experimentation, it was determined that a 100 bands using Gaussian sensitivity as displayed in Figure 2.31 and fully covering the visible spectrum was optimal in order to obtain a simulation as accurate as possible.

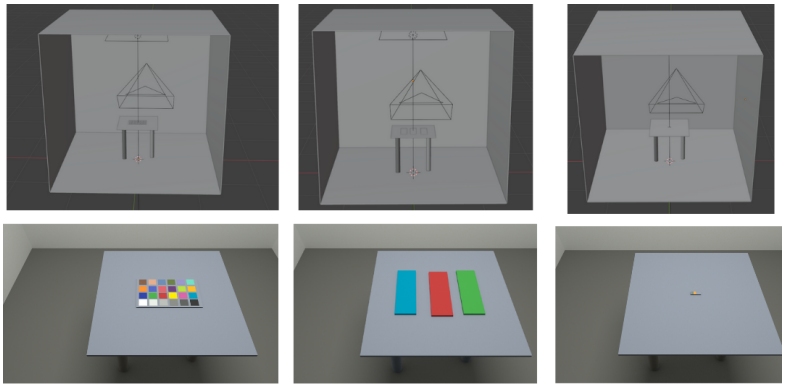

Figure 2.30: Simulation of the light booth in three configurations (top: Blender models, bottom: Render).

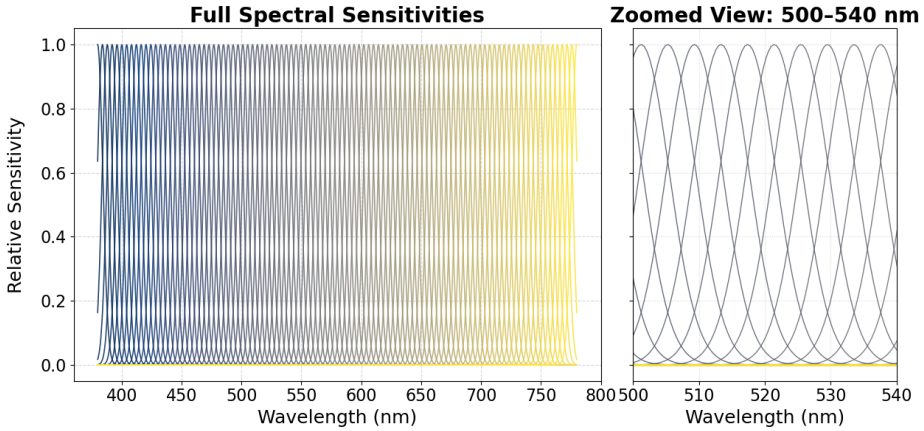

Figure 2.31: The camera's 100 Gaussian bands covering the visible spectrum.

Although the simulation is not able to produce an exact digital twin of the light booth, it nevertheless allowed to simulate different settings for the light booth. The simulation was tested with various lighting conditions and was compared to the ground truth measured inside the light booth, on the experiment table. Figure 2.32 shows the difference of SPD that was obtained when testing one of the light spectra considered. This particular example, although close visually, still featured a noticeable difference in chromaticity of the light spectrum with a $\Delta_{E,00} \approx 1$.

This work allowed us to explore the idea of simulating the experiments in order to identify possible biases induced by the light booth environment. More precisely, the inclusion of colored objects inside the light booth was studied in order to evaluate their influence on the lighting conditions. Figure 2.33 shows the difference induced by adding an orange wall facing the camera on the light spectrum measured. In this example, the difference in environment produces a noticeable chromaticity difference of the light received on the experiment table and further confirms the need for a neutral colored environment for

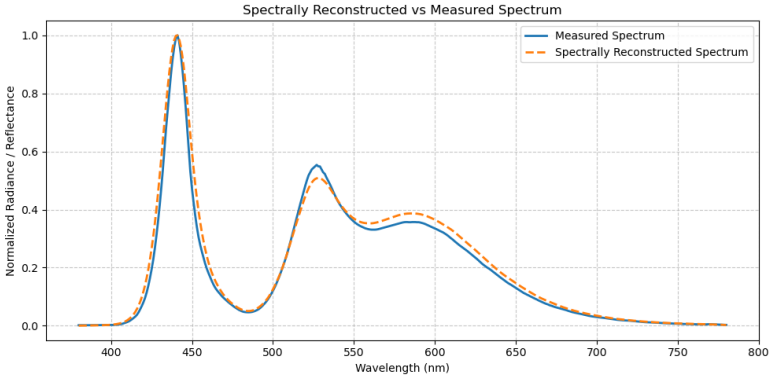

Figure 2.32: Comparison of the real and simulated light spectra.

experimentation. With further research, such simulations could be used to assess lighting performance and potential chromaticity shifts in more complex environments closer to those encountered in everyday life.

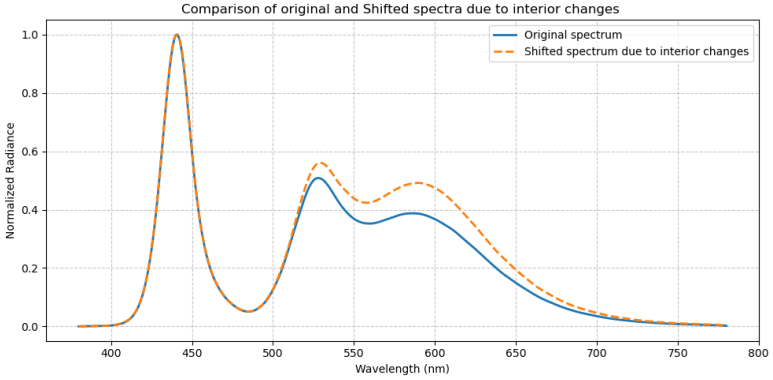

Figure 2.33: Simulated spectra with and without an orange wall.

2.4 Visual Impairment Simulation Tools

There are strict requirements for working with low vision people including safety and hazard assessment which make it difficult to perform experiments easily. Moreover there are important variations between people affected by low vision making it difficult to form a uniform and large panel of observers for the experiments. Therefore, it was decided to first use simulation methods before starting experimentation with real low vision patients. In this section, the selection of the simulation methods will be explained with starting with the attempt to use mixed reality (MR) headset to simulate low vision and the limitations that were found, then the simulation goggles that were used for the psychophysical experiments will be presented.

2.4.1 Mixed reality headset

Mixed reality headsets consist in virtual reality headset complemented with front facing cameras allowing for real time display of the environment in front of the wearer. Since this technology is more advanced than augmented reality (AR), the advantages of such a device are many, especially for supplementing the vision of the user. With advanced processing power, it is now possible to modify in real time the vision of someone wearing such a headset.

Thanks to these abilities, it is possible to consider using their capabilities to develop a simulation device for a wide range of low vision conditions. This idea was explored by Acevedo et al. [37] prior to the preparation of the experiments conducted in this thesis. Using a combination of a virtual reality (VR) headset and a stereo camera a low vision simulator was developed and able to simulate complex visual impairments. The simulated low vision conditions are the following:

- Cataract
- Myopia
- Astigmatism
- Age-related Macular Degeneration (AMD)

Visual impairments were simulated by applying specific alterations to the visual input. Blurry vision was reproduced using Gaussian filtering, as well as distance-dependent blur to reflect refractive errors. Color shifting was applied to emulate conditions such as cataracts, which affect color perception. Contrast loss was modeled by compressing the images lightness range, while glare discomfort was introduced through controlled glare enhancement. Finally, localized visual field loss was simulated using masking, localized Gaussian blurring, or spatial distortions. These alterations were done in real-time thanks to parallel computing as well as GPU calculation using CUDA as described by the pipelines of Figure 2.34.

Although the simulation tool described in this subsection is capable of reproducing complex visual impairments, several limitations render it unsuitable for the experiments in this thesis. First, the reliance on a stereo camera rather than the cameras integrated into the VR headset introduces unnecessary complexity, requiring additional devices and extensive calibration. More critically, since the objective of this thesis is to examine the influence of spectral light composition on color vision performance, the use of a three-primary display cannot faithfully reproduce the full range of colors present in real-world scenes.

2.4.2 Simulation goggles

Since the virtual reality headset proved to be inadequate for the type of psychophysical experiments needed in this work, it was decided to use commercially available simulation goggles. These goggles consist in a completely enclosed mount with opening for the eyes covered with special lens depending on the type of visual impairments they aim at

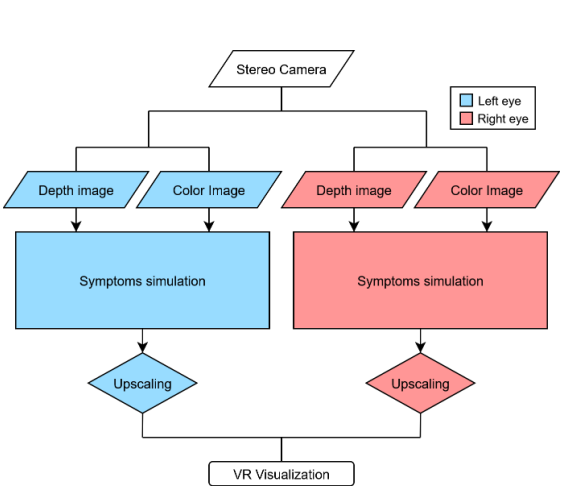

(a) Stereo vision pipeline.

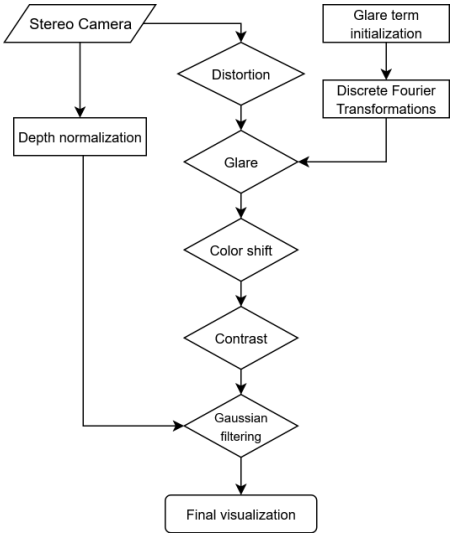

(b) Vision alteration pipeline.

Figure 2.34: Pipelines for the simulation of visual impairments using a stereo camera and a VR headset. Image from [37].

simulating. The goggles used throughout this work were manufactured by A Fork in the Road [38], it contains various low vision conditions including:

Figure 2.35: Simulation goggles used in this work (blurry vision top left, tunnel vision top right, central scotoma bottom)

- Blurry vision,
- Central scotoma,
- Tunnel vision,
- Diabetic retinopathy,
- Cataract,

- Hemianopsia.

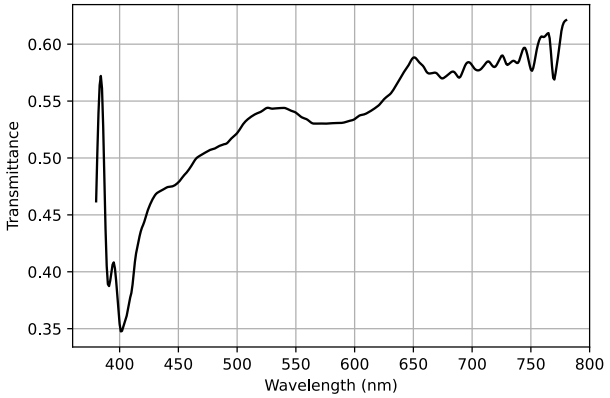

Figure 2.36: Transmittance of the blurry lenses of the low vision simulation goggles

In this study, we focused on three specific low vision conditions: blurry vision, central scotoma, and tunnel vision. The goggles simulating blurry vision were selected to represent a visual acuity of 20/400. Those designed to replicate central scotoma shared the same visual acuity as blurry vision simulation goggles but included an opaque plastic disk in the center of the lens, simulating a 10° field loss. Lastly, the tunnel vision goggles simulated a visual acuity of 20/80 and were mostly covered in opaque material, leaving only a 10°a central field unobstructed to replicate the experience of severe peripheral vision loss. The transmittance of the blurry parts of the goggles was measured with the JETI spectroradiometer and is plotted in Figure 2.36. We can observe that there is a significant absorbtion peak at 400 nm, however it falls outside of the range considered in this study since all the channels selected are contained in the range 441-686 nm.

There are several limitations to using simulation goggles for this kind of experiment. First, the lenses do not accurately replicate the transmittance characteristics of a visually impaired eye. Second, they reduce the amount of light reaching the retina. Finally, they cannot track eye movements, which is particularly problematic when studying localized visual impairments. However, despite these limitations, simulation goggles can provide a useful approximation of vision loss and serve as a starting point, as they enable a large panel of observers to experience the same visual impairment.

2.5 Chapter Summary

This chapter presented the fundamental background necessary to investigate LED lighting in relation to human visual performance. It began with a detailed description of the human visual system, presenting the structure and function of each component contributing to visual perception. Particular attention was given to color vision and its underlying mechanisms. The main causes of visual impairments were also discussed, highlighting the

challenges they pose both for affected individuals and for the design of the psychophysical experiments that were carried out in this work and will be presented in Chapters 4 and 6.

Since this thesis is centered around the study of color vision, it relies heavily on colorimetry. Therefore an introduction to the mathematical tools employed throughout this thesis was provided. The chapter covered the characterization of light through its spectral power distribution (SPD) and explained how perceptual colors are quantified and calculated from physical light spectra using the CIE 1931 XYZ color space. All relevant color spaces used throughout this work were presented, together with the transformations required to perform the conversion between them. The concept of color difference was introduced with its different iterations, and the CIEDE2000 ($\Delta_{E,00}$) metric was selected to be use in subsequent analyses due to its improved perceptual uniformity compared to the previous versions.

Significant emphasis was placed on light quality metrics developed to assess how lighting conditions influence visual performance, as these metrics are a key component in the study of lighting. Among these, the IES TM-30, and more specifically the report it produces, was adopted as the preferred approach to easily communicate the characteristics of light sources. The chapter also detailed the technical aspects of the tools for light and color measurement that were used throughout this work.

A major part of this chapter was dedicated to characterizing the experimental environment in which all subsequent experiments were conducted. Extensive measurements were carried out inside the lighting booth, including all surface properties and LED panel behavior across all channels, drive levels, and during extended time periods to assess thermal effects. The spatial uniformity analysis revealed that the LED panel provides a stable illuminated area of approximately 60 x 60 cm, a key factor in the design of the experiments presented in the following chapters. This complete characterization led to the simulation of the lighting booth using a light engine simulator, allowing virtual testing in different lighting configurations. Overall, this section established a rigorous methodology for controlling experimental lighting environments, leading to the development of a procedure that enables both the exhaustive exploration of the capabilities of a tunable LED panel and the implementation of a light stabilization algorithm for such systems that will be presented in Chapter 5.

Finally, this chapter addressed the simulation of low vision conditions. In this work, the decision was made to first investigate the influence of light under simulated low vision before generalizing the results to individuals with actual visual impairments. This approach allows to have a larger group of participants while ensuring uniformity of the simulated viewing conditions. Two main approaches were evaluated: mixed reality headsets and simple simulation goggles. While mixed reality offers promising flexibility and realism, current limitations, particularly in color accuracy and color range of displays, make it unsuitable for the present research. Consequently, simple simulation goggles were identified as the most practical solution for approximating low vision conditions in psychophysical experiments investigating the effects of spectral composition of light on visual performance.

The following chapter will introduce various methods developed to assess low vision, as well as the psychophysical procedures that can be employed to study visual perception under different conditions. These foundations will serve as the basis for designing experiments that evaluate lighting performance in the context of low vision, which is central to the

problem addressed in this thesis.

Chapter 3

Low vision Assessment, Aids and Lighting Research

Although vision is humanity's sharpest sense, it is also extremely fragile. Indeed, the many complex physiological interactions underlying human vision can easily be damaged by traumatic injuries, diseases or environmental factors. Visual impairments are particularly common, especially for the elderly, and are sometimes impossible or too severe to fully correct. The everyday life consequences for people affected are many, manual activity, reading, watching television, mobility and independence can be severely hindered. Therefore, low vision has been subject to extensive research in order to reduce the risk of vision loss as well as finding new medical procedures and low vision aids to alleviate visual impairments.

Low vision aids in particular have been receiving growing attention with the development of electronics and the new prospects offered by smartphones. Furthermore, the role of public infrastructure and the suitability of home settings have been increasingly recognized in supporting accessibility for individuals with visual impairments. More specifically, with the recent developments in solid state lighting, attention has focused on the importance of promoting appropriate lighting, both in terms of brightness and color rendering.

This chapter focuses on the current research on low vision rehabilitation, starting with a presentation of the main visual functions that are affected for low vision individuals and the corresponding tests commonly used to assess the severity of visual impairments. It then describes the available low vision aids, ranging from traditional optical solutions to newer developments such as advanced reality headsets, along with their respective advantages and limitations. Finally, the chapter introduces psychophysical experimentation and reviews recent developments in light optimization to enhance visual performance.

3.1 Assessment of Visual Functions

Accurately characterizing an individual's visual impairment is essential to provide personalized and suitable solutions in order to assist them in everyday tasks. low vision conditions affect the visual system and its functions in diverse ways, consequently optometrist and ophthalmologists have access to a range of tests developed to assess specific aspects of

visual performance.

In addition to low vision conditions affecting the clarity, sharpness or field of vision, color vision deficiencies are also common. While they are primarily associated with color blindness, aging and various low vision conditions have also been linked to alterations in color perception. A variety of color vision tests are available, each offering different levels of accuracy in assessing color vision performance.

This section focuses specifically on the tests used in the medical field to evaluate visual functions including visual acuity, visual field, contrast sensitivity as well as a special emphasis on color vision assessment, thus providing insight into the visual functions affected by low vision and outlines the essential considerations for assessing visual performance in psychophysical experiments.

3.1.1 Clinical tests for low vision assessment

Vision when unimpaired is our most sensitive sense, allowing us to perceive our surroundings in great details When this ability is impaired but not entirely lost, the condition is classified as low vision. The World Health Organization (WHO) defines low vision as moderate to severe visual impairment based on two primary visual functions: visual acuity, which describes the clarity and sharpness of central vision, and visual field, which represents the extent of the functional area of vision. Additionally, some have argued that contrast sensitivity should also be considered as a critical visual function in the definition of low vision [39].

Visual acuity:

Visual Acuity (VA) corresponds to the spatial resolution of the visual system. It is the ability of the human visual system to perceive small details and detect them as individual stimuli [40, 41]. However, this definition is not sufficiently specific and therefore the expression of visual acuity is test-dependent [42]. The expression of visual acuity varies depending on tests conducted and regional preferences, however the most common method compares the distance at which the tested visual system can see the finest details to the distance at which a normal visual system can see the same details. This forces the test to be performed at a set distance, however, it is possible to express visual acuity independently of distance by measuring the Minimal Angle of Resolution (MAR) which corresponds to the minute of arc of the finest detail the observer is able to discern. Equation 3.1 summarizes the different ways to express visual acuity.

$$VA = \frac{1}{MAR} = \frac{6}{D_{metre}} = \frac{20}{D_{feet}} \tag{3.1}$$

Various tests exist to measure visual acuity, but they all share a common principle. Characters or symbols, known as optotypes, are presented in different sizes, and the patient is asked to read or identify them from a set distance until they can no longer do so accurately. Since their introduction by Heinrich Küchler in 1843, different optotypes have been proposed, each with their strengths and weaknesses, accompanied by significant research on their size progression within visual acuity charts [43]. The following are notable tests used to assess visual acuity.

The most common type of test in the western countries are tests using Latin letters. Early visual acuity charts such as Snellen's or Monoyer's scales were extensively used since their introduction in the late XIXth century [44, 45]. Snellens visual acuity charts (Figure 3.1a) comprise eleven lines of letters, with the largest at the top. Each subsequent line contains more letters, decreasing in size following a geometric progression with a factor between 1.25 and 1.5 [43].

Snellen's charts have received some criticism over the years, pushing for newer and improved visual acuity charts. One of these criticism was the geometrical progression of the size reduction of letters which led to the development of many LogMAR charts such as the Bailey-Lovie charts or the Early Treatment Diabetic Retinopathy Study or ETDRS charts (Figure 3.1b) [46, 47]. These charts trade the geometrical progression with a logarithmic progression more fitting for human perception and improving the accuracy of the visual acuity assessment.

The last visual acuity test presented in this section is the Landolt C test [48] which consists in a series of broken rings or Cs of different sizes and orientations (Figure 3.1c). This test does not assume literacy and the patient only has to point out the direction of the opening of the ring. The size progression of Landolt's broken ring are also available in logarithmic scale. Although it became an ISO standard [49], reading charts are still extremely popular.

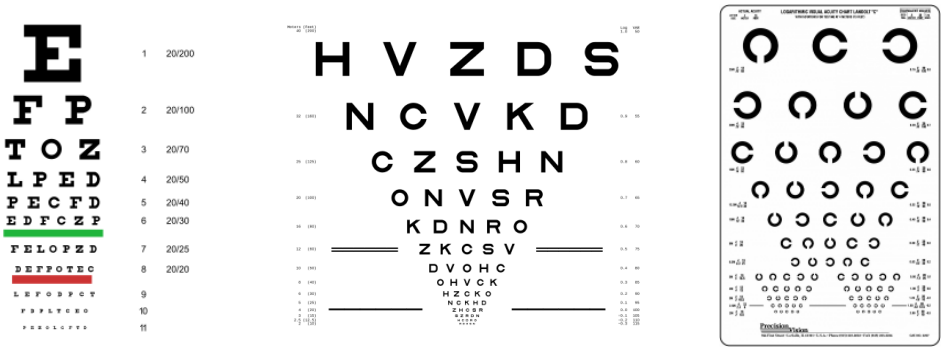

(a) Snellen chart. Image from [50].

(b) ETDRS chart. Image from [47].

(c) Landolt C chart. Image from [51].

Figure 3.1: Visual acuity assessment charts.

Visual field:

Visual field is defined as the portion of space visible without any movement from the eye. Normal visual field for a single eye consists in the central portion of 30°, 60° toward the nose and 100° in the opposite direction, 60° upward and 75° downward [52]. Visual field defects are diverse, and depending on the medical conditions affect by creating blind or blurry spots in different portions of the visual field. For example, glaucoma typically results in peripheral vision loss, macular degeneration affects the central portion of vision, and hemianopia involves the loss of vision in one-half of the visual field. The visual field is usually expressed in degrees representing the remaining field of view. The diversity of

visual field loss has led to the need of objective mapping of the regions and the development of perimetry.

The easiest method to quickly assess the extent of visual field loss is called Confrontation visual field testing. It is performed by having the patient with one eye covered stand in front of the examiner and stare at him in the eye and by moving his fingers in the field of view, the examiner can detect the portions that are still functional when the patient reports seeing the fingers. Although useful as a quick testing method, confrontation testing suffers from low sensitivity of the test for certain visual impairments and is therefore insufficient by only providing qualitative assessment of visual field loss [53, 54].

The first method to accurately measure visual field loss is the tangent screen method [55]. It consists in a 1 or 2m screen featuring a target, as shown in Figure 3.2 positioned in front of the examinee. The examiner then points to various areas of the target using a pointer to identify non-functional regions of the visual field [56]. The main limit of this method is that it is only able to measure the visual field in the central 30° degrees of the field of view.

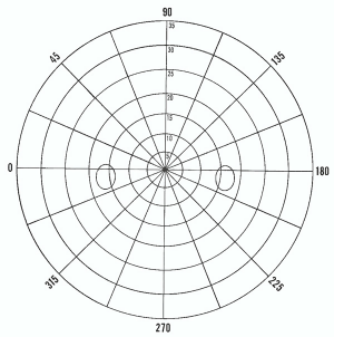

Figure 3.2: Target of the tangent screen. Image from [57].

A major improvement in visual field testing with the introduction of the Goldmann perimeter in 1945 [58], the device is shown in Figure 3.3a. It uses a hemispherical field uniformly illuminated, where a target can be projected statically of in movements in different sizes, luminance or colors [55]. Subsequent improvements automated the process using computers in the 1970s, with new perimeters such as the Octopus shown in Figure 3.3b.

Contrast sensitivity:

Even with good visual acuity and no visual field loss, some people can still suffer from visual impairment: age, high myopia or astigmatism can affect a third and distinct visual function, contrast sensitivity [39]. Contrast sensitivity is the ability of the visual system to detect differences in luminance between an object and its background [61].

There are two types of tests used to assess contrast sensitivity. First similar letter charts as the ones used for visual acuity are available but differ in the fact that letters gradually fade into the white background. The patients have to read the letters until they cannot discern the next one. These tests are available either using same-sized letters like the

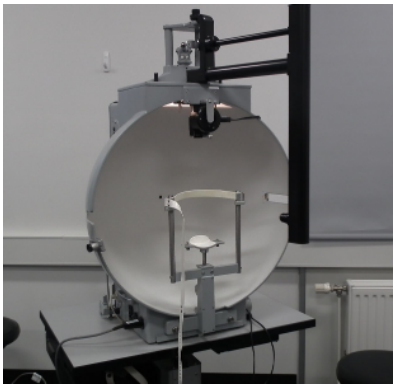

(a) A Goldmann perimeter. Image from [59].

(b) Octopus 900 perimeter. Image from [60].

Figure 3.3: Comparison between a Goldmann perimeter and a modern automatic perimeter.

Pelli-Robson charts (Figure 3.4a) [62] or different sizes like the Regan charts [63].

Other types of test use gratings with varying frequencies and orientations. The gratings can be sine waves like in Arden or Vistech (Figure 3.4b) tests or square waves like in the Cambridge low contrast test [61]. In this type of tests, the patients have to indicate the orientation of the gratings.

(a) Pelli-Robson chart. Image from [64].

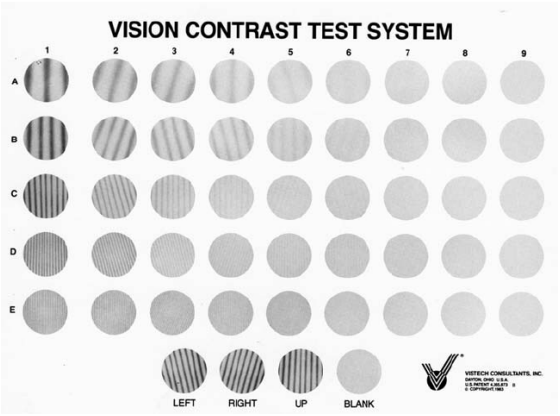

(b) Vistech VCTS 6500 chart. Image from [65].

Figure 3.4: Two types of contrast sensitivity test.

3.1.2 Color vision testing

Research on color vision relies extensively on psychophysical experiments, which often draw inspiration from established clinical tests used to evaluate color perception. These assessments focus primarily on color discrimination, the capacity of the visual system to differentiate between colors that are close in hue, saturation, or lightness. Since accurate

color discrimination is fundamental to many daily tasks, its evaluation provides valuable insight into both normal and impaired visual function. This section presents an overview of the most commonly used tests to assess this ability.

Pseudoisochromatic plates:

The most popular type of tests used to screen for color vision deficiencies are the pseudoisochromatic plates. Although many types exist, the principle remains similar: these plates consist in many small colored dots that form a figure, a number or a shape, hidden withing a background of dots in different hues and lightness levels. While individuals with normal color vision can easily distinguish the figures, those with certain color vision deficiencies may not see it at all or see something different. By exploiting how different types of color blindness affect the perception of certain colors, pseudoisochromatic plates provide a quick and effective way to identify and classify visual impairments.

The most well-known and commonly used pseudoisochromatic plate set are the Ishihara test plates created by Shinobu Ishihara in 1917 [66] which is designed to detect red-green color vision deficiency. The test consists in 38 plates (Figure 3.5a) in its full version, with shorter versions containing fewer plates. Each plate displays a number formed by dots of varying colors. Some plates are designed to be read by both individuals with normal color vision and those with color vision deficiency, others are unreadable for people with color vision deficiency, and a few are specifically designed to be readable only by individuals with such deficiencies [67].

Other types of plates have also been developed, for example the Hardy, Rand and Rittler (HRR) test which uses symbols in different corners of the square plate as shown in Figure 3.5b. Compared to the Ishihara plates, the HRR test is able to detect blue-yellow color deficiencies in addition to the red-green deficiencies [68].

In order to achieve the most accurate results possible, it is recommended to perform the test in a well lit environment and with a light with good color rendering performances [69].

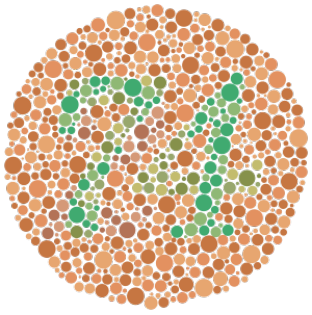

(a) Ishihara test plate. Image from [70].

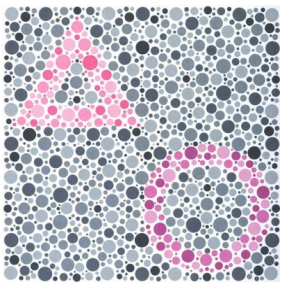

(b) HRR test plate. Image from [68].

Figure 3.5: Two types of pseudoisochromatic plates.

Arrangement Tests:

One of the main limitation of the use of pseudoisochromatic plates in the context of

(a) FM100 hue test. Image from [71].

(b) Farnsworth D-15 test. Image from [72].

Figure 3.6: Two arrangement tests for color vision deficiency.

psychophysical experimentation is their inability to assess numerically the severity of color vision deficiencies [67]. Arrangement tests on the other hand solve this issue by using a more complex task for the observer: arrangement of color caps in the right hue order.

The most widely used of these types of tests is the Farnsworth-Munsell 100 hue test [73]. The original test used 100 colored caps of different hues justifying its name, but the current test only features 85 different colored caps now. The Farnsworth-Munsell 100 Hue Test (FM100) is a color vision test generally used to screen for color blindness. The 85 color caps of the FM100 are arranged in four trays (Figure 3.6a). The observer's objective is to sort the caps in the correct hue order according to subtle color variations. Each cap is numbered from 1 to 85 with the number printed on its underside indicating its correct position in the sequence. The results of the FM100 test can be expressed as a numerical score, defined as follows. Let s_i represent the score for the cap at position i, obtained by summing the absolute differences between the index of the current cap and the indices of its two adjacent caps:

$$s_i = |n_i - n_{i-1}| + |n_i - n_{i+1}| \tag{3.2}$$

where n_i is the number of the cap at position i and n_{i-1} and n_{i+1} the numbers of the adjacent ones.

The partial scores of the Farnsworth-Munsell 100 hue test can be reported in a polar plot, an example is available in Figure 3.7. This type of plot can be interpreted by observing which hue regions have the highest values, corresponding to the greatest deviations from the correct hue sequence, i.e. the hues that were harder for the observer to discriminate. In this particular example provided, the highest error peaks are located in the yellow-red (YR) and blue-green (BG) regions which highlights significant difficulties in discriminating colors within these ranges of the hue spectrum.

A smaller variant using only 15 samples in one tray is available as the Farnsworth-Munsell D15. It is able to detect the most prevalent types of low vision including red-green and blue-yellow colorblindness. It is less precise than the Farnsworth-Munsell 100 hue test but is often used for occupational screening when good color vision is necessary [74].

Anomaloscope:

An anomaloscope (see Figure 3.8) is a specialized optical device used to diagnose and quantify color vision deficiencies. It works by presenting the observer with a split field: one half displays a fixed color (the test color), while the other shows a mixture of colors

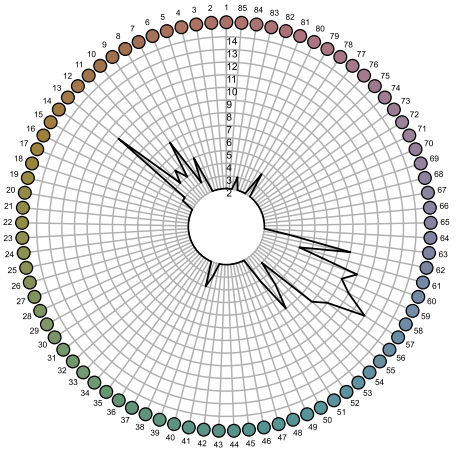

Figure 3.7: Polar representation of the scores derived from the Farnsworth-Munsell 100 Hue Test (FM100).

that can be varied. The user adjusts the ratio of the color mixture in order to match the test color. The mixture needed to match the color for the observer reveals the type and severity of the color vision deficiency.

Figure 3.8: An anomaloscope. Image from [75].

There are different types of matches available for anomaloscopes, nowadays the only two types still produced are the following:

- Rayleigh match: a yellow monochromatic test light at 589nm and two mixture lights red and green at respectively 545nm and 670nm. This type is used to detect red-green deficiencies [76].
- Moreland Match: a cyan-blue test light composed of lights at 480nm and 580nm, and blue and cyan mixture lights respectively at 436nm and 490nm. This type is used to detect blue-yellow deficiencies [77].

The anomaloscopes are considered the most precise way to quantify red-green and blue-yellow color deficiencies. However, they come at a high price and need special training to be used [67], limiting them to color vision studies.

Digital tests:

With the developments and increasing affordability of displays capable of faithful rendition of colors, many color vision tests have been developed to be performed digitally [78]. This has major advantages compared to the physical tests:

- Cost-effectiveness: digital tests are less expensive and are not subject to wear and deterioration over time.
- Time-efficiency: they can be completed without direct supervision by a practitioner, therefore saving time for both examiner and participant.
- Flexibility: they can be randomized and/or dynamically adapted based on the observer's responses, reducing the risk of memorization and enhancing accuracy.

Despite these advantages, digital color vision testing faces the challenge of ensuring standardized testing conditions, as variations in display characteristics and viewing environments may significantly affect results [79].

Some of the traditional tests have been ported to digital versions and validated to different degrees of success such as the Ishihara plates [80] or Farnsworth D-15 [81]. Other tests like the Cambridge colour test [82] were developed specifically to be performed on a computer. This test uses pseudoisochromatic plates featuring Landolt Cs as shown in Figure 3.9. The color difference between the motif and the background is dynamically adapted to estimate the discrimination thresholds [83]

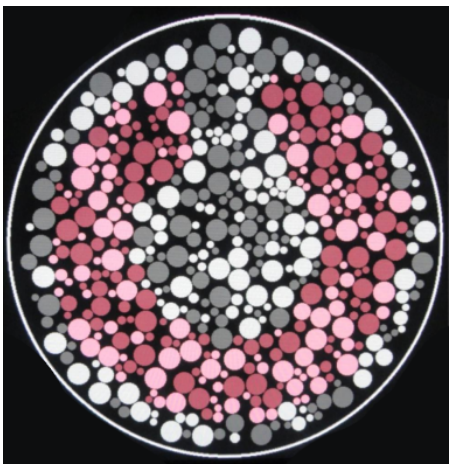

Figure 3.9: An example of Cambridge colour test plate. Image from [82].

Another approach is the Color Vision Assessment and Diagnosis which presents moving colored patterns on a neutral background. Participants have to identify the direction of these patterns, allowing the test to determine the smallest detectable color difference along specific color axes [84]. Example of patterns can be observed on Figure 3.10.

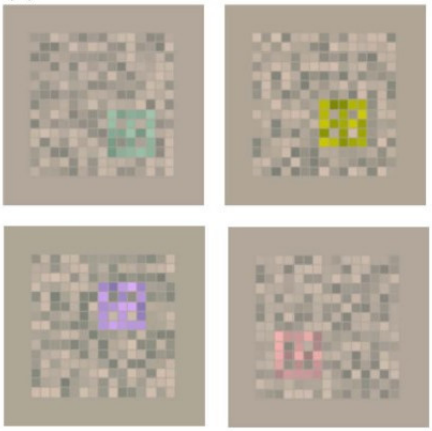

Figure 3.10: Example of patterns for the Color Vision Assessment and Diagnosis test.

3.2 Low Vision Aids and Assistive Technologies

A wide range of solutions exists to support individuals with low vision in their daily activities. Traditional approaches often involve training patients to make optimal use of their residual vision, maximizing their functional abilities. In recent years, however, advances in electronics have led to the development of innovative assistive technologies: from smartphones to virtual reality (VR) headsets, these devices have opened new possibilities for enhancing visual performance.

This section will first go over the traditional aids and training techniques that have been proposed to patients until now, before presenting some of the newer approaches and future prospects of low vision aids.

3.2.1 Optical aids

Optical aids encompass a wide range of tools designed to passively adjust incoming light through the means of an optical system. This type of low vision aids can enhance vision thanks to their refraction, magnification or field expansion effects. Optical aids for low vision are widely used due to their ease of manufacture, broad availability and practicality, as they generally require no electricity or external power.

Magnification tools are also a common aid available to low vision people in a variety of shapes. Simple hand magnifiers can be used and transported in order to improve reading at close range, while stand magnifiers can help for extended reading sessions. Similar functionality can also be achieved with high-powered glasses-mounted lenses improving practicality.

Telescopic systems are another common solution for individuals with low vision, enabling the magnification of objects at intermediate to long distances, at the cost of a reduced field of view. These can be monocular or binocular, feature manual or in more complex versions automatic focusing, and may be mounted directly onto eyeglass frames. They are useful for a variety of tasks, including outdoor navigation and watching television from a

distance.

Standard eyeglasses can also be adapted with additional optical components. Filters, for example, may be used to reduce glare or enhance contrast, while prisms can be incorporated to redirect light toward a functioning area of the retina in cases of reduced visual field. These adaptations allow for targeted improvements in visual performance, tailored to the specific needs of the user.

3.2.2 Non-optical aids

In addition to optical aids, everyday tasks can be facilitated for low vision individuals by adapting their environment to their needs. This includes enhanced contrast, increased size or tactile and auditory cues that can simplify the use of many objects that would otherwise be impractical to operate with magnification only.

This can be easily achieved first by increasing the size of text or symbols to allow for easier reading with residual vision [85]. There is a variety of objects adapted to use large-printed materials such as large print books, increased font for instruction labels or large-button telephones and computer keyboard.

Use of high contrast can be really beneficial in many situations. In a closed environment such as a kitchen high contrasted cutting board, or kitchen utensils can help locate and use them. High contrasted tracks can be used to guide low vision people indoor or outdoor, for example the Tenji blocks used in Japan (See Figure 3.11). Areas that need specific carefulness including stairs, crossings, train docks or doors can be contrasted against the background to help alert and locate them [86].

Using other senses can also help to facilitate many tasks. Some crosswalks are equipped with speakers to inform when it is safe to cross. Other devices like watches, calculators or kitchen timers are sometimes fitted with a speaker to be able to hear the readings.

Figure 3.11: Tenji blocks. Image from [87].

3.2.3 Mobility aids

The white cane is the most common and recognizable low vision aid aimed at improving mobility. It serves two main purposes: first allows visually impaired people to scan their surrounding while moving, second identifies them as visually impaired to the sighted people for them to watch out. It can come in multiple shapes and lengths depending on the

severity or specificities of the visual impairments. Although the long white cane is the most commonly used type, shorter or foldable variants are also available for greater convenience. Some canes are designed primarily for identification rather than mobility assistance, for example identification canes are shorter and lighter and are used by individuals with mild visual impairments to signal their condition to others. In the same idea, support canes exist in white color to have the dual purpose of supporting and identification as low vision person.

Guide dogs are highly trained service animals that assist individuals with severe visual impairments or blindness by helping them navigate their environment safely and independently. Unlike canes, guide dogs can actively avoid obstacles, indicate changes in elevation, and find specific locations such as doors or crossings. Their use is however rather limited, with only about twenty thousand dogs in service globally currently due to the cost and complexity of the training process.

3.2.4 Electronic and digital aids

With new advances in miniaturized electronics, display technologies, and software development, digital devices have been growing rapidly as a category of assistive technologies for low vision people. Unlike traditional optical and non-optical aids, these devices can combine image processing, magnification, contrast enhancement and text-to-speech functionalities in a single portable or stationary platform. Their main advantage lies in their adaptability, with customized settings fitting the user's preferences and specificities in vision capabilities.

One of the most common electronic solutions is the closed-circuit television (CCTV) system (Figure 3.12),in which a camera captures an image of reading material or an object and displays it on a screen with adjustable magnification and contrast. Modern CCTVs may be desktop-based with large monitors for extended reading, or portable and handheld for greater flexibility. Digital magnifiers, often in tablet or handheld form, offer similar functions with the added advantage of portability and battery-powered operation.

The main issue of specialized tools is their high price due to low production and can be difficult to use proficiently, leading to low usage by low vision patients. However, with the progression of smartphones, it becomes increasingly easier to have a device with cameras and high computation power, allowing many different applications for the low vision.

Nowadays, smartphones themselves are fitted with many accessibility settings, like font size customization, different color modes for the display such as color inversion or enhanced contrast, and text to speech to read any page displayed. This allows for easier use of the smartphones by low vision patients and through their daily use make familiarization to the device simpler.

One of the most common usage of smartphones by low vision patients is through the integrated camera, which even though it does not feature an optical zoom, still is useful with digital zoom to magnify details from both afar and close range [88]. Different apps have also been developed that use the computational power of the smartphones in order to use image processing for various tasks. Text to speech applications are available and are able to detect text in an image and read it out loud. Some smartphone applications have more specialized goals, for example counting physical currencies or detecting pedestrian crossing lights. Other apps are more generalist and allow to describe the environment

while filming it, with the help of volunteers or an AI model [89].

Figure 3.12: A collection of electronic and optical magnifiers. Image from [90].

3.2.5 Future directions in low vision aids

Thanks to developments in optics, electronics and computer science, the field of low vision rehabilitation continually evolving. Although traditional aids remain essential for low vision individuals, new solutions are being developed to enhance residual vision even further. This section will present ongoing research and prospects for the future of low vision aids.

Sensor-based solutions:

White canes are essential tools that enhance autonomy for individuals with visual impairments, however, they present several limitations, such as the inability to detect obstacles above cane level, moving objects within the users path, or irregularities in the ground surface. To address these issues, researchers have developed augmented canes equipped with a variety of sensors allowing the cane to emit alerts through sounds or vibrations. Cameras, in particular, have been extensively employed across numerous applications, especially with the rapid advancement of artificial intelligence models [91, 92]. In addition to cameras, ultrasonic [93, 94], infrared [95, 96], and light detection and ranging (LIDAR) sensors [97] have been integrated to improve obstacle detection accuracy, while ultra-wideband (UWB) radars [98] have also been investigated. In most cases, multiple sensors are combined in order to achieve more reliable and robust environmental perception. Other shapes have also been proposed for this type of aids including bracelets [99, 100], pendants [101] or waist belts [102, 103], with the aim of improving ergonomics.

Indoor environments present fewer dangers for visually impaired individuals, as their layout is generally more stable and predictable than outdoor settings. Therefore, numerous beacon-based mobility aids have been proposed to facilitate safe navigation . These systems typically rely on technologies such as Bluetooth Low Energy (BLE) [104], Radio Frequency Identification (RFID) [105], UWB [106] or Augmented Reality markers [107] to provide

location information and guidance. Objects can also be fitted with such beacons in order to identify them [108]

Head-mounted devices:

A major drawback of handheld aids is that they require one functional hand to be continuously occupied, which can limit usability in daily activities. To overcome this limitation, head-mounted devices have been proposed as an alternative. Such systems can function as head-up displays (HUDs) that superimpose information onto the visual field, or as image-processing devices that modify the visual scene to enhance residual vision. There are currently two forms of head-mounted devices that are actively being researched as solutions for low vision people: Mixed Reality (MR) headsets and smart glasses.

Augmented Reality headsets are partially or fully enclosed displays equipped with lenses and worn in front of the eyes. Unlike Virtual Reality (VR) headsets, AR devices use video feeds captured by forward-facing cameras to present the surrounding environment on the display. Real-time image processing can then be applied to enhance visual perception through techniques such as contrast adjustment [109], edge enhancement [110, 111], localized magnification [112], or text-to-speech conversion via integrated speakers. Additional functionalities, including face recognition and contextual information overlay [113], further expand their potential for supporting individuals with visual impairments.

Smart glasses, by contrast, closely resemble conventional eyeglasses and incorporate see-through displays capable of projecting information onto the lenses (Figure 3.13). Compared to AR headsets, they offer improved ergonomics through reduced weight and size; however, their image-processing capabilities are considerably more limited. Smart glasses typically function as head-up displays (HUDs), highlighting relevant details or obstacles [114, 115] and assisting with wayfinding [116] through integrated cameras.

Figure 3.13: Rayban meta smart glasses. Image from [117].

Vision language models:

The increasing accessibility to mobile high performance computing have also allowed vision language models (VLMs) to be considered for the aid of low vision people. These models are designed to interpret visual information in natural language, allowing to generate coherent textual or auditory descriptions of images, documents, or real world scenes. VLMs can perform complex reasoning tasks such as recognizing object, their disposition as well

as provide a contextual description of a scene. While they are increasingly integrated into smart glasses, their applications can extend to a wide range of devices such as smartphones. By using speakers or connected audio interfaces, devices using VLMs can provide real-time descriptive feedback, significantly enhancing accessibility for individuals with low vision [118, 119].

Implants and sensory substitution:

In addition to external aids, several surgical and implantable approaches are being investigated to rehabilitate vision in cases of severe visual impairment. Standard intraocular lenses, already widely used in cataract surgery, can correct refractive errors and improve visual function at the cost of reduced accommodation capabilities [120], while intraocular telescopic lenses are designed to magnify retinal images [121]. Retinal prostheses, including epiretinal and subretinal implants, attempt to restore visual perception by electrically stimulating surviving retinal cells [122]. Alternatively to retinal implants, strategies such as the BrainPort device have been developed, which transmit visual information through electrotactile stimulation of the top of the tongue, allowing sensory substitution [123].

Limitations of high-tech solutions:

Recent developments in low vision aids have been largely technology-driven, however, only a small fraction of proposed solutions ultimately reach widespread use. Cost remains the primary barrier [124], worsened by low adoption rates among potential users. Limited access to trained professionals further reduces the adoption of the more complex aids, as many individuals with low vision remain unaware of available aids or perceive them as overly difficult to use [125, 126]. Reliance on battery power also limits the practicality of these aids, as it reduces their autonomy, increases their weight, and often compromises user comfort. Head-mounted displays exemplify these issues: while technologically sophisticated, they are often cumbersome, expensive, and produce only modest improvements in quality of life [127]. Moreover some have pointed out that high-tech solutions are not preferred by low vision individuals compared to standard aids and that preference does not only rely on performance [128]. Societal stigma associated with aids too visible, along with the desire to avoid standing out, have also been cited as significant factors limiting the adoption of new assistive technologies [129, 130]. Similarly, surgical interventions, although offering the closest approximation to vision restoration, need highly specialized surgeons and carry elevated risks of postoperative complications [131].

3.3 Lighting for Low Vision and Optimization of Light

Lighting plays a critical role in the performance of the human visual system, influencing not only the clarity of visual perception but also comfort, eye fatigue, and safety in daily activities. This is particularly important for individuals with low vision, who often have access only to inadequate lighting conditions. Moreover, current lighting standards fail to adequately account for the specific needs of low vision individuals, highlighting the necessity for more inclusive guidelines that maximize accessibility and visual capabilities.

This section examines the current literature studying the ability of lighting to enhance the visual capabilities of individuals with low vision. It will begin by discussing the integration of lighting with conventional low vision aids, followed by an overview of the current general recommendations for lighting for the visually impaired. Next, attention will be given to existing methods for assessing color vision and the psychophysical techniques commonly employed in such research. Finally recent advances in the optimization of lighting will be reviewed in order to give insights on the possibilities it offers in the context of low vision.

3.3.1 Lights for low vision aids

Individuals suffering with low vision can often benefit from improved lighting conditions. To support their daily activities, they frequently rely lamps in various shapes. These may be stationary lamps placed at strategic locations in ones home, such as the kitchen for cooking or the couch for reading, or they can be portable, providing greater flexibility and illumination precisely where it is needed. Portable solutions such as flashlights further enhance accessibility and independence, while headlamps also allow for hands-free utilization. Lamps can be used either as standalone aids or in combination with other low vision devices. Moreover, certain assistive tools are equipped with integrated lighting to further enhance their effectiveness in supporting daily tasks. Examples include handheld and stand-mounted magnifiers, whether optical or electronic, as well as reading glasses fitted with built-in lamps to facilitate reading.

3.3.2 General lighting recommendations

The importance of lighting for ensuring both visual performance and visual comfort has led to the development of formal lighting standards. These standards primarily address workplace environments in order to promote visual efficiency, safety, and energy economy. Their specifications vary by geographical region: for example, EN 12464-1 [132] is applied within the European Union, while ANSI/IES RP-1 [133] was developed for the United States. The European standard provides task-dependent recommendations for minimum illuminance levels and emphasizes the importance of uniform light distribution. It also defines acceptable glare levels, sets maximum thresholds, and describes strategies for glare reduction. By contrast, the treatment of color is relatively limited, focusing mainly on correlated color temperature (CCT) classifications warm, intermediate, and cool, as summarized in Table 3.1. Recommendations for color rendering are expressed using the CIE Ra index, with a minimum CRI of 80 for general indoor environments and values above 90 for specialized applications such as medical examinations or color-critical inspection tasks.

In the context of residential indoor lighting, there are no formal standards, instead, guidance is provided through recommendations issued by organizations such as the Commission Internationale de l'Eclairage (CIE) and the Illuminating Engineering Society (IES). For example, the IES suggests target illuminance levels depending on the activity and space: approximately 100-200 lux for living and dining rooms, 200-500 lux for bathrooms and kitchens, and 500-1000 lux for areas dedicated to visually demanding tasks such as cooking

Colour appearance	CCT (K)
Warm	below 3300 K
Intermediate	3300 to 5300 K
Cool	above 5300 K

Table 3.1: Lamp colour appearance groups (EN 12464-1).

or reading. However, most homes fall short of these recommended lighting levels, which poses an even greater challenge for individuals with low vision, since existing standards and recommendations are typically based on assumptions of normal vision. Therefore, it has been suggested that people with low vision would benefit greatly from lighting standards for low vision as well customizable lighting solutions fitting specifically their visual needs to the tasks they perform [134, 135, 136].

The CIE 227:2017 report "Lighting for Older People and People with Visual Impairment in Buildings" [137] gives specific guidances for indoor lighting and environments in order to be adapted to the elderly as well as low vision people. It describes in detail the changes the visual system is subjected to with aging and visual impairments in order to provide guideline for designing lighting in buildings to be as inclusive as possible. The report highlights the need for illuminance to be adapted for the tasks performed, while providing strategies to limit glare discomfort. Moreover, special emphasis has been given on the importance of color contrast when designing interiors.

Although this report provides detailed recommendations for adapting lighting to the needs of people with low vision, significant gaps remain in understanding the specific effects of light on color vision. In particular, few studies offer precise guidance on the spectral composition of light or the impact of correlated color temperature on color discrimination. To address this, it is necessary to use experimental approaches that objectively measure visual performance under varying conditions. Psychophysical experimentation provides the methodology to investigate the impact of lighting on color vision, particularly in the context of low vision.

3.3.3 Psychophysical experiments in color vision research

To investigate human vision, it is essential to quantify the performance of the visual system under varying conditions. The focus of this thesis is the impact of lighting on color discrimination ability, therefore it is necessary to define the field of psychophysics, the scientific discipline studying the relationship between physical stimuli and the perceptions and sensations they provide, and present the methodological framework and techniques it proposes. The following section presents an overview of psychophysical experimentation as applied to color vision research [138].

Comparison-based methods:

Comparison-based methods are a simple way to study how people perceive color. These methods present two or more color stimuli simultaneously, and observers are asked to answer a forced-choice question. By analyzing these choices it is possible to gain insight

into how the colors are perceived and what is the detection threshold for the varying parameter.

Paired comparison is the most commonly used comparison method because its simplicity allows for fast and intuitive experiments. In this type of experiment, participants are presented with two stimuli and asked to make a choice, for example, selecting the one that appears lighter, more saturated, or differs in another perceptual aspect [139]. Alternatively, they can be asked whether the two stimuli are identical, which eliminates the need for the participant to understand the specific perceptual property being studied and helps reduce bias.

More complex designs involve three or more stimuli presented at once. In some cases, observers are asked to identify the odd one out, that is, the stimulus that differs from the others [140]. In other tasks, one stimulus is designated as a reference, and participants must decide which of the remaining samples matches it. These extended comparison tasks provide richer information about perceptual relationships and are especially useful for exploring subtle differences between stimuli.

Despite their usefulness, comparison-based methods present certain limitations and practical challenges that need to be taken into account when devising such an experiment. One major concern is the selection and design of the stimulus set: if stimuli are poorly chosen, clustered too closely, or unevenly distributed within the perceptual space, the resulting judgments may be biased or fail to capture meaningful differences. Another difficulty lies in the scalability of these methods. As the number of stimuli increases, the total number of possible comparisons grows rapidly, leading to excessive testing time, increased participant fatigue, and potentially reduced data reliability.

Scaling methods:

Another important class of psychophysical procedures is scaling methods. Unlike comparison-based methods, which rely on binary judgments, scaling methods require the observer to quantify their perception along a continuous or discrete scale. In this way, the observer does not simply state which stimulus is lighter or more saturated, but instead provides a graded response that reflects the magnitude of the perceptual attribute under study.

Several techniques exist to establish such scales. For example, in gray scaling methods, observers arrange or rate samples according to a perceptual parameter (for example color difference) by comparing them to a predefined series of gray samples. These gray samples are constructed with constant steps in lightness, providing a perceptual reference scale against which the stimuli can be evaluated [141, 142, 143].

Other approaches may use numerical rating scales, category judgments, or magnitude estimation [144], where observers freely assign values to indicate perceived intensity. These methods are especially useful to study more complex and subjective aspects such as preference or naturalness.

Finally, arrangement tasks such as the Farnsworth-Munsell 100 hue test also constitute a type of psychophysical scaling procedure, where the observers have to rank color chips in order of hues and provide precise information on color discrimination ability.

Color matching methods:

Color-matching procedures are another approach to psychophysical experimentation on color perception. In these tasks, the observer adjusts the parameters of one stimulus until it appears perceptually identical to a reference stimulus. The goal is to determine the specific parameter settings, for example intensity, chromaticity, or luminance, at which two stimuli are perceived as matching.

Color matching can be implemented using a forced-choice procedure. In this approach, several candidate stimuli are presented simultaneously, and the observer must select the one that most closely resembles the reference stimulus. This design simplifies the task for the observer, since it avoids the need for continuous adjustments, but it requires a more careful and systematic selection of the stimulus to ensure reliable results.

Color matching experiments can also be conducted using adjustment procedures [145]. In this approach, the observer directly manipulates the parameters of one stimulus until it perceptually matches the test stimulus. Adjustment methods provide a more precise and individualized measure of color equivalence, though they require a higher level of attention and consistency from the observer. Classic examples include the anomaloscope, used to assess color vision deficiencies, and the experiments of Guild and Wright, which led to the development of the CIE 1931 color space.

Another approach is to use cancellation methods, where the goal is not to match two stimuli but to nullify a specific perceptual property. In this type of experiment, an additional stimulus is adjusted or added until the targeted perceptual aspect is effectively canceled out, leaving the observer with a neutral or balanced stimuli. This technique has been widely used in color vision research, particularly in studies of opponent-color processing [146, 147].

The psychophysical methods described in this subsection provide different experiments that can be used to quantify visual performance under different conditions. In the context of studying lighting and its impact on color vision performance, these approaches can be adapted to optimize illumination, allowing us to design light conditions that can enhance visual performance, for example color discrimination. More specifically, the advanced customizability of LED lighting offers new opportunities to implement these findings, allowing for lighting solutions specifically designed to support individuals with low vision.

3.3.4 Optimizing light for visual performance

Light is responsible for our ability to see our environment and its spectral composition defines how well the visual system can perform. The rapid adoption of LED technology and its flexibility in spectral output have increased the interest in understanding spectral properties of light and its influence on human vision. This section provides an overview of the history and underlying principles of light-emitting diodes, followed by a presentation of research that takes advantage from the advanced customizability of LED lighting to optimize illumination, with a specific focus on applications in the context of low vision.

Light-emitting diodes, principle and development:

Electroluminescence is the property of certain materials to emit light when an electrical

current passes through them. The phenomenon was first observed in semiconductors in 1907 by Henry Joseph Round, who discovered that silicon carbide crystals emitted light when a voltage was applied to it. Two decades later, in 1927, Oleg Losev developed the first light-emitting diode (LED), also using silicon carbide. However, no practical application was found at the time due to the materials low light-emission efficiency.

As illustrated in Figure 3.14a, an LED consists of two main leads: the anvil and the post, connected to the anode and cathode, respectively. The anvil also serves as a support for the semiconductor die, which is mounted on a reflective cavity designed to direct the emitted light outward. The semiconductor die itself is composed of two regions: the n-type region, which contains free electrons, and the p-type region, which contains mobile electron holes. When a voltage is applied, electrons from the n-region migrate to fill holes in the p-region, allowing current to flow in only one direction, forming the basic principle of all diodes. In light emitting diodes, the materials are specifically selected so the holes have a lower energy than the electrons in the n-region, forcing the electrons to release excess energy through emission of a photon. This process is summarized in Figure 3.14b. The wavelength of the light emitted depends on the band gap energy of the materials selected.

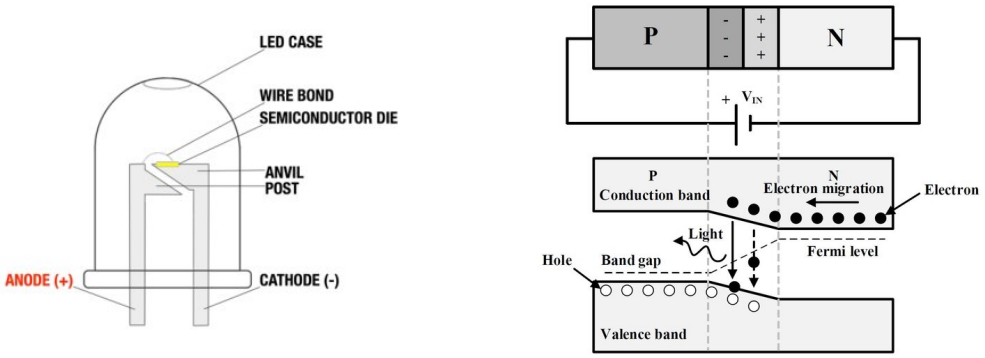

(a) Schema of a basic LED. Image from [148]. (b) Light emitting diode principle. Image from [149].

Figure 3.14: LED structure and principle.

During the 1960s, significant progress was made in developing LEDs through the use of new semiconductor materials, which enhanced both efficiency and brightness, while advances in manufacturing techniques helped reduce costs. By the late 1960s, LEDs began replacing incandescent bulbs as indicator lights and Nixie tubes in digital displays. Early LEDs could emit light from the near-infrared to the yellow region of the spectrum [150]. However, despite rapid improvements in brightness, their use in general lighting remained unfeasible due to the absence of high-performance LEDs capable of emitting in the blue region of visible light.

The first blue LEDs were developed in the 1970s, but their extremely low efficiency restricted their use for example for digital displays. A major breakthrough came in 1993, when Shuji Nakamura created the first high-brightness blue LED, leading the way to practical lighting applications. This advancement enabled the production of white LED lamps. Although it can be achieved by combining red, green, and blue LEDs, it is done

more efficiently and with better color rendering by pairing a bright blue LED with a phosphor coating that converts part of the emission into green and red light through fluorescence [151]. Thanks to important energy efficiency and lifetime as well as rapid progress in both brightness and color rendering, LED lighting has almost entirely replaced incandescent and fluorescent lamps in a wide range of applications [152, 153].

LEDs have become the main source of light for many applications including residential lighting, automotive systems, and advanced display technologies such as MicroLED. In the context of home lighting, continuous improvements in brightness, color rendering, and affordability have made high-quality lighting solutions widely accessible. More recently, the customizability of lighting has become mainstream, with tunable bulbs offering adjustable color temperatures or even fully customizable light colors, providing users with greater control over their lighting environments. For professional and research purposes, tunable LED panels have further enabled precise color management and more accurate investigations into the effects of lighting [154].

Optimization of LED lighting:

Thanks to the newly available customizability offered by LED lighting, it is possible to design an infinite number of spectra with vastly different characteristics, making it possible to consider optimizing the light to improve visual performances, more particularly in the context of low vision.

The optimization of LED lamps with respect to their color-rendering characteristics has been extensively explored with the hypothesis of normal vision. Color rendering metrics provide an easy way to evaluate the performances of a light and are therefore commonly used as cost functions to derive theoretically optimal spectra according to a specific characteristic. For white LEDs, optimization can be achieved with improved composition of the die and different types of phosphor coatings which allows to produce different spectral properties: He et al. developed white LEDs featuring red, green and blue phosphors to achieve high CRI [155], while Xiao et al. proposed a white LED with green and orange phosphors to improve the CIE R_f for road lighting applications [156]. Another approach takes advantage of the ease of integrating multiple LEDs within a single package, allowing the spectral output of the lamp to be customized through the use of multiple independently controlled channels. This method has been used extensively to achieve high CRI LED lamps, for example He et al. proposed the addition of a red LED to a white phosphor coated LED to achieve good color rendering [157]. Advanced LED lamps and tunable panel allow for even more control with multiple individual and have been used to design light spectra maximizing specific metrics, Zhang et al. developed a method based on a genetic algorithm to achieve light spectra with high CRI, CQS as well as Luminous Efficacy of Radiation (LER) [158]. In addition, specialized indices have been considered for specific applications such as the Cyanosis Observation Index (COI) for clinical settings [159] or the Melanopic Efficacy of Luminous Radiation (MELR) by Saw et al. [160] or the Circadian Action Factor (CAF) by Zheng et al. [161].

Although color rendering metrics are useful tools to efficiently quantify and communicate the properties of different light sources, they were only designed taking into account normal vision, Furthermore, they do not always correlate with actual visual performance,

particularly in the case of spectra produced by LED lighting [24]. Therefore, despite being more time consuming, psychophysical experiments are essential either as an optimization method or as a mean of validating results with real observers. Such experiments are particularly valuable when the studied property is not easily described by quantitative measures, for example the perceived naturalness of a scene, lighting preference or the subjective colorfulness of an environment [162]. Furthermore, in the context of non-standard vision, psychophysical experimentation becomes particularly important, as existing models and light quality metrics generally fail to capture the specificities of such visual conditions. Consequently, efforts have been made to design lighting solutions that go further than faithful color rendering and instead aim to enhance the visual capabilities of individuals with non-standard vision. Flinkman et al. have proposed light spectra that successfully enhance color discrimination for people affected by red-green color vision deficiency [163]. Similarly, people with low vision could benefit from lighting specifically adapted to different types of visual impairments. While the impact on color perception is typically less pronounced than in the case of colorblindness, many visual impairments significantly alter perception and affect color vision [164, 165]. Moreover, aging itself exerts a noticeable influence on color vision performance, further emphasizing the importance of adaptive lighting solutions [166]. These advances in optimizing lighting have been achieved not by relying solely on traditional metrics, but by implementing precise, targeted experiments that directly measure visual performance under controlled conditions.

Different approaches have been proposed in order to experiment on the ability of light to improve visual performances of low vision individuals. Katemake et al. [167] conducted a series of psychophysical experiments, including obstacle course navigation and practical tasks such as kitchen activities under varying lighting conditions. Their findings demonstrated that appropriate lighting can significantly enhance everyday activities by improving color contrast, optimizing light positioning for precision tasks, and incorporating features such as illuminated edges. They however found that in the context of mobility, the variations in illumination levels and correlated color temperature tested in the experiment did not show significant influence. Wolffsogn et al. [168] similarly concluded that correlated color temperature (CCT) has no significant influence on reading performances. However, color and illuminance alone are insufficient to fully characterize the diversity of spectra that can be produced. Consequently, efforts have been made to study light directly in terms of its spectral composition. Some aids have been proposed, taking advantage of the ability of LED device to output a completely customized light, such as the multispectral light reading aid proposed by Ramane et al. [169]. Yang et al. [170] proposed a LED-based lighting approach to assist individuals with specific visual impairments. Through psychophysical experiments using a multispectral lighting system, they demonstrated that tailored spectral mixes can significantly improve color perception compared to standard white LEDs.

3.4 Chapter Summary

This chapter focused on presenting the available methods used to study low vision. It began with an overview of the clinical tests commonly employed to detect visual impairments and assess their severity. Three major visual functions, visual acuity, visual field, and

contrast sensitivity were described, along with the most common tests used to evaluate each of them. This provided an understanding of how visual impairments affect vision and illustrated the types of procedures required for their study.

Particular attention was given to tests evaluating color vision, as they are especially relevant to this work. These tests are not only widely used in clinical settings but are also often used in psychophysical experiments, including those investigating the influence of color vision performance. Special emphasis was placed on the Farnsworth-Munsell 100 Hue Test, which is a standard clinical tool but has also been used in lighting studies. This test is of major importance to this thesis and a modified version of it will be presented in Chapter 4.

A significant portion of this chapter was focused on the existing assistive technologies and aids for individuals with low vision. Traditional aids such as canes and magnifying glasses were introduced, followed by the different environmental adaptations that can be made to make spaces more accessible and navigable. A presentation was also made on more recent developments include electronic and digital aids, which offer greater flexibility and adaptability to the specific needs of the user and environmental conditions. The use of smartphones as visual aids was also described, illustrating how widely available technology can support accessibility.

Additionally, several research prototypes were presented, including systems based on LIDAR or ultrasonic sensors that can detect obstacles and alert users through auditory or tactile feedback. Among emerging technologies, Augmented Reality (AR) headsets and smart glasses have attracted a lot of attention, as they can integrate advanced computer vision and AI models to dynamically enhance contrast, highlight important visual features, and adapt to individual visual impairments.

The chapter also highlighted the limitations and challenges associated with current aids, which range from high cost and lack of comfort to dependence on battery life and reticence of some users to use devices that make their condition visible of fear of standing out. However, one of the main advantage of these advanced solutions is the ability to enhance contrast in order to improve visibility which cannot be achieved using passive optical aids only. This reinforces the idea that optimizing light to enhance color contrast by using optimized spectral characteristics would be promising approach to improve scene visibility without the need for specialized interior or wearable devices.

Then, the chapter examined existing recommendations and research on lighting for people with low vision. It was shown that there are major gaps in most standards and guidelines, as they primarily take into account luminance levels for different visual tasks but neglect other characteristics such as color temperature, color rendering, and spectral distribution. Moreover, conventional light quality metrics, such as the CRI, are based on the standard observer model which does not take into account the perceptual characteristics of low vision individuals.

Although some studies have attempted to optimize lighting conditions to improve visual performance, most have been conducted for normal vision with the aim to maximize different light quality metrics. Very few investigations have specifically addressed the needs of low vision individuals or explored how variations in the spectral content of light influence their color perception and discrimination abilities [167, 170].

For this reason, the following chapter presents the first psychophysical experiment of

this thesis which designed to investigate how light wavelength affects color discrimination depending on the type of low vision. This experiment will establish a basis for a better understanding of how lighting can be optimized to improve visual performance for people with low vision.

Chapter 4

Color Discrimination under Monochromatic LEDs in Simulated Low-Vision Conditions

This chapter presents the initial phase of a series of experiments that aim at optimizing the white light spectrum for visually impaired people. This initial phase is focused on evaluating the influence of monochromatic LED light on color perception in a low vision context with the goal to determine the minimal number of LED channels required to produce white light that enhances color discrimination. To this end, the experimental protocol leverages the additive properties of light which allow the optimization of a white light source by mixing different spectral bands [171, 172, 173]

A detailed overview of the preparatory stages for this work is provided in Section "Experimental setup". The psychophysical experiment carried out to collect data is then detailed in Section "Psychophysical Experiment Based on the Farnsworth-Munsell 100 Hue Test", emphasizing the requirements to deal with. Section "Automatic Score Calculation" outlines the solutions developed to address the experimental challenges. The collected data are analyzed and the key trends derived from the results are discussed in Section "Results". Finally, the outcomes of these first investigations will be analyzed.

4.1 Psychophysical Experiment Based on the Farnsworth-Munsell 100 Hue Test

The psychophysical experiment was designed to obtain as much information as possible on color discrimination under different colored lights within a simulated low vision context. To this end, participants were asked to sort color samples under different and carefully controlled lighting setups.

4.1.1 Experimental setup

The psychophysical experiment presented in this chapter was carried out in a 2.5 x 2.5 x 2.5 meter light booth in order to precisely control lighting conditions. The illumination was provided by a a spectrally tunable LED panel, the Dittosizer Light Player from Telelumen that was fully characterized in Chapter 2. Their settings were then adjusted to meet the needs of the study [2]. Special care was also taken in preparing the light booth and its installed equipment. The viewing area consisted in a 1 x 1 meter wide experiment table covered in neutral gray cardboard. While the position of the participant was not fixed in one place due to the duration of the experiment, the viewing distance is approximately 30 cm.

Characterization of the channels highlighted significant variations in illuminance on the experimental table when they were all set at their maximum drive levels. Since the experiment focuses on the influence of SPD on color discrimination, it was essential to standardize illuminance across all 13 channels in order to ensure that any difference in perception could be attributed to wavelength effects rather than illuminance variations. To achieve this, the weakest channel was used as the baseline and all other channels were adjusted to match its illuminance [2]. This weakest channel corresponds to the bluest one (RB1 in Table 2.4 that was provided in Chapter 2) and it provided 80 lux on the surface of the experimental table. Such an illuminance of 80 lux aligns with the CIE guidelines for minimum required visibility while ensuring controlled and unbiased experimental conditions for studying wavelength effects on color discrimination [137]. This setup balances practical visibility requirements with the need for spectral consistency in the study.

As illustrated by Figure 4.1, participants were monitored with a ZED Mini stereo camera during each session. In addition, a Canon EOS 5D Mark IV was placed in a corner of the light booth to record the final positions of the color samples on the table at the end of the experiment. Finally, two computers were used to control the different equipment, one for the two cameras and one to manage the lighting system.

4.1.2 Color sample selection

Three standard sets of color samples are commonly and widely used in psychophysical experiments: the Munsell Color System (MCS), the Natural Color System (NCS) and the Farnsworth Munsell 100 Hue Test (FM100).

In order to have a complete hue circle for a sorting task, color samples from both the MCS and NCS can be selected with a fixed lightness and chroma. To meet such a constraint, MCS samples should have a value of 6 and a chroma of 6 while NCS samples should be chosen with 20% blackness and 50% chromaticness. These criteria yield 40 distinct samples in each set. By design, the FM100 forms a full hue circle and comprises 85 color caps.

To identify the most suitable set of color samples, we analyzed the ΔE_{00} color difference between consecutive samples in each set. As shown in Figures 4.2, 4.3 and 4.4, the FM100 caps have both lower and more consistent ΔE_{00} values across the hue circle. Based on these results, the FM100 was selected as the optimal set for our study. In addition, the FM100 offers several practical advantages. Colors samples are encased in a black hard

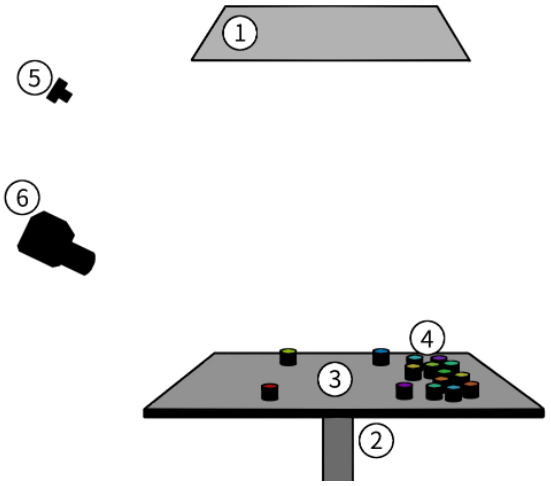

Figure 4.1: Setup in the light booth : (1) Telelumen multispectral LED panel, (2) Neutral gray experimental table, (3) Four references samples, (4) Samples to sort, (5) ZED Mini stereo camera, (6) Canon EOS 5D Mark IV camera

plastic shell which not only makes them easier to handle but also protects colored surfaces from direct finger contacts, helping to preserve their spectral reflectance characteristics. This contrasts with the more fragile and less ergonomic formats of the MCS and NCS paper samples. Moreover, the FM100 includes 85 different color caps providing a greater flexibility in selecting a subset tailored to our specific experimental requirements.

The color caps selected have a visual angle of XXX at the typical distance for this experiment. Moreover, for all types of simulated visual impairment used in this experiment, multiple samples can be viewed at the same time.

4.1.3 Experimental requirements

The goal of the experiment is to map the color discrimination ability of participants wearing different types of low vision simulation goggles under the 13 selected spectral channels of the LED panel. Although the FM100 is supposed to be performed under a standard illuminant (typically D65 or D50), previous studies have also used it under colored lights to assess color discrimination for unusual illumination conditions [174]. This supports our decision to select the FM100 instead of the MCS and the NCS for the reasons outlined above. However, several adaptations are required. First, the standard FM100 is a time-consuming procedure. Given that our psychophysical experiment needs as many participants as possible to be relevant, the number of color samples had to be reduced to make the task achievable. Moreover, since the lights used in the experiment are nearly monochromatic, participants may confuse colors located on opposite sides of the hue circle. To address this, the original arrangement of color caps in four separate trays was replaced by a single square layout containing all the color samples. Four reference caps were placed at the corners of this layout to guide the sorting task (see Figure 4.8).

To balance accuracy with a reasonable experiment duration, the number of color samples

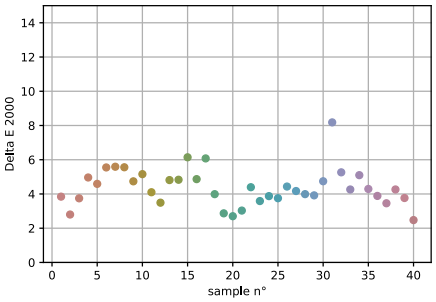

Figure 4.2: ΔE_{00} under illuminant D65 between consecutive samples of the MCS with a value of 6 and a chroma of 6.

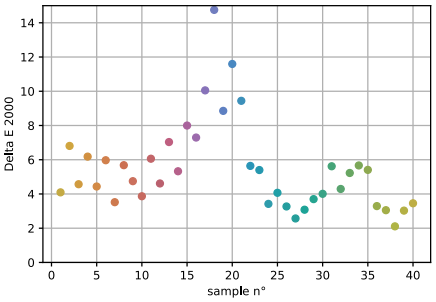

Figure 4.3: ΔE_{00} under illuminant D65 between consecutive samples of the NCS with 20% blackness and 50% chromaticness.

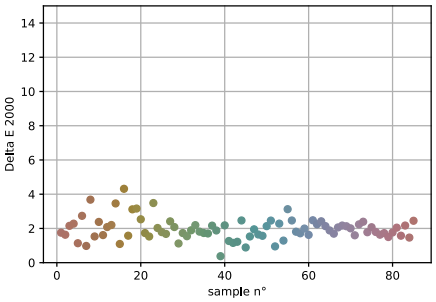

Figure 4.4: ΔE_{00} under illuminant D65 between consecutive samples of the FM100.

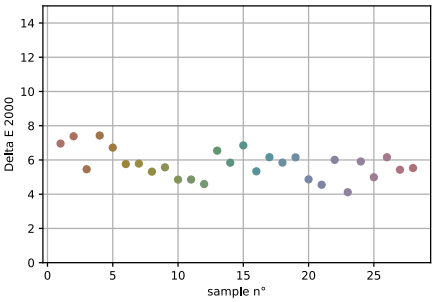

Figure 4.5: ΔE_{00} under illuminant D65 between consecutive samples of the subset selected from the original FM100.

was reduced by approximately two-thirds. A selected subset of 28 caps was chosen to maintain minimal variability in color differences between consecutive samples as shown in Figure 4.5. The ΔE_{00} values for this subset have an average of 5.7 with a variance of 0.7, ensuring both consistency and perceptual relevance in line with our experimental requirements.

4.1.4 Experimental protocol

The psychophysical experiment was divided into two sessions, each lasting approximately one hour. Depending on individual preferences and availability, the sessions could be scheduled either consecutively or on separate days. All participants were volunteers with normal or corrected-to-normal vision. Upon arrival, each person received an information sheet presenting the general purpose of the experiment, warning the use of colored lights and providing details regarding the nature of the data being collected. After reviewing this information and after asking any necessary questions, volunteers were free to decline

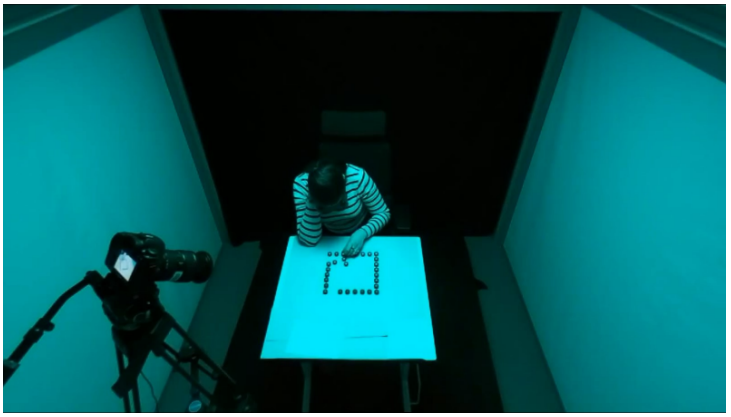

Figure 4.6: A participant taking part in the experiment.

participation without any obligation. Finally, before starting the psychophysical experiment itself, participants performed an online simplified version of the FM100 Hue Test available on X-Rites website.

A total of 57 participants completed both sessions of the experiment over a two-month period. They were divided into 4 groups as follows:

- G1: control group (no low vision simulation goggles), 10 participants
- G2: central scotoma simulation goggles, 16 participants
- G3: blurry vision simulation goggles, 15 participants
- G4: tunnel vision simulation goggles, 16 participants

After the color blindness checking step, each participant entered the light booth and was given time to sit and adjust the chair. According to the assigned group, the observer was then provided with the appropriate low vision simulation goggles. Once comfortably seated, the following simple and concise instructions were given: You will have 28 colored samples in front of you. Four of them are already placed and serve as references. You have to arrange the remaining 24 samples in the correct hue order. If clarification was needed, the following explanation was provided: Arrange the samples similarly to how you did during the visual test you performed a few minutes ago, except that the reference samples are now placed at the corners of a square. If participants, especially those wearing simulation goggles, had difficulty locating the sample cutouts on the table, the instructor briefly entered the light booth to provide assistance. This gave confidence to observers who were afraid of making a mistake specifically during the first manipulations at the beginning of the experiment. The disposition of the light booth is illustrated in Figure 4.6.

During this start-up step, the light booth was illuminated with a D65 daylight setup to provide the same illuminance of 80 lux given by each of the 13 channels on the surface of the experimental table (see Section “Experimental setup”). When the participant was ready to begin the sorting task, one of the 13 selected channels was turned on using

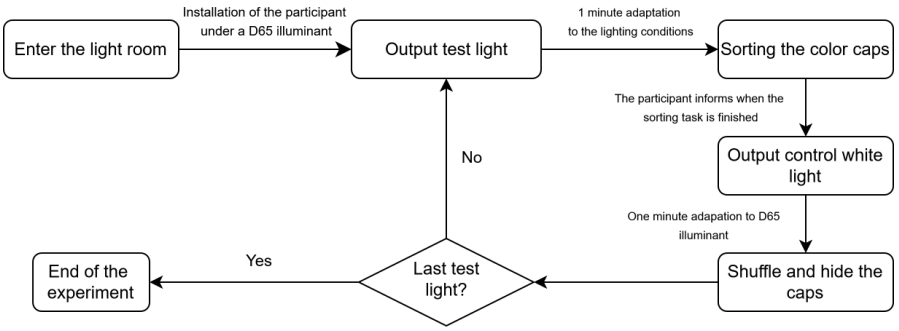

Figure 4.7: Flowchart describing the experimental protocol.

a smooth gradient transition. After one-minute adaptation period under the colored light, the observer started to sort the colored samples in free time. The different LED channels were cycled one after the other once the sorting task was completed. Between each channel, the booth was again illuminated with D65 white light. To avoid potential bias related to the order of lighting conditions, five predefined lighting sequences were used with participants randomly and evenly distributed among them. An overview of the full experimental protocol is given by the flowchart shown in Figure 4.7.

At the end of a sorting task, there were three possibilities: (1) If it was not the end of one of the two sessions, the participant remained seated in the light booth while the next task was being prepared by the instructor. (2) If it was the end of the first session, the participant exited the light booth without receiving any performance feedback. (3) If it was the end of the second session, the participant was shown the results of his/her final round and invited to share his/her feedback through a short interview.

4.2 Automatic Score Calculation

As explained in the previous section, participants were asked to sort 28 color samples a total of 13 times. Manually recording the position and number of each sample would be both tedious and very time-consuming, especially as the caps have to be turned over since identification numbers are printed on their back. This would slow down the experiment considerably. Participants would have to wait a long time between each sorting task, creating boredom and lassitude that could alter the quality of the results and introduce experimental bias. To address this issue, an algorithm was developed to automatically detect the positions and order of the color samples. This algorithm processes a unique 14-bit RAW image of the experimental area and accurately reports the order of the caps.

4.2.1 Image capture

Images of the experimental area were captured using a Canon 5D Mark IV camera which is able to provide high-resolution 14-bit RAW depth color pictures. The camera was positioned in the corner of the light booth and directed towards the table where participants ordered the color samples (see Figures 2.1 and 4.1). Image capture was performed under the D65

white adaptation light which was setup to provide an illuminance of 80 lux on the surface of the experimental table. F-number and exposure time settings were optimized to have a clear and sharp image across all 28 samples. An example of captured image is shown in Figure 4.8.

4.2.2 Sample detection

Due to slight misalignments in cap placement or potential camera shifts between sessions, an automatic detection of sample positions was required. Then, the algorithm begins by converting the 14-bit RAW color image to grayscale as shown in Figure 4.9. A cross-correlation operation is performed between this grayscale image and a small reference image of a single cap. Local maxima are then extracted in order to determine the position of each cap (see Figure 4.10). A bounding box is then drawn around the detected sample positions.

4.2.3 Order detection

Inside each bounding box, a 10x10 pixel region of interest (ROI) is centered to extract the color information from the original 16-bit image (see Figure 4.11). The average color within each ROI is computed in sRGB color space and stored in an array with sample positions indexed starting from the cap closest to the camera and proceeding clockwise. In the next step, the average sRGB values are converted to the CIE L*C*h color space. The resulting array is then sorted by the hue (h) component. This ordered array reflects the effective relative positions of the caps as sorted by the participant.

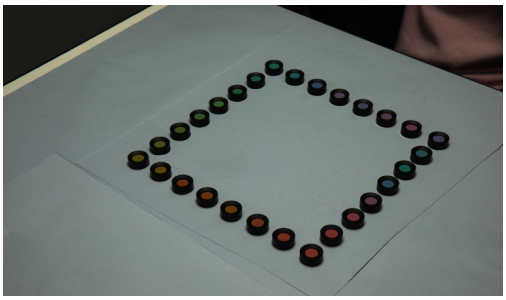

Figure 4.8: Original color image.

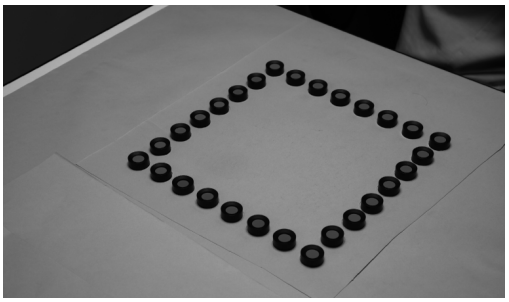

Figure 4.9: Grayscale image.

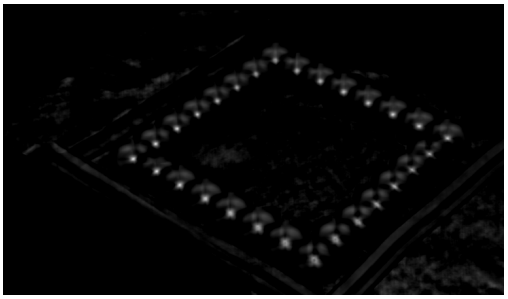

Figure 4.10: Cross-correlation result.

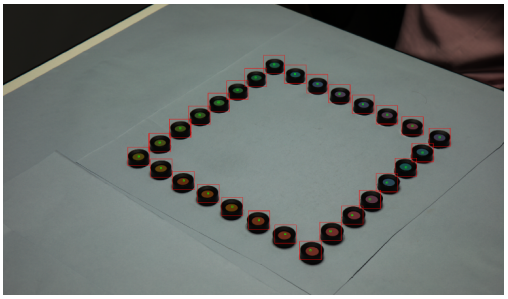

Figure 4.11: Original image with bounding boxes (red) and Regions of Interest (green).

4.2.4 Score calculation

Once the sample order is obtained, the score can be calculated. Because the modified test uses only 28 of the original 85 samples and the caps are arranged in a square with references placed at the corners instead of in four trays, an adaptation of the Farnsworth-Munsell 100 Hue Test scoring method was required. The calculation we used is as follows:

$$s_i = \begin{cases} 28 - |n_i - n_{i-1}| & \text{if } |n_i - n_{i-1}| > 14 \\ |n_i - n_{i-1}| & \text{otherwise} \end{cases} + \begin{cases} 28 - |n_i - n_{i+1}| & \text{if } |n_i - n_{i+1}| > 14 \\ |n_i - n_{i+1}| & \text{otherwise} \end{cases} \tag{4.1}$$

4.2.5 Algorithm robustness

The algorithms outputs were validated using data from the first ten participants. In addition to photographing the colored samples, the true sorting order was manually recorded and compared with the algorithms results. This provided 130 trials (10 participants x 13 lighting conditions) for which the ground truth was known. Across all trials, the algorithm consistently returned the correct sorting order with no observed failures. It was therefore considered that the algorithm was robust enough to provide the correct sorting order.

4.3 Results

The ordering of the color samples provides valuable information about the influence of lighting conditions on color discrimination. By analyzing how selected caps were arranged by participants, it could be possible to identify trends that would reflect how channels affect color perception according to the selected simulated visual impairment.

4.3.1 Acquired data

A ZED stereo camera was used to capture the unfolding of each experimental session in order to analyze participants' strategies (see Figure 4.12). This approach provides a comprehensive data set that can be referenced if an observer's data seems aberrant during statistical analysis and needs to be discarded.

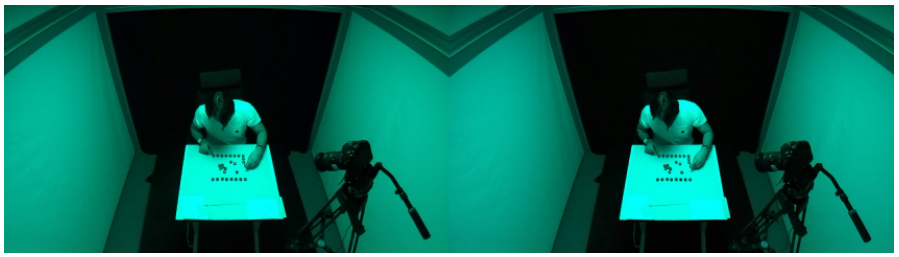

Figure 4.12: Recording of one of the sessions using a ZED stereo camera.

Moreover, since the camera is binocular, it supports the application of AI-based models to track hand and body movements in three dimensions. While a detailed analysis of participants' strategies is beyond the scope of this article, such an investigation will be useful to extend the present result analysis and for the design of our future psychophysical experiments.

The order of the 28 color samples was recorded for each participant under all 13 selected channels of the LED panel ($l = 1, \dots 13$). The collected numerical data are the scores for each individual color sample ($i = 1, \dots 28$) under each lighting conditions for all participants ($n \in \mathrm{G}_k$) in a given group ($k = 1, \dots 4$). These data can be noted as follows:

$$\{s_{i,l,n}\}_{i\in[\![1,28]\!],l\in[\![1,13]\!],n\in G_k} \tag{4.2}$$

with $k \in [\![1, 4]\!]$

The Total Error Score (TES) related to the original Farnsworth-Munsell 100 Hue Test describes the overall ability of an observer to discriminate colors. It is calculated by summing the scores of all the colored caps. In this study, TES aims to evaluate the effectiveness of each lighting channel in allowing an accurate color discrimination. It is calculated as shown in Equation 4.3. The TES distributions for the 4 groups of participants are presented in Figure 4.13.

$$\forall l \in [\![1, 13]\!], \forall n \in G_k, \quad TES_{l,n} = \sum_{i=1}^{28} s_{i,l,n} \tag{4.3}$$

The lower the TES is the better the ranking.

The lowest error scores for the control group G_1 are observed for channels B2 and C, i.e. channels 4 and 5 (see Figure 2.25 and Table 5.1), with average TES values lower than 150. In contrast, the highest error scores are obtained for channels RB2, R1, R2 and DR1, i.e. channels 2, 11, 12 and 13, with average values exceeding 250. In overall, the TES values for the control group G_1 are lower for most channels (except for the poorest ones)

compared to the other groups. The standard deviation is another important parameter to consider in the cross-analysis of scores.

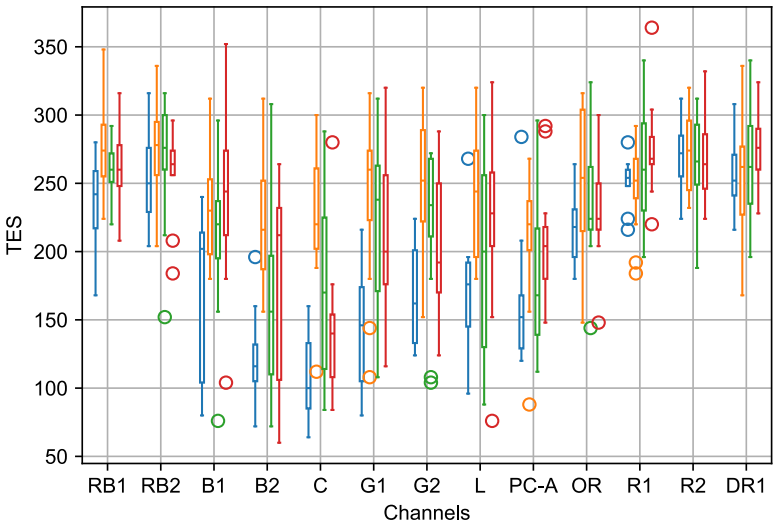

Figure 4.13: Box plots showing the distribution of Total Error Scores (TES) for the 4 groups across the 13 lighting channels used in the experiment: G_1=Control Group (in blue), G_2=Central Scotoma (in orange), G_3=Blurry Vision (in green), G_4=Tunnel Vision (in red)

.

Equation 4.4 introduces an extended metric, the Extended Total Error Score (ETES), to quantify the overall ability of an observer to discriminate colors under all 13 channels. This allows a comparative analysis of group performance and the influence of low vision simulation goggles. The distribution of ETES values for each group is shown in Figure 4.14.

$$\forall n \in G_k, \quad ETES_n = \sum_{l=1}^{13} TES_{l,n} = \sum_{l=1}^{13} \sum_{i=1}^{28} s_{i,l,n} \tag{4.4}$$

In Figure 4.14, the control group G_1 exhibits the lowest ETES values, while the central scotoma group G_2 shows the highest ETES. It is interesting to note that group G_2 also has the lowest standard deviation, suggesting a more uniform performance despite poorer average results. Groups G_3 (blurry vision) and G_4 (tunnel vision) have similar ETES values but group G_3 presents a higher standard deviation.

From this preliminary analysis, three distinct types of data need further investigation: (1) sample scores $s_{i,l,n}$ $(i = 1, \dots 28)$ that give an information how well each color samples are distinguished under specific lighting conditions (channels $l = 1, \dots 13$) by participants in groups $n \in (G_k)$ with $(k = 1, \dots 4)$); (2) the $TES_{l,n}$ that gives a rating for a specific

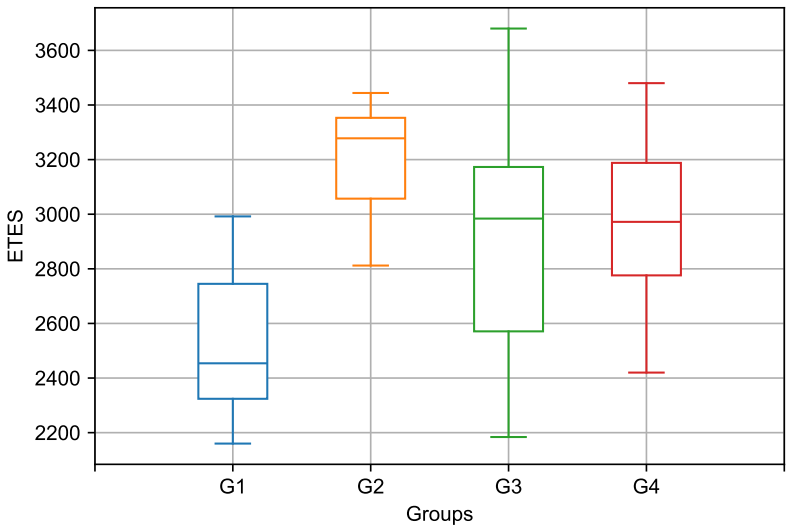

Figure 4.14: Box plots showing the distribution of Extended Total Error Scores (ETES) for the four participant groups: G_1=Control Group, G_2=Central Scotoma, G_3=Blurry Vision, G_4=Tunnel Vision.

channel across the hue circle within each observer group; (3) the $ETES_n$ that allows cross-group comparisons of global color discrimination performance.

4.3.2 Statistical analysis

The results of the statistical analysis of experimental data are presented in Tables 4.1 to 4.6. In these Tables, green cells indicate p-values below the significance threshold $\alpha = 0.05$ while red cells correspond to p-values above this threshold.

1st analysis : Global performance comparison between groups

In this first part of the statistical analysis, the global color discrimination performance is compared across the 4 groups of observers. Let us define $ETES^k$ as the set of Extended Total Error Scores for participants in group G_k:

$$\mathbf{ETES}^k = \{ETES_n\}_{n \in G_k}$$

Pairwise comparisons between groups were performed using Welch's t-test on $\mathbf{ETES}^i$ and $\mathbf{ETES}^j$ for all $i \neq j$. This statistical test is suitable for comparing two independent samples that may have unequal variances [175].

	G_1	G_2	G_3	G_4
G_1		7.6e-6	1.0e-2	1.5e-3
G_2			3.2e-2	2.1e-2
G_3				7.6e-1
G_4				

Table 4.1: Welchs t-test p-values for pairwise group comparisons across LED channels l ($l = 1, \dots 13$).

Hypothesis $\boldsymbol{H_0}$: There is no significant global performance difference between the two groups G_i and G_j, for $i \neq j$.

Hypothesis $\boldsymbol{H_1}$: There is a significant global performance difference between the two groups G_i and G_j, for $i \neq j$.

If the p-value is lower than $\alpha = 0.05$ the Hypothesis $\boldsymbol{H_0}$ is rejected indicating a statistically significant difference.

Table 4.1 presents the results of the pairwise comparisons of the four groups. Green cells denote statistically significant differences which means that Hypothesis $\boldsymbol{H_0}$ is rejected. Red cells indicate non-significant results when Hypothesis $\boldsymbol{H_0}$ cannot be rejected. The comparison between the blurry vision group G_3 and the tunnel vision group G_4 does not lead to a significant difference suggesting similar global color discrimination performance for these two simulated visual impairments. In contrast, all three low vision simulation groups performed significantly worse than the control group G_1. This is especially emphasized for central scotoma group G_2 which exhibits significantly poorer performance than both the blurry vision and tunnel vision groups.

2nd analysis : Group performance comparison across LED channels

In this second part of the statistical analysis, group performance across the different LED channels is examined. Since both the groups and channels are independent, Welchs t-test remains appropriate. Let $\mathbf{TES}_l^k$ denote the total error score for group G_k under LED channel l defined as:

$$\mathbf{TES}_l^k = \{TES_{l,n}\}_{n \in \mathrm{G}_k, l \in [\![1,13]\!]}$$

Hypothesis $\boldsymbol{H_0}$: The different groups perform the same under different lighting conditions i.e. $\mathbf{TES}_l^i = \mathbf{TES}_l^j \quad \forall i, j \quad i \neq j$.

Hypothesis $\boldsymbol{H_1}$: The different groups perform differently under different lighting conditions i.e. $\mathbf{TES}_l^i \neq \mathbf{TES}_l^j \quad \forall i, j \quad i \neq j$.

	G_1 / G_2	G_1 / G_3	G_1 / G_4	G_2 / G_3	G_2 / G_4	G_3 / G_s4
01	9.0E-03	6.3E-02	7.8E-02	9.9E-02	1.7E-01	9.5E-01
02	9.0E-02	3.0E-01	6.9E-01	4.9E-01	9.9E-02	4.1E-01
03	1.1E-02	8.0E-02	1.0E-02	2.5E-01	7.3E-01	2.1E-01
04	2.3E-06	6.1E-02	3.0E-02	5.0E-03	3.5E-02	6.4E-01
05	1.0E-07	5.6E-03	6.5E-02	7.8E-03	1.7E-05	1.8E-01
06	1.3E-04	3.1E-03	6.4E-03	2.8E-01	1.2E-01	6.7E-01
07	6.5E-05	4.5E-03	4.4E-02	1.5E-01	1.6E-02	3.2E-01
08	1.6E-03	2.4E-01	2.5E-02	4.6E-02	3.7E-01	2.8E-01
09	2.7E-02	3.4E-01	3.2E-02	1.4E-01	9.0E-01	1.7E-01
10	7.3E-02	2.0E-01	3.2E-01	4.7E-01	3.0E-01	7.4E-01
11	9.2E-01	3.5E-01	2.5E-02	3.5E-01	3.2E-02	3.6E-01
12	9.6E-01	6.2E-01	9.4E-01	5.7E-01	8.9E-01	6.7E-01
13	7.6E-01	6.5E-01	2.1E-01	4.9E-01	1.6E-01	5.0E-01

Table 4.2: Welchs t-test p-values for all pairwise group comparisons. (G_1=Control Group, G_2=Central Scotoma, G_3=Blurry Vision, G_4=Tunnel Vision)

Table 4.2 presents the results of Welch's t-test for each LED channel l ($l = 1, \dots 13$) across all pairwise group comparisons G_i vs G_j with $i \neq j$. As in the previous section, green cells indicate statistically significant differences where the null hypothesis is rejected and red cells correspond to non-significant differences where the null hypothesis is retained.

The analysis shows that the majority of statistically significant differences are observed for channels 3 to 9. The central scotoma group G_2 and the tunnel vision group G_4 exhibit the greatest deviations from the control group G_1, while the blurry vision group G_3 appears most similar to the control group with only three significant differences (green cells) across all channels. Once again, no significant differences appear between the tunnel vision and blurry vision groups for any channel. G_4 presents eight significant differences in Table 4.2 while G_3 shows seven. In this Table, the distribution of green cells is as follows: four for channels 4, 5, and 7; three for channels 6 and 8; and two for channels 3 and 9. As a preliminary conclusion, color discrimination appears the poorest under both short-wavelength (channels 1 and 2) and long-wavelength (channels 10 to 13) lighting conditions.

3rd analysis : Paired comparison of LED channels within groups

To further investigate the impact of lighting conditions, each group was individually analyzed to determine whether different LED channels significantly affect color discrimination within that group. More precisely, all possible pairs $\boldsymbol{TES}^k_{l_1}$ and $\boldsymbol{TES}^k_{l_2}$ where $l_1, l_2 \in [\![1, 13]\!], l_1 \neq l_2$ for a given group G_k were compared. Since each participant experienced all lighting conditions, the data are paired. Therefore, a paired t-test was used to analyze the intra-group differences.

Hypothesis H_0: For a given group, different light spectra have no significant impact on color discrimination.

Hypothesis H_1: For a given group, different light spectra significantly affect color discrimination.

If the p-value is lower than $\alpha = 0.05$ the Hypothesis $\boldsymbol{H_1}$ is statistically verified (green cells in the Tables), otherwise the Hypothesis $\boldsymbol{H_0}$ is verified (red cells in the Tables).

Tables 4.3, 4.4, 4.5 and 4.6 present the results of the paired t-test for all channel pairs i, j with $i = 1, ...13$, $j = 1, ...13$ and $i \neq j$. While it is challenging to completely summarize the results of the statistical tests in a condensed way, several observations are interesting to note. First, the diagonal of the tables points out if there is a significant difference between two consecutive channels (i.e. channels i and i+1). For example, channels 3 and 4 have a different impact on color discrimination for groups G_3 and G_4 oppositely to channels 6 and 7. Channels 7 and 8 as well as channels 12 and 13 have the same impact on color discrimination for all groups.

Table 4.3, presenting the results for the control group, shows that there is no significant difference between channels 4 and 5 corresponding to the best-performing channels in terms of color discrimination with TES values lower than 130 (see Figure 4.13). Likewise, no significant difference is observed between channels 6 and 9 which correspond to the next best channels in terms of color discrimination (TES between 130 and 160). There is also no significant difference between channels 3, 7 and 8 which have TES between 160 and 200. Color discrimination is significantly worse for all other channels (i.e. channels 1-2 and 10-13) with TES values upper exceeding 200. Note that the average TES for the control group ranges between 130 and 270.

In Table 4.4, presenting the results for the central scotoma group, the paired t-tests show few significant differences across LED channels which is consistent with Figure 4.13 where poor color discrimination is observed for all channels. The average TES values range from 220 to 280 indicating uniformly bad performance.

In Table 4.5, presenting the results for the blurry vision group, no significant differences are found between channels 4 and 5, or between channels 5 and 9, again corresponding to the best-performing conditions with TES values lower than 160 (see Figure 4.13). All other channels (13, 68 and 1013) show significantly worse performance with TES values exceeding 200. The range of average TES for this group spans from 160 to 280.

Figure 4.13 shows that, for the tunnel vision group, the best color discrimination is obtained for channel 5 (with a TES lower than 140), followed by channel 7 (with a TES lower than 190). According to Table 4.6, there is a significant difference between channels 5 and 7. This Table also indicates no significant difference between channels 4, 6 and 9 which are the next best channels in terms of color discrimination (with a TES between 190 and 220). Color discrimination is worse for all other channels (i.e. channels 1-3, 8 and 10-13) which have TES values exceeding 220. Overall, TES values range from 140 to 280.

Further observations can be drawn from the next figures. Figure 4.15 supports the assumption that channels 4, 5 and 6 are the best for color discrimination for the control group. In this figure TES values are mapped onto the hue circle for each color sample

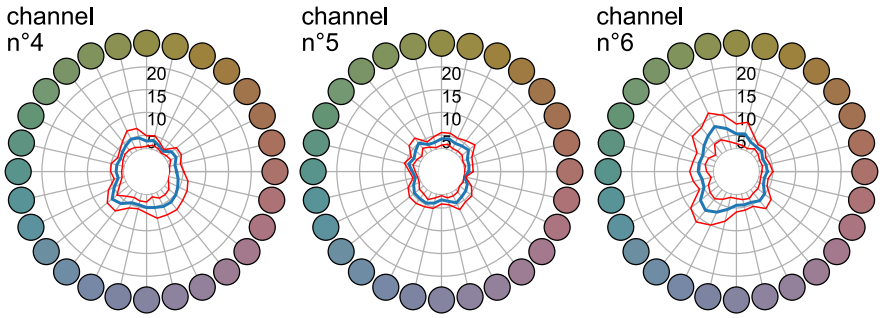

Figure 4.15: Average error score of the 10 participants in the control group for channels 4, 5 and 6 (blue: average error, red: confidence interval).

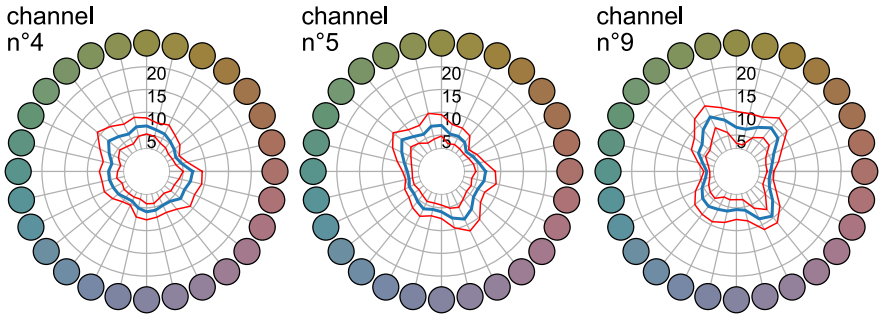

Figure 4.16: Average error score of the 15 participants in the blurry vision group for channels 4, 5 and 9 (blue: average error, red: confidence interval).

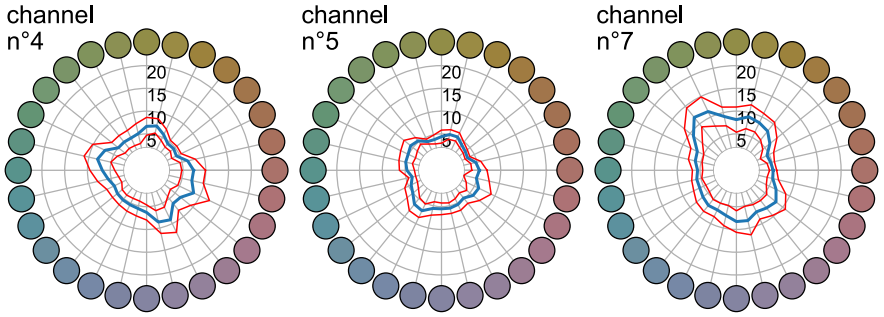

Figure 4.17: Average error score of the 16 participants in the tunnel vision group for channels 4, 5 and 7 (blue: average error, red: confidence interval).

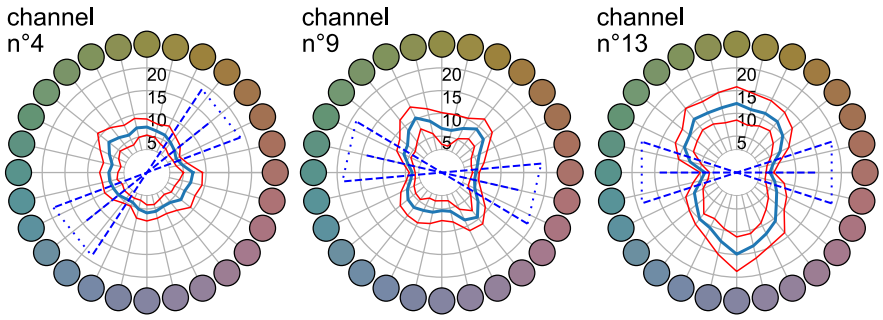

Figure 4.18: Average error score of the 16 participants in the blurry vision group for channels 4,9 and 13 (blue: average error, red: confidence interval).

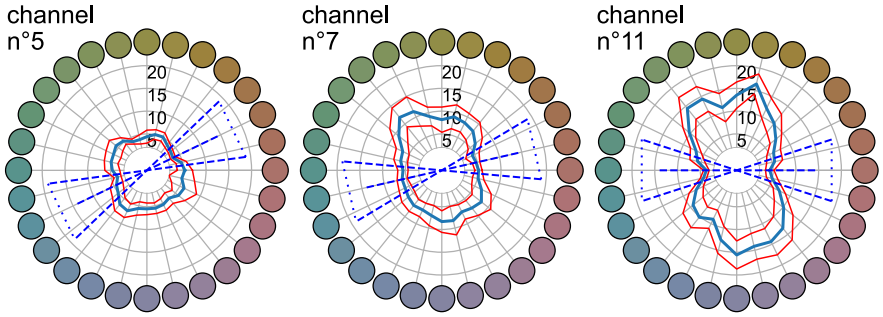

Figure 4.19: Average error score of the 16 participants in the tunnel vision group for channels 5,7 and 11 (blue: average error, red: confidence interval).

($i = 1, \ldots 28$). The average error is drawn in blue with the standard deviation for all participants ($n \in G_1$) in red. These plots demonstrate that channel 4 provides better color discrimination than channels 5 and 6 across all hues. The worse color discrimination is for channel 6 having a peak wavelength at 517 nm (see Table 5.1), especially for hues in the green (G), yellow (Y), purple (P), and purple-blue to blue (PB-B) regions.

Figure 4.16 confirms the assumption regarding the best-performing channels (i.e. channels 4, 5 and 9) for the blurry vision group. These plots demonstrate that color discrimination is generally easier (i.e. lower TES) for the control group than for the blurry vision group for channels 4 and 5 across all hues. Among the three, channel 4 provides the best color discrimination while channel 9 (PC-A, an orange LED) is the worst especially in the green-yellow-red (G-YR) and PB-B regions.

Lastly, Figure 4.17 confirms that channels 4, 5 and 7 are the best for the tunnel vision group. Discrimination under channel 5 is better for tunnel vision than for blurry vision across all hues while performance under channel 4 is similar between the two groups. Channel 5 outperforms channels 4 and 9 overall. Channel 7 provides the worst performance of the three, especially in the G-Y and PB-B regions.

To sum up:

- Channel 4 (B2, peak wavelength at 478 nm) provides the best color discrimination for both the control and tunnel vision groups;
- Channel 5 (C, peak wavelength at 500 nm) provides similar performance as channel 4 for the control group but less effectively for the blurry and tunnel vision groups;
- Channel 6 (G1, peak wavelength at 517 nm) provides relatively good color discrimination performance only for the control group, though TES is twice as high for blue hues compared to red;
- Color discrimination with monochromatic LEDs is generally more challenging for simulated blurry vision than for normal vision group.

In Figures 4.18 and 4.19, the two blue sectors represent the hue ranges (of 36° each) for which the color discrimination is optimal i.e. where the TES values are the lowest. The dashed blue line connecting these sectors corresponds to the axis formed by the two color samples with the best discrimination performance.

For the blurry vision group:

- The best channel in the cyan region (channels 3 to 6) is channel 4 offering improved discrimination for blue and yellow-orange color samples;
- The best channel in the yellow-green region (channels 7 to 10) is channel 9 for which discrimination is better for blue-green and red color samples;
- The least poor channel in the red region (channels 11 to 13) is channel 13 and does only provide acceptable color discrimination for blue and red color samples.

Figure 4.18 shows that channels 4 and 9 appear complementary in terms of color discrimination whereas channel 13 does not contribute as effectively. Importantly, none of

the 13 LED channels allows a strong color discrimination in the green and in the purple regions.

For the tunnel vision group:

- The best channel in the cyan region (channels 3 to 6) is channel 5 which enhances discrimination for orange and blue samples;
- The best in the yellow-green region (channels 7 to 10) is channel 7, which improves discrimination for red and cyan samples;
- The least poor in the red region (channels 11 to 13) is channel 11 and does only provide acceptable color discrimination for red and cyan color samples.

Figure 4.19 shows channels 5 and 7 appear complementary in terms of color discrimination while channel 11 provides weaker contribution. None of the 13 LED channels allows a strong color discrimination in the green-yellow and in the purple-blue hue ranges.

4.3.3 Participant feedback

This section reports the participants' comments regarding the difficulties and issues they may have met during the experiment.

The sorting task was well understood by all observers with very few questions arising once the experiment began. The preliminary reduced FM100 hue test conducted on a computer prior to the first experimental session was helpful to familiarize participants and make them confident with the nature of the sorting activity.

Some participants reported neck pain after the experiment. Such a discomfort may be due to improperly adjusted seating and the use of goggles that required an awkward head position to view samples located nearest to them. This issue may also have been reinforced by the fact that some participants reported that they sometimes cast shadows on nearby color samples. These concerns will be further explored in future studies thanks to data collected from the stereo camera used to monitor the experiment. In addition, motion tracking will be explored to identify ergonomic problems in order to improve future experimental setups.

Participants also frequently mentioned eye strain following the experiment. This was especially associated to some of the channels that were deemed as more unpleasant. As anticipated, the broader band channels in the center of the visible spectrum were generally preferred. However, there was no consensus on which specific channels were the most straining. Some observers reported greater discomfort from the reddest channels while others found the bluest channels more unpleasant. Moreover, several participants expressed concern that under some lighting conditions they were ordering samples based on perceived lightness rather than hue as they could not accurately distinguish color differences.

4.4 Chapter Summary

This chapter investigated the impact of light spectra on color discrimination for individuals with simulated low vision. A psychophysical experiment was conducted using a fully

	1	2	3	4	5	6	7	8	9	10	11	12	13
1		2.6e-01	1.7e-02	3.4e-05	1.0e-06	7.2e-04	1.2e-03	5.6e-03	2.6e-03	2.5e-01	8.3e-02	3.0e-02	1.0e-01
2			1.2e-03	1.5e-06	1.5e-05	1.3e-04	1.6e-03	2.2e-03	3.8e-04	3.1e-02	8.5e-01	2.7e-01	7.6e-01
3				5.3e-02	8.1e-03	1.8e-01	9.5e-01	9.6e-01	7.7e-01	3.6e-03	5.2e-03	7.6e-04	3.7e-03
4					3.0e-01	1.3e-01	2.7e-02	5.7e-03	4.6e-03	7.9e-05	2.1e-06	5.2e-07	2.0e-06
5						1.3e-02	6.4e-04	7.1e-04	1.8e-03	9.7e-07	1.4e-07	7.6e-08	2.6e-07
6							2.5e-01	1.9e-01	2.9e-01	4.2e-04	1.1e-04	1.3e-05	2.6e-05
7								8.4e-01	8.7e-01	5.4e-03	1.3e-04	1.7e-06	4.0e-06
8									6.0e-01	1.0e-02	4.7e-04	1.0e-04	2.3e-04
9										2.9e-03	4.4e-04	1.3e-04	6.6e-04
10											1.7e-02	3.0e-03	1.8e-02
11												1.5e-01	4.1e-01
12													2.2e-01
13													

Table 4.3: P-values from paired t-tests comparing LED channels for the control group (G1)

	1	2	3	4	5	6	7	8	9	10	11	12	13
1		7.3e-01	3.7e-03	3.3e-03	6.3e-04	6.2e-02	1.6e-01	2.0e-02	2.5e-04	1.8e-01	2.7e-02	6.8e-01	1.5e-01
2			1.5e-03	3.0e-04	3.4e-03	7.7e-02	1.0e-01	1.7e-02	4.2e-04	7.4e-02	3.4e-02	4.7e-01	5.3e-02
3				5.3e-01	5.3e-01	5.4e-01	2.6e-01	6.7e-01	9.7e-02	2.3e-01	2.2e-01	3.2e-02	1.2e-01
4					8.8e-01	3.1e-01	1.2e-01	3.4e-01	5.3e-01	1.1e-01	4.0e-02	2.5e-03	4.1e-02
5						2.4e-01	1.8e-01	3.1e-01	1.4e-01	1.5e-01	6.3e-02	1.3e-02	7.5e-02
6							6.0e-01	9.1e-01	3.4e-02	6.2e-01	5.8e-01	1.4e-01	4.8e-01
7								5.6e-01	1.3e-02	9.3e-01	9.8e-01	1.5e-01	8.1e-01
8									4.4e-02	6.0e-01	4.5e-01	2.8e-02	3.9e-01
9										1.4e-02	5.1e-03	3.6e-04	1.7e-02
10											9.6e-01	1.9e-01	7.4e-01
11												9.0e-02	7.6e-01
12													3.1e-01
13													

Table 4.4: P-values from paired t-tests comparing LED channels for the central scotoma group (G2)

	1	2	3	4	5	6	7	8	9	10	11	12	13
1		3.3e-01	2.4e-03	1.8e-05	2.5e-05	1.6e-02	1.3e-02	1.6e-03	8.7e-05	3.2e-02	7.6e-01	6.9e-01	5.9e-01
2			4.4e-03	1.5e-05	1.6e-05	7.2e-03	6.8e-03	3.9e-04	6.5e-05	3.6e-03	6.3e-01	5.6e-01	6.9e-01
3				2.2e-03	1.0e-02	8.0e-01	5.1e-01	3.3e-01	1.1e-01	6.8e-02	3.9e-03	2.9e-03	2.1e-03
4					5.9e-01	1.9e-03	8.6e-04	1.7e-02	4.5e-02	5.9e-05	2.8e-05	1.8e-05	9.8e-07
5						1.9e-03	5.6e-03	2.2e-02	2.2e-01	1.6e-05	3.0e-06	2.1e-05	1.0e-05
6							7.1e-01	1.3e-01	5.0e-02	2.4e-01	1.7e-02	1.4e-02	7.9e-03
7								1.9e-01	2.6e-02	4.1e-01	1.9e-02	1.1e-02	3.9e-03
8									3.9e-01	1.6e-03	1.1e-03	7.2e-04	6.3e-04
9										1.2e-03	1.4e-04	1.5e-04	1.9e-06
10											2.5e-02	1.2e-02	1.4e-02
11												9.4e-01	8.7e-01
12													9.0e-01
13													

Table 4.5: P-values from paired t-tests comparing LED channels for the blurry vision group (G3)

	1	2	3	4	5	6	7	8	9	10	11	12	13
1		9.4e-01	1.5e-01	3.5e-04	1.3e-07	2.4e-03	1.9e-03	2.0e-02	1.9e-04	4.1e-02	1.7e-01	4.5e-01	2.2e-01
2			2.7e-01	7.6e-04	5.6e-07	4.6e-03	1.7e-03	5.0e-02	6.1e-04	8.2e-03	5.7e-02	3.9e-01	2.0e-01
3				4.0e-03	2.3e-05	7.6e-02	5.1e-02	3.7e-01	1.2e-01	6.4e-01	5.0e-02	7.3e-02	9.8e-02
4					4.0e-02	8.6e-02	4.9e-02	1.2e-02	8.4e-02	1.3e-02	1.7e-04	6.5e-05	3.4e-04
5						7.7e-04	2.8e-07	3.8e-04	7.4e-06	5.2e-06	2.2e-08	7.6e-07	1.4e-07
6							8.3e-01	3.8e-01	9.9e-01	9.5e-02	1.9e-03	8.6e-04	3.1e-03
7								3.3e-01	7.8e-01	6.4e-02	1.6e-05	7.4e-04	2.6e-04
8									4.7e-01	6.1e-01	1.2e-02	1.9e-03	1.0e-02
9										7.0e-02	4.1e-05	8.3e-04	1.8e-04
10											1.9e-03	5.8e-03	2.7e-03
11												5.9e-01	8.5e-01
12													6.8e-01
13													

Table 4.6: P-values from paired t-tests comparing LED channels for the tunnel vision group (G4)

characterized spectrally tunable LED system from which 13 distinct channels were selected and calibrated to maintain isoluminance. The experiment was based on a modified version of the Farnsworth-Munsell 100 Hue Test, using 28 carefully selected color caps arranged in a square layout instead of the traditional four-tray configuration. This setup, coupled with an automated scoring algorithm, allowed efficient and consistent assessment of participants' performance. This significantly reduced session duration, allowing 57 participants divided into four groups (control, central scotoma, blurry vision, and tunnel vision) to complete the experiment over a two-month period.

The results exhibit substantial differences in color discrimination across the groups, especially with the central scotoma group which displayed the poorest performance under all 13 spectral lighting conditions. Additionally, the light channels produced varied effects across participant groups with the most notable group differences observed within the 460-630 nm spectral range. These observations underscore the critical role of spectral composition in color perception especially in low vision conditions.

This work provides valuable insights into how specific light wavelengths affect color discrimination for people suffering from different types of visual impairments. These results are a keystone for future research aimed at optimizing lighting environments to enhance visual performance of low vision people. Upcoming and future studies will build upon these first results to achieve the broader goal of optimizing spectral lighting to develop white light systems tailored to the visual needs of the visually impaired.

The work described in this chapter was presented at the ENVISION 2025 conference in Dallas, where the findings were shared with professionals in low vision rehabilitation. In addition, the study has been submitted for publication and is currently undergoing peer review.

This chapter studied the influence of individual light channels on color discrimination ability. However, since everyday lighting applications require the production of white light, the next chapter will describe the process developed to explore and generate the various white light conditions that the panel is capable of producing.

Chapter 5

LED Light Mixing and Stabilisation

The first experiment that was performed during this thesis, which was described in Chapter 4, allowed us to study the influence of different colored channels on color discrimination performance for different types of visual impairments. However, for everyday tasks, white light remains the most suitable illumination condition and what is most adapted to the human visual system. To exploit these results and propose practical applications, it is therefore essential to devise methods to design, optimize, and generate specific white light spectra.

The characterization carried out in the first phase of this work, as detailed in Chapter 2, provided a clear understanding of the extent of the capabilities of the available LED panel. However, the goal of reproducing a target spectrum through individual channel control raises two key research questions: what are the different spectra can the panel actually generate, and what drive levels are required for each channel to achieve the desired output? These questions are essential, as the lighting conditions designed for the different experiments may be constrained by the practical limitations of the lighting system used in this study in terms of spectral and intensity capabilities.

This section focuses on the methods that were used in this thesis for the psychophysical experiments that were conducted, in order to produce white light. First, the procedure that was done in order to obtain light with a specific chromaticity will be detailed, followed by the algorithm that was developed to ensure stability over time of the spectral output of the panel as well as spectral match. Finally the parameters selected and the way these algorithm implemented in this work will be discussed.

5.1 Light Mixing Algorithm

After analyzing the influence of individual light channels on color discrimination, the next step is to determine how these channels can be combined to produce an optimal white light spectrum that enhances the visual performance of individuals with low vision. To specifically investigate the impact of spectral composition, the chromaticity and illuminance

were fixed so that the spectral power distribution was the only variable in the experiment described in the following chapter.

Although no universally accepted definition of white light exists, chromaticities commonly used in lighting applications are generally recognized as falling within this category. Therefore, the lights generated for the following experiment were designed to match the chromatic appearance of standard illuminants or typical consumer lighting.

This section describes the methodology employed based on the algorithm described by Finlayson et al. [176] to generate white lights with a specified chromaticity and the procedure used to systematically explore the metamer set, corresponding to all possible light spectra sharing the same chromaticity, that can be generated by the LED panel.

5.1.1 Simple spectrally tunable LED system output model

As explained previously in Chapter 2, the output of a tunable LED panel can be simply written as the sum of the contribution of each of its channels. If one were to measure the different channels individually it would be possible to measure the resulting output as summarized by Equation 5.1:

$$S(v, \lambda) = \sum_{i=1}^{13} S_i(v_i, \lambda) \tag{5.1}$$

with $S(v, \lambda)$ the total spectral output of the panel, $S_i(v_i, \lambda)$ represent the SPD of the i^{th} channel and $v = (v_1, \ldots, v_{13})$ are the drive levels of the 13 selected channels, $v_i \in [0, 1]$ where $v_i = 0$ corresponds to when the channel is turned off and $v_i = 1$ corresponds to its maximum output power.

However in order to use Equation 5.1, it is required to measure the spectral output of each channel at every possible drive level, which is not possible in practice. To address this, an approximation must be introduced to model the channel behavior as a function of each drive levels. Although the output of an LED is not linearly proportional to its driving current, tunable systems often employ calibrated drive levels to approximate a linear control of the brightness of the different channels. In this case, the spectral power distribution of a channel can be approximated as linear with respect to the drive level, as shown in Equation 5.2:

$$\forall i \in [\![1, 13]\!], \quad S_i(v_i, \lambda) \approx v_i \cdot S_i(1, \lambda) \tag{5.2}$$

This approximation allows us to interpolate the spectral power distribution of all the channels only from their measurement once at their maximum intensity, in turn giving us an approximation of the total output of the panel:

$$S(v, \lambda) \approx \sum_{i=1}^{13} v_i \cdot S_i(1, \lambda) \tag{5.3}$$

which can also be written in matrix form as:

$$\mathbf{S_v} \approx B \cdot v \tag{5.4}$$

with B the matrix containing the spectra of the 13 channels.

Figure 5.1 displays the approximation for channel 7 when lit at 50% of its maximum ouput.

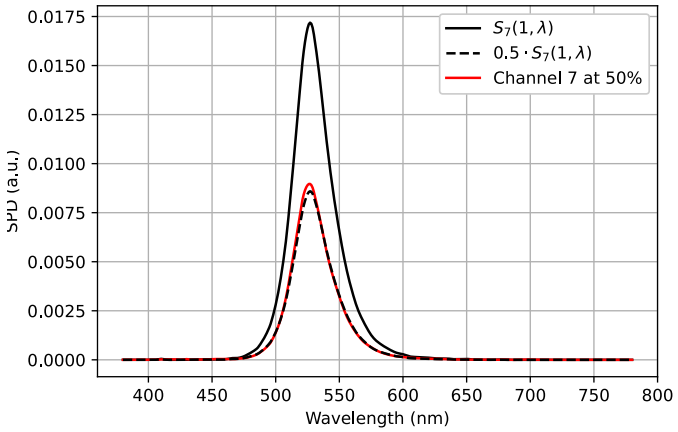

Figure 5.1: Comparison between the linear approximation and the measured SPD.

5.1.2 Solution for 3 channels

According to CIE 1931, any color can be represented as a combination of three tristimulus values X, Y, and Z. Therefore, at least three independent channels are required to reproduce a broad range of colors. To illustrate the requirements for generalization to a greater number of channels, the simple case in which only three channels are used will be detailed in this section.

In order to describe the chromaticity of a light, the tristimulus values in the CIE1931 XYZ color space will be used. The formula given in Chapter 2 to compute the XYZ values from a spectra can also be written in matrix form as described by Equation 5.5:

$$\mathbf{X} = S \cdot M_{XYZ} \tag{5.5}$$

with $\mathbf{X} = (X, Y, Z)$ the tristimulus values, S the SPD of a light and M_{XYZ} the matrix containing the color matching functions.

Using the approximation given by Equation 5.2 the color output of the LED panel can be expressed by:

$$\mathbf{X} = B \cdot XYZ \cdot v \tag{5.6}$$

With three channels, the matrix $B \cdot XYZ$ is a square 3 by 3 matrix and v the array containing the drive levels of the three selected channels.

If this system of equation has a solution, then the unique combination of drive levels required to match the chromaticity XYZ can be calculated by solving an $ax = b$ linear matrix equation:

$$(B \cdot XYZ) \cdot v = \mathbf{X} \tag{5.7}$$

5.1.3 Generalization to N channels

As illustrated in the the previous section, finding the spectrum that match specific tristimulus values requires to solve a system of equations with 3 equations and N unknown variables with N the number of channels used. This means that the dimension of the solution space is equal to $N - 3$. Therefore, by increasing the number of channels, the complexity to solve and explore all possible solutions quickly rises.

In their article, Finlayson et al. [176] described an algorithm that returns the complete set of solutions, the metamer set. While the mathematical formulation of the algorithm will not be presented in full detail, this section will provide a general outline of its operation and implementation in this work.

In order to compute all the spectra that match the desired chromaticity, the algorithm returns two values, σ_p a particular solution to the problem (i.e. a solution to the Equation $v \cdot B \cdot M_{XYZ} = \mathbf{X}$), which might not be a physically achievable solution and Ψ which is the basis for the metameric black solution space (i.e. solving the equation $v \cdot B \cdot M_{XYZ} = \mathbf{0}$).

Using these two values, all solutions σ can be written as:

$$\mathcal{S} = \left\{\sigma = \sigma_p + \alpha \cdot \Psi | \alpha \in \mathbb{R}^{N-3}\right\} \tag{5.8}$$

However, the solution space $\mathcal{S}$ also contains solutions that are not physically realizable with the LED panel, including negative drive levels or values exceeding the panels maximum output.

Therefore, the algorithm also returns 2 sets of constraints:

$$B\Psi\alpha \geq -B\sigma_p \tag{5.9}$$
$$B\Psi\alpha \leq 1 - B\sigma_p \tag{5.10}$$

with $\alpha \in \mathbb{R}^{N-3}$.

When applied to the solution space $\mathcal{S}$, these constraints define a bounded and convex region of a $N - 3$ dimensional space which can then be sampled in order to explore all possible spectra that match the desired chromaticity.

5.1.4 Visualisation of the metamer set

The algorithm previously described is particularly useful to display the full range of spectra possible matching a given chromaticity. In this section, the method is illustrated for a system with $N = 5$ channels. In this case, the solution space of possible spectra has a dimensionality of $N-3 = 2$, which allows for convenient two-dimensional representation while still having a wide diversity of spectral distributions. In this example, five channels were selected (Figure 5.2) to produce the metamer set matching the chromaticity of 4000K white LED lights.

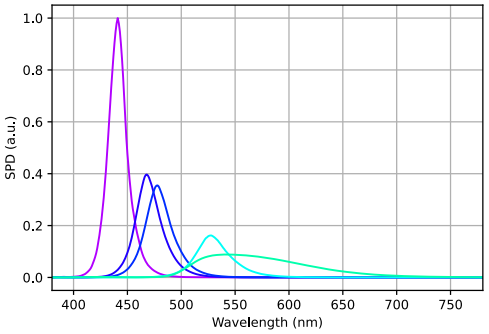

Figure 5.2: Five selected channels for this example.

In order to explore all the possible solutions, it was decided to use a Poisson point process to randomly and uniformly sample the solution space as shown in Figure 5.3a. This process generates a large amount of random values $\alpha = (\alpha_1, \alpha_2)$ that verify the constraints defined in the previous subsection. With enough sample points it is possible to explore the full diversity of spectra that match the desired chromaticity that the panel is capable to produce with the selected channels, which translates to the different spectra shown in Figure 5.3b.

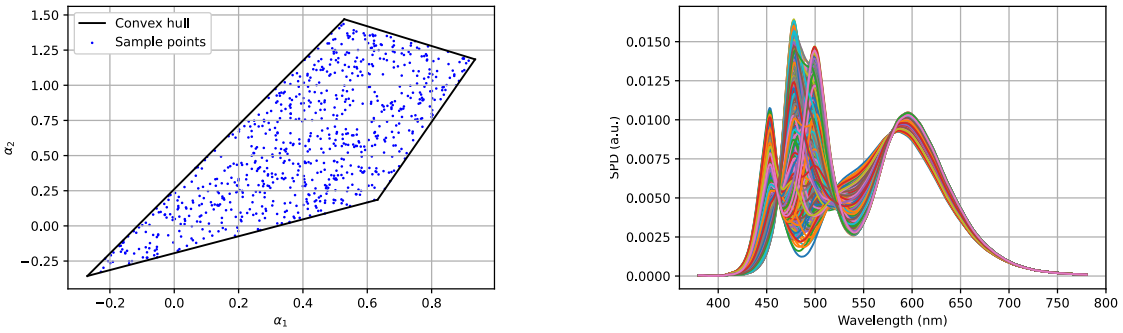

(a) Poisson point process to sample the solution space (∼2000 points).

(b) The different solution spectra.

Figure 5.3: Visualisation of the metamer set.

In addition of the representation of the diversity of spectra available we can also display the available characteristics of the lights and compare the different color rendering indices such as CIE R_a in Figure 5.4a and CIE R_f in Figure 5.4b.

5.1.5 Non-linearity and the complex version of the algorithm

When testing in practice however, even on a calibrated LED panel the predicted drive levels to match the target spectrum generally produce an output slightly different than

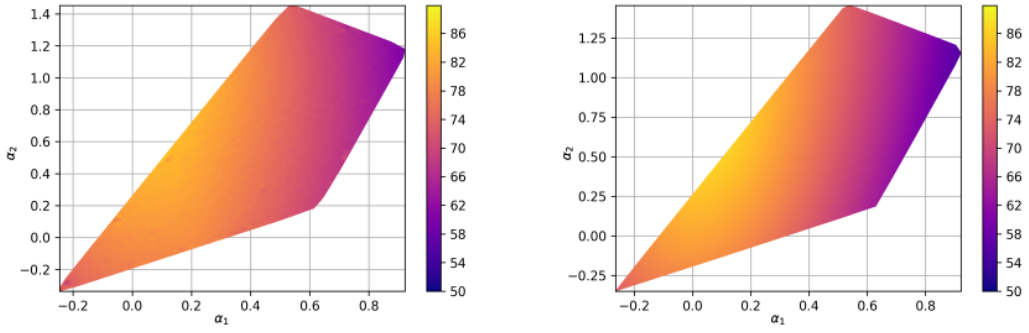

(a) CIE R_a values of the metamer set.

(b) CIE R_f values of the metamer set.

Figure 5.4: Comparison of achievable CIE R_a and CIE R_f

expected. This is due to the fact that channels don't behave exactly linearly and the approximation in Equation 5.2 can be true to varying degree depending on the channel considered and is especially true for small drive levels.

Finlayson et al. proposed an improved version of the algorithm using a much finer interpolation method to predict the output of the LED channels. Instead of measuring each channel once, the channels are measured at different drive levels and the predicted spectrum is interpolated from this data, as summarized by Equation 5.11. Figure 5.5 shows the example for channel 7 set at 50% with measurements done at 40 and 60%.

$$S_i(v_i, \lambda) \approx (1-a) \cdot S_i(v_i^j, \lambda) + a \cdot S_i(v_i^{j+1}, \lambda), \quad a = \frac{v_i - v_i^j}{v_i^{j+1} - v_i^j} \tag{5.11}$$

with $\left\{ S_i\left(v_i^j, \lambda\right) \right\}_{i \in [\![0,13]\!], j \in \mathbb{N}}$ the measurement of the channels at different drive levels.

Depending on the choice of intermediate measurements for the interpolation, this version of the algorithm allows for more accurate prediction of the spectral output as illustrated by Figure 5.6, however it adds a lot of complexity to the calculation of the metamer set. The complex version of the algorithm described by Finlayson et al. is only different in the fact that it requires to compute the metamer set for each possible combination of measurements, i.e. to compute the full metamer set using N channels measured at K different drive level each, we need to compute K^N different sets. For example with 5 channels measured at 10 drive levels, 100000 sets have to be calculated which even with optimization and parallel processing takes about 25 seconds to complete using python on a modern computer equipped with an i7 12700H. It also makes the analysis of the results much more complicated, since instead of having one single solution space, we have a union of multiple spaces.

Despite the use of a more sophisticated interpolation model and precise prediction algorithm that significantly improves spectral match to a desired spectrum, in practice, the output still tends to drift from the target spectrum over extended periods of operation. This drift cannot be corrected simply by increasing measurement precision or refining

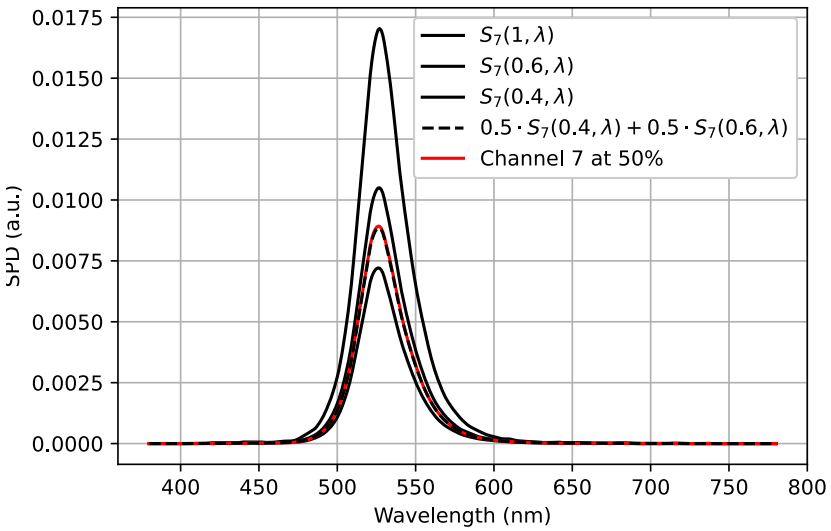

Figure 5.5: Comparison between the complex approximation and the measured SPD.

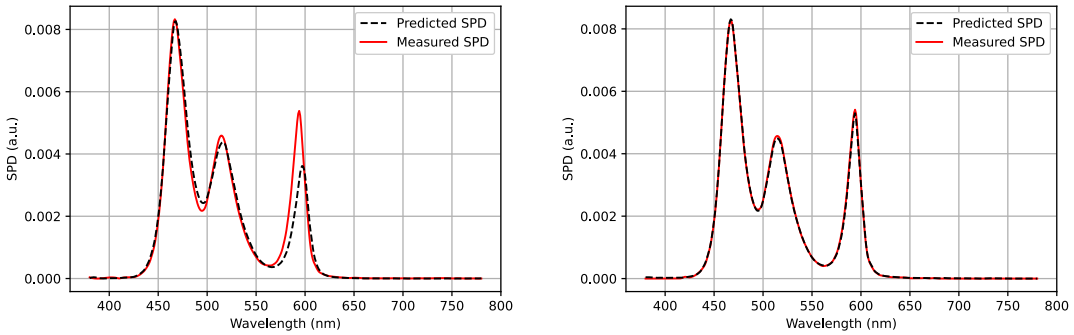

(a) Prediction with the linear approximation. (b) Prediction with the complex approximation.

Figure 5.6: Comparison of the two approximation methods.

the matching algorithm, since it is tied to the properties of LEDs: their spectral power distribution and light efficacy are inherently dependent on junction temperature. To achieve full real-time control of the emitted light, particularly for use in psychophysical experiments, a dedicated light stabilization system was therefore developed. The following section details the design and implementation of this stabilization algorithm.

5.2 LED Light Stabilization Algorithm

Although the algorithm described in the previous section, and more specifically the complex version, allows us to produce spectra that match accurately the desired chromaticity, it cannot take into account the variation of light produced by LEDs as their junction temperature rises. In practice, the spectral output and intensity of an LED change as its junction temperature rises, and the magnitude of this effect can vary from one LED to another leading to a drift of the chromaticity of the light output.

The next step in this research is to conduct a psychophysical experiment to assess human observers ability to discriminate small color differences under a given lighting condition. In this context, maintaining a stable and controlled light source is essential. In this section, we detail a method for stabilizing multi-LED illuminants that we have developed specifically for the experimental protocol that will be described in chapter 6.

5.2.1 Junction temperature and influence on the light output

To design an effective stabilization method, it is first necessary to understand how LED junction temperature affects light output. This subsection reviews the influence of temperature on both spectral distribution and luminous efficacy of the individual channels.

The measurement values obtained at the minimum (30° C) and the maximum (45° C) temperature of the heatsink are summarized in Table 5.1. The measurement results clearly show that temperature affects all channels to varying degrees.

Channels V1 to B1 are less sensitive and have reduced loss of luminous efficacy and no perceptible spectral shift. B2 to G2 have a more pronounced loss of luminous efficacy as well as a slight spectral shift. Channels L to FR3 exhibit significant intensity loss, reaching a maximum of 30% on channel R1, accompanied by a significant spectral shift towards the longer wavelengths of the visible range. This shift is gradual with increasing temperature (noted as "grad" in Table 5.1).

Additionally, peak amplitude was measured to check its proportionality with the drive level at different temperatures. It was confirmed that all selected channels exhibit almost linear properties, although the slope decreases with decreasing luminous efficacy.

These variations induce both a color shift as well as a decrease in illuminance which could influence the results of a psychophysical experiment. To illustrate this effect, an X-Rite ColorChecker chart was photographed under LED illumination closely matching a D65 illuminant. The chart was first captured immediately after the panel was switched on and then again after 30 minutes of continuous operation. Figure 5.7 shows the corresponding $\Delta_{E,00}$ color differences between the two images.

5.2.2 Theoretical optimization

In theory, as discussed previously, with a comprehensive characterization of the device and a detailed understanding of all relevant parameters, it would be possible to accurately predict the input drive levels required to replicate a target spectrum.

Table 5.1: Characterization of the 13 selected channels (Subsection 2.3.2).

	RB1	RB2	B1	B2	C	G1	G2
Peak wavelength (nm)	441	454	468	478	500	517	528
Amplitude attenuation	4%	3%	4%	5%	16%	1%	15%
Peak shift (nm)	no	no	no	<10	<10	<10	<10

	PC-A	OR	R1	R2	DR1	L
Peak wavelength (nm)	594	624	636	654	686	544
Amplitude attenuation	8%	27%	30%	28%	6%	2%
Peak shift	grad	grad	grad	grad	grad	grad

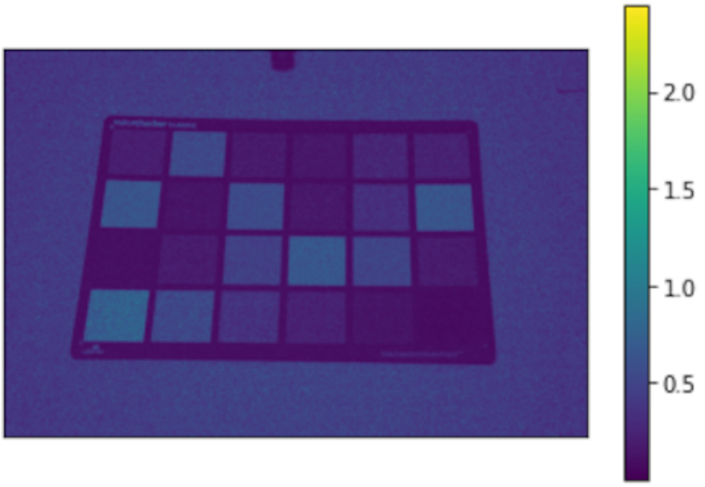

Figure 5.7: $\Delta_{E,00}$ difference after 30 minutes.

Since the output of an LED device is the combined emission of its individual channels, the precise output can be predicted using the following calculation:

$$\forall \lambda \in [380, 780], S_{T,I}(\lambda) = \sum_{i=0}^{L-1} S^i_{T^i,I^i}(\lambda) \tag{5.12}$$

where λ is the wavelength ranging from 380 to 780 nm, L is the number of channels and $S^i_{T^i,I^i}(\lambda)$ is the spectral distribution of the i^{th} channel at temperature T^i and drive level I^i.

Different types of minimization can then be performed. Both Mean Squared Error

(MSE) and Mean Absolute Error (MAE) were evaluated. No significant differences were noticed in stabilization performance. Consequently, MSE was selected for this task:

$$I^{new} = \min_{I} \int_{380}^{780} \left(Ta(\lambda) - \sum_{i=0}^{L-1} S^i_{T^i,I^i}(\lambda) \right)^2 d\lambda \tag{5.13}$$

with $Ta(\lambda)$ the target SPD to match.

However, in the absence of a complete device characterization, the values of $S^i_{T^i,I^i}(\lambda)$ cannot be directly obtained. Since a full characterization is not realistic, a method was developed that requires only a single measurement per channel at maximum intensity. The following subsection first introduce the approach used to approximate these values by estimating the effect of increasing junction temperature for each individual channel.

5.2.3 Approximation of the impact of the temperature

It is possible to approximate the output of a LED at any drive level using the spectrum of the output of the maximum drive level with a linear approximation (Subsection 5.1.1):

$$S_{T_0,I_0}(\lambda) = I_0 S_{T_0,1}(\lambda) \tag{5.14}$$

with $S_{T_0,I_0}(\lambda)$ the SPD of an LED at the temperature T_0 and drive level I_0, and $S_{T_0,1}(\lambda)$ the SPD at its maximum drive level.

The main limitation of this approximation is its viability only under constant temperature conditions. However, we can model the impact of temperature on channel output can be represented by incorporating an intensity offset dI and a wavelength offset $d\lambda$ such as:

$$S^i_{T_1,I_0}(\lambda) = (I^i_0 + dI^i) S^i_{T_0,1}(\lambda + d\lambda^i)$$

We can obtain these deviations by minimizing the MSE criterion with a single measurement of the device output.

$$(dI_{min}, d\lambda_{min}) = \min_{dI,d\lambda} \int_{380}^{780} \left(M(\lambda) - \sum_{i=0}^{L-1} (I^i + dI^i) S^i_{T_0,1}(\lambda + d\lambda^i) \right)^2 d\lambda \tag{5.15}$$

with $M(\lambda)$ the measured spectrum.

This approximation makes it possible to evaluate the impact of both peak intensity reduction and spectral shift for each individual channel. This is achieved by only measuring the total light output of the panel and estimating the spectral power distribution of the individual channels by comparing it with the measurements done during the short characterization process, effectively updating the measurements used for the prediction as will be shown in the next subsection.

5.2.4 Optimization of the drive levels

Ultimately, to determine the updated drive levels, we propose to simply substitute the theoretical values in Eq. 5.13 with the approximation obtained with Eq. 5.15:

$$I^{new} = \min_{I} \int_{380}^{780} \left(Ta(\lambda) - \sum_{i=0}^{L-1} (I^i + dI^i_{min}) S^i_{T_0,1}(\lambda + d\lambda^i_{min}) \right)^2 d\lambda \tag{5.16}$$

with $Ta(\lambda)$ the target spectrum.

This minimization procedure provides a prediction of the required drive levels to achieve a spectral match to the target, based on the updated approximations of the spectral power distributions of the individual channels. To illustrate the performance of the algorithm, the following subsection presents several examples using different target spectra.

5.2.5 Stabilization results

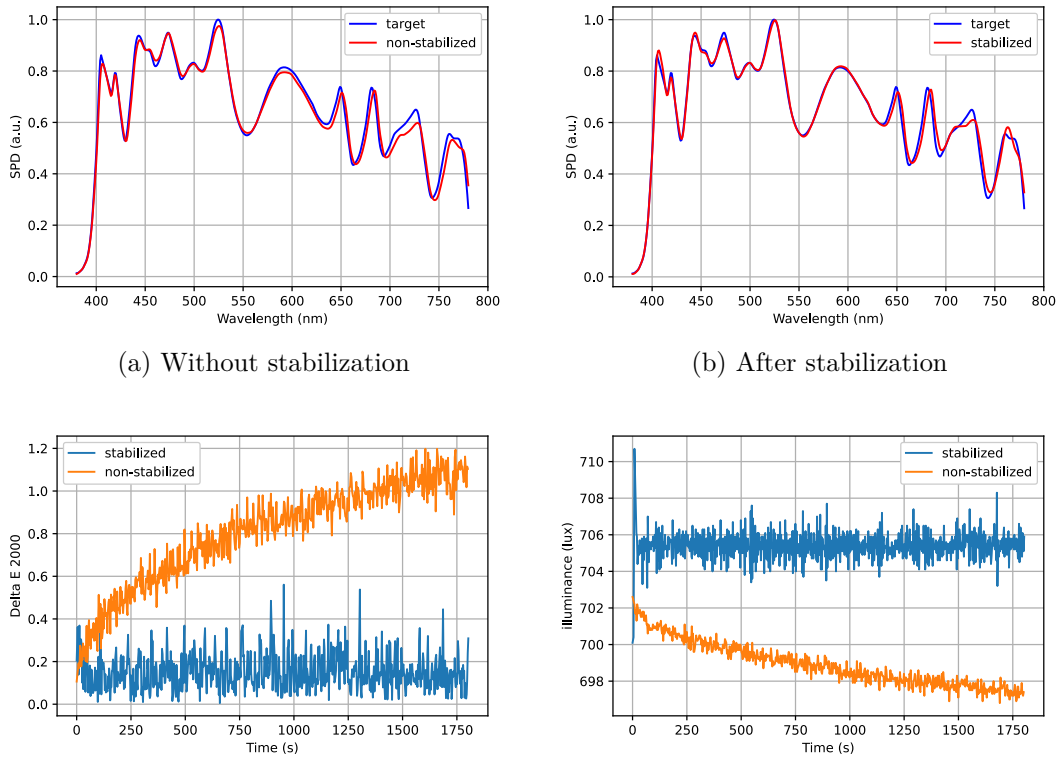

(a) Without stabilization

(b) After stabilization

(c) Evolution of the ΔE_{00} differences.

(d) Evolution of the illuminance.

Figure 5.8: Comparison of the output with (blue chart) and without (orange chart) stabilization for illuminant D65.

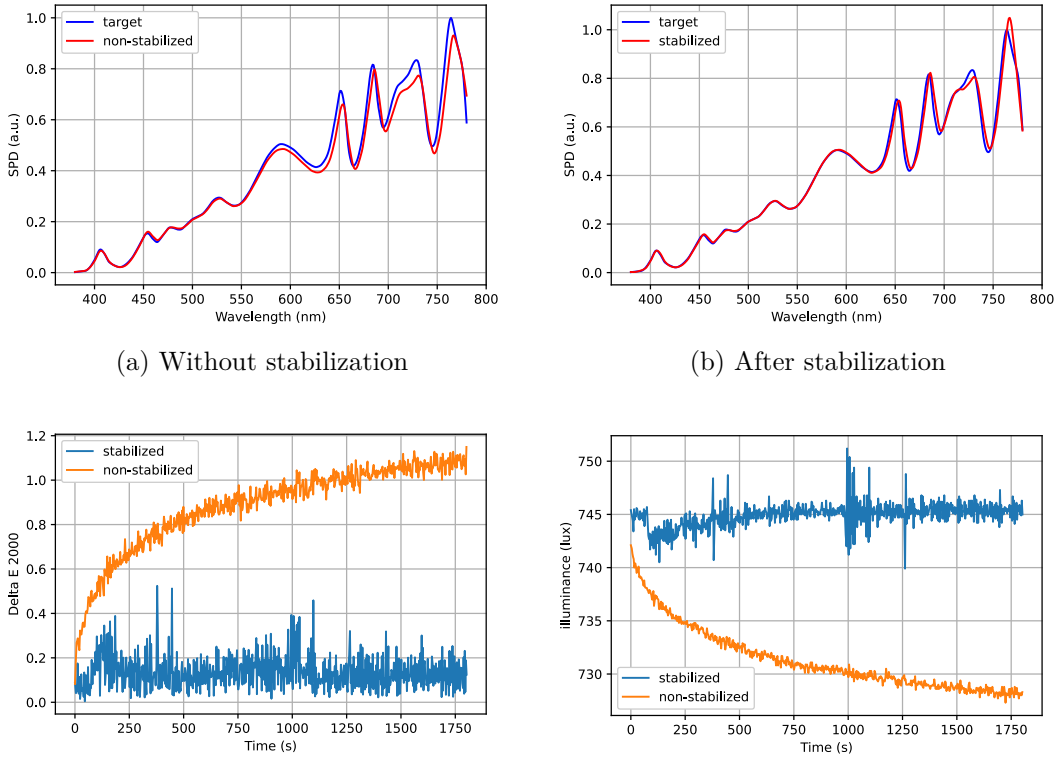

(a) Without stabilization

(b) After stabilization

(c) Evolution of the ΔE_{00} differences.

(d) Evolution of the illuminance.

Figure 5.9: Comparison of the output with (blue chart) and without (orange chart) stabilization for Illuminant A.

The algorithm was validated using several spectral power distributions (SPDs). The best performance was observed when all channels were active as this provides greater flexibility for corrections. Figures 5.8 and 5.9 show two examples of SPDs close to the illuminant D65 and illuminant A, respectively. Figures 5.8a and 5.9a highlight a significant spectral shift away from the target when the light output is not stabilized. This shift is particularly noticeable in the channels corresponding to longer wavelengths as they are more sensitive to heat. In contrast, Figures 5.8b and 5.9b illustrate how the stabilisation algorithm improves the spectral match between the light output and the target spectrum. This improvement in spectral matching comes with a decrease in color differences relative to the target as shown in Figures 5.8c and 5.9c. In these two examples, the not stabilized light output exhibits a ΔE_{00} color difference exceeding 1 which corresponds to a perceptible color difference. With stabilization, the ΔE_{00} is reduced to a value below 0.4 making the color difference imperceptible. Additionally, the illuminance is stabilized as illustrated in Figures 5.8d and 5.9d.

5.2.6 Limits and possible improvements

Although the stabilization algorithm presented in this section improves greatly the accuracy of the light output, several practical considerations should be noted when using it.

The first point concerns the gradual decrease in brightness of a channel as its temperature rises. While this effect can generally be mitigated by incrementally increasing the drive level, the compensation becomes impossible when a channel is already operating at 100% output, a situation that can occur when producing white light at high illuminance levels. A practical approach to address this issue is to include a margin when selecting the target spectrum, ensuring that stabilization can be achieved without exceeding the maximum output of the channels.

The second point relates to spectral shifts of the LED channels. Certain channels are more prone to drift toward longer wavelengths during operation, which can influence color stability. The algorithm maintains the spectral match by dynamically adjusting the drive levels of individual channels, therefore it performs particularly well for spectra that use multiple overlapping channels and should be applied with care for spectra that feature narrow or isolated peaks.

Finally, the third consideration is linked to the algorithms optimization criterion. When a perfect spectral match cannot be maintained, the algorithm minimizes the spectral difference, without taking into account the resulting perceptual color of the light. In such cases, the correction process may prioritize spectral fit over small color deviations, and users should be aware of this trade-off when using this algorithm.

To address these limitations, future work could involve designing a more sophisticated cost function that takes into account both the minimization spectral and color differences. Another idea would be the real-time integration of the algorithm proposed by Finlayson et al. which could be implemented to dynamically compute the metameric set and select the optimal trade-off between spectral accuracy and color fidelity.

5.2.7 Combined operation of the light mixing and stabilization algorithms

The use of both previously described algorithms allowed us to produce a highly accurate white light output on the Telelumen LED panel. This gives us the ability to generate and maintain accurate white light conditions which is one of the main requirements for the psychophysical experiment presented in the next chapter. By ensuring both spectral accuracy and stability over time, the combined use of both of these algorithms give us the the ability to conduct experiments in rigorous conditions.

The procedure to generate the lights used in further experiments can be summarized as follows: the light mixing algorithm was first used to explore the full range of spectra that could be produced by the LED panel. This process made it possible to select and define specific target spectra to use in the experiment. Then, the light stabilization algorithm was applied to optimize the drive levels sent to the panel, ensuring the produced light closely matched the desired targets. Finally, this algorithm operated continuously in a feedback loop during the experimental sessions, compensating for variations such as the gradual temperature increase of the LED channels that could otherwise bias the light output.

Another significant advantage of the light stabilization algorithm was its ability to effectively correct the nonlinear behavior inherent to the LED channels. This correction allowed us to use the simplified version of the light mixing algorithm without compromising spectral accuracy.

5.3 Chapter Summary

This chapter presents the pipeline that was developed to be able to compute all lights that we would be able to produce and use, given the spectrally tunable LED system that is available for this study.

First, the algorithm presented by Finlayson et al. was presented and successfully implemented both in its simple version and a more complex and accurate version. This algorithm is particularly important in this work since it allows us to compute the full metamer set, i.e. all the lights that match a given chromaticity, with any set of active LED channels. This algorithm was used to good extent in the next chapter as it was the way to explore exhaustively all the lights we could use. Moreover, since we want to investigate the influence of spectral power distribution on color discrimination, we decided to select lights with the same chromaticity.

The complete characterization procedure presented in Chapter 2 showed that rising temperature of the device influenced the light output of the LED channels, furthermore, the extent and nature of this modification is different depending on the channel considered. Therefore, no characterization procedure, even extremely precise, could allow us to have a stable light output during extended periods of time, which would be necessary for psychophysical experiment sessions. Therefore, a light matching and stabilization algorithm was devised, that uses only a single measurement of each of the channels. This algorithm was first presented at the Computational Color and Imaging Workshop (CCIW) in Milan in September 2024 and was subsequently featured in an article published in the Journal of Imaging [2].

Finally, this chapter showed that the combined use of the two previously mentioned algorithm allowed for simple management of the LED panel output: the metamer computation set allows to explore and find drive levels that match a desired chromaticity, while the light matching and stabilization algorithm helps maintain the light output to the desired target spectrum. This ability to conduct experiment under highly controlled lighting conditions are instrumental to the final set of psychophysical experiments that will be presented in the next chapter.

Chapter 6

Color Discrimination under White Light in Simulated Low Vision Conditions

The next step of this study was to design different spectra of white light with the objective of increasing color discrimination ability. To do that, we needed to propose a psychophysical experiment that would be both quick and accurate. However, preliminary tests showed that fast arrangement tests like what was done in the experiment of Chapter 4 were too simple under white light even for low vision conditions, therefore a new type of experiment was needed. This chapter presents the final phase of this thesis, which integrates all previous developments into a psychophysical experiment with the objective of identifying an optimized light spectrum able to enhance color discrimination abilities for individuals with low vision.

In order to achieve this goal, a new experimental protocol has been developed based on a simple color discrimination task. By using pairs of closely related color samples to assess the ability of participants to distinguish subtle chromatic differences under different lighting conditions. To ensure rigorous experimental conditions and reproducibility, a detailed procedure was established to calibrate an inkjet printer for the production of customized color samples. Furthermore, the LED stabilization method described in Chapter 5 was employed to maintain consistent lighting conditions during the experiment.

The color management process of the inkjet printer is detailed in Section 6.1, followed by details on the design of the experimental protocol in Section 6.2. Next, section 6.3 presents the pilot experiment that was conducted without simulation goggles to confirm the ability of the experiment to assess color discrimination ability under varying lighting conditions. Finally, the experiment that was conducted with simulation goggles is described in Section 6.4.

6.1 Methods Used for the Selection of Color Pairs

To conduct a psychophysical experiment on color vision, one approach involves using pairs of color samples [177, 140, 141], each consisting of two color patches with small color differences.

Two main options can be considered: either using pre-existing standard color patches (e.g., Pantone, Munsell Book of Color, RAL colors) or creating custom patches using a colorimetrically calibrated printer. The first option provides only limited control over the characteristics of the patches, making it less flexible for specific experimental needs. The second option, more suitable for experiments on color vision, involves printing custom color patches with an inkjet printer designed for high-quality photographic printing. For our study, we selected the Canon image PROGRAF PRO-300, which uses 10 color ink cartridges. The patches were printed on matte paper, an ideal choice for the goals of a color discrimination experiment.

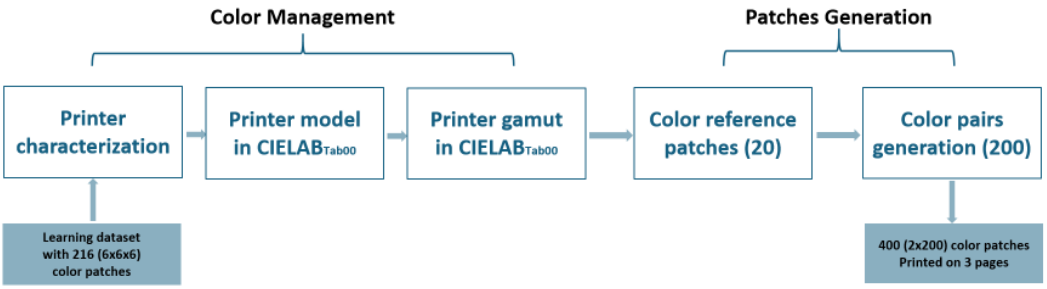

Figure 6.1: The different steps of the color workflow used to print color pairs. 20 reference colors were selected, then 10 color values were generated for each reference colors, which resulted in the printing of 400 colored patches forming 200 color pairs. See details in Sub-Section 6.1.5.

In the following subsections, we detail the new method we propose for sampling the printer's color gamut to generate N reference color patches from a selected sampling grid where all neighbours of an element of the grid are equidistant for a chosen color distance formula.

We also introduce an additional method designed to select pairs of color samples that are equidistant and colorimetrically close (see Figure 6.1). For both methods, we used the printer's native RGB color space to produce the targeted color patches. This approach bypasses the default color management of the operating system, giving us more precise control over the printed samples.

6.1.1 Sampling $CIELAB$ color space with $CIEDE00$ metrics

The $CIEDE00$ (ΔE_{00}) metric is widely considered as one of the most accurate methods for assessing just noticeable color differences [178]. Even if other metrics have been introduced recently [141] we used it to evaluate small color differences between color

patches. $CIEDE00$ is a color difference formula specifically designed to account for the non-uniformity of the $CIELAB$ color space in regards to lightness, chroma and hue differences [179]. However, one main limitation of the $CIEDE00$ metric is its lack of Euclidean structure [178, 180, 181]. This limitation complicates its application in some computational tasks, such as uniform sampling within a color space, where it is essential to generate color patches that are equidistant from one another in a colorimetric sense based on a defined sampling grid.

Sampling based on non-Euclidean Color Difference Formulas (CDFs) presents numerous challenges [182, 183]. Colantoni et al. proposed a robust algorithmic method in [184] to sample the $CIELAB$ color space with a non-Euclidean CDF allowing the use of the Euclidean metric for a chosen CDF. This approach relies on a tabulated sampling of the $CIELAB$ color space[1] derived from the $CIEDE00$ distance which has been used to define the base color values of the patches required to carry out the psychophysical experience described in Section 6.3.

The sampling forms a cubic grid of size $(152 \times 321 \times 312)$. Each element of the grid corresponds to a $CIELAB$ color (defined by its (L^*, a^*, b^*) coordinates), ensuring that the $CIEDE00$ distance from its 6 neighbours is equal to 0.5. This grid is centered on the color coordinate $(50, 0, 0)$ and serves as the basis for a new tabulated color space named $CIELAB_{Tab00}$. Figure 6.2 illustrates the distribution of the tabulated color values in the chromatic diagram (a^*, b^*), highlighting a red zone where calculated values are sub-optimal. For further details on the accuracy of this sampling, refer to [184].

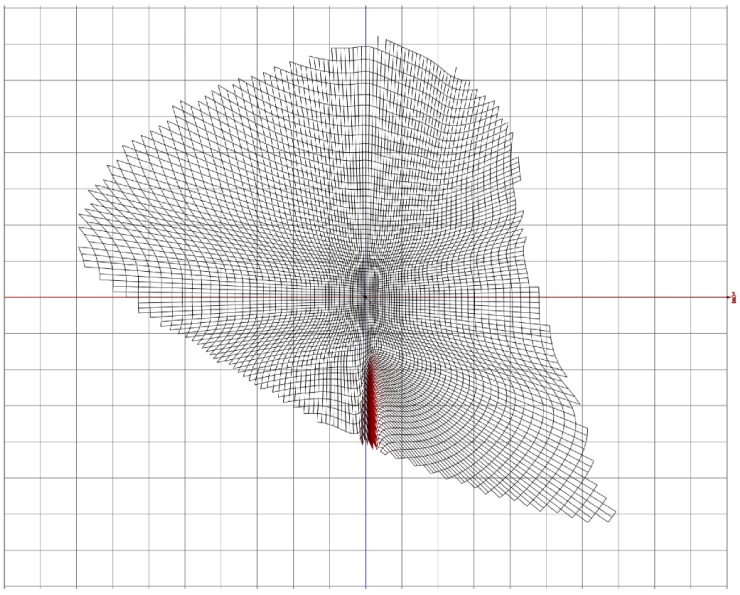

Figure 6.2: The distance is here set to 1 to visualize a slice of the $CIELAB_{Tab00}$ tabulated values in the chromatic plane $(a*, b*)$ of the $CIELAB$ color space. Image from [184].

[1]The corresponding color values for this sampling are available at: `https://www.couleur.org/deltaE/d00.h`

To convert color values from this $CIELAB_{Tab00}$ tabulated color space into (L^*, a^*, b^*) coordinates, we use the values from the grid combined with a trilinear interpolation. Image from [184].

For the inverse transformation from (L^*, a^*, b^*) coordinates to tabulated $CIELAB_{Tab00}$ color values, we construct a tetrahedral structure from the original sampling grid by dividing each cube into 6 tetrahedra. When converting a (L^*, a^*, b^*) color, we first identify the tetrahedron containing the color and then apply tetrahedral interpolation to calculate the corresponding $CIELAB_{Tab00}$ tabulated color value.

6.1.2 Color management

Printer color management techniques rely on either traditional methods such as those described in [185] or machine learning approaches [186, 187]. These techniques use standardized color profiles, mainly ICC and iccMAX profiles [188, 189], or direct measurements of pre-printed color patches. Their goal is to maximize the colorimetric capabilities of the device and, most importantly, ensure consistent color reproduction across various devices.

As stated previously, we chose to work within the printer's RGB color space. This RGB color space is influenced not only by the printer hardware but also by the color management system implemented by the operating system driving the printer (in this case, Windows 10). To link the RGB values used to control the printing of selected color patches (i.e. those defined by the tabulated color space $CIELAB_{Tab00}$) to the measurements derived from their printing, it is essential to implement a color management system that is both accurate and straightforward. To achieve this, we propose a method originally designed for characterizing and calibrating monitors.

Printer characterization and color profiles

To characterize the printer, we used the color management process introduced in [190].This robust method, originally designed for displays, is essential for achieving accurate cross-media color reproduction. The technique introduced aims to predict displayed color stimuli from given RGB inputs using polyharmonic spline interpolation for the forward direction (RBG to $CIELAB$) and tetrahedral interpolation for the backward direction ($CIELAB$ to RGB) (see Figure 6.3). This approach relies on an optimally optimized set of color patches measured on a screen, enhancing accuracy without technology-specific assumptions. The forward model mapped RGB inputs to the $CIELAB$ color space, while the backward model enable to compute RGB values for specific $CIELAB$ targets. An iterative selection of color patches improves the training data set, thereby refining model precision across various displays. However, since the dynamic selection of color patches is not possible for printers, as in [190] we opted for a straightforward discretization of the RGB space. For the training set, we used 216 patches arranged in a $(6 \times 6 \times 6)$ grid. For the test set, we used 125 patches in a $(5 \times 5 \times 5)$ grid (see Figure 6.4).

After printing the $216 + 125$ patches on matte paper, we measured them using a spectrocolorimeter (I1 Pro 3 from X-Rite) and used the resulting reflectance factors to obtain the $CIEXYZ$ and $CIELAB$ values under illuminant D65, chosen as the reference illuminant. Based on the 125 test patches, we estimated the optimal parameters for the

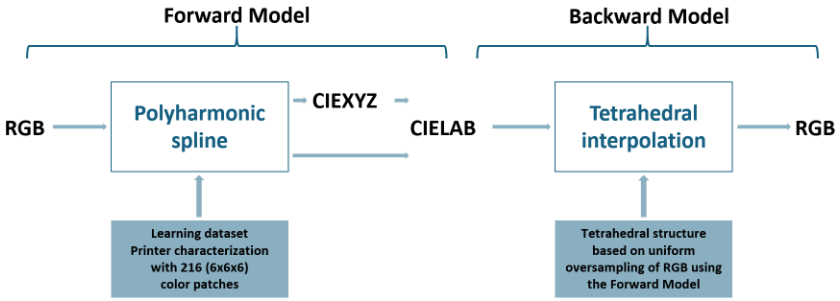

Figure 6.3: Forward and backward models. Image from [184]

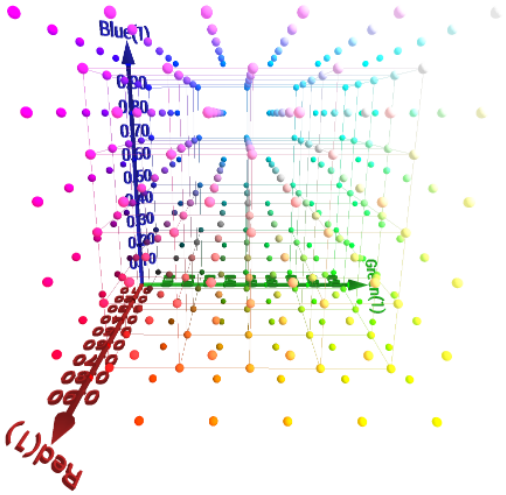

Figure 6.4: *RGB* color space discretization with $216 + 125$ patches. The 125 patches correspond to color samples linked by segments. Image from [184]

forward model (also used for the backward model): the polyharmonic kernel (linear, cubic or thin-plate), the target space ($CIELAB$ or $CIEXYZ$) and the smoothing factor.

Our forward model uses $CIELAB$ as default target. This does not imply that we have to use this space as target for the polyharmonic kernel. In fact, we considered two choices. We can use either $CIELAB$, which seems to be the most logical target, or $CIEXYZ$ associated with a (X, Y, Z) to (L^*, a^*, b^*) color transformation. The use of different color spaces as targets gives us another degree of freedom. We estimated the forward model for the three possible kernels and the two target color spaces ($CIEXYZ$ and $CIELAB$) across a range of smoothing factor values. The model that minimizes the mean ΔE_{00} error was selected as the optimal configuration. For the printer used in this study, the optimal parameters are the following:

- Polyharmonic kernel: Cubic
- Target space: $CIEXYZ$

- Smoothing factor: 0.0025

The average, maximum errors and the 95 percentile of the corresponding forward and backward models are presented in Table 6.1. Figure 6.5 illustrates the error for each color of the test set compared to the corresponding estimated values.

Table 6.1: Comparison of errors using **CIEDE76** and **CIEDE00** metrics

Metric	**CIEDE76**	**CIEDE00**
Forward model		
ΔE - Mean	1.56	0.83
ΔE - Max	7.01	5.56
ΔE - 95 percentile	3.57	1.66
Backward model		
ΔRGB - Mean	0.03	0.03
ΔRGB - Max	0.15	0.15
ΔRGB - 95 percentile	0.10	0.10

After determining the optimal parameters, we generated a profile file containing all 341 RGB, $CIEXYZ$, and $CIELAB$ values from the characterization, as well as the model parameters.

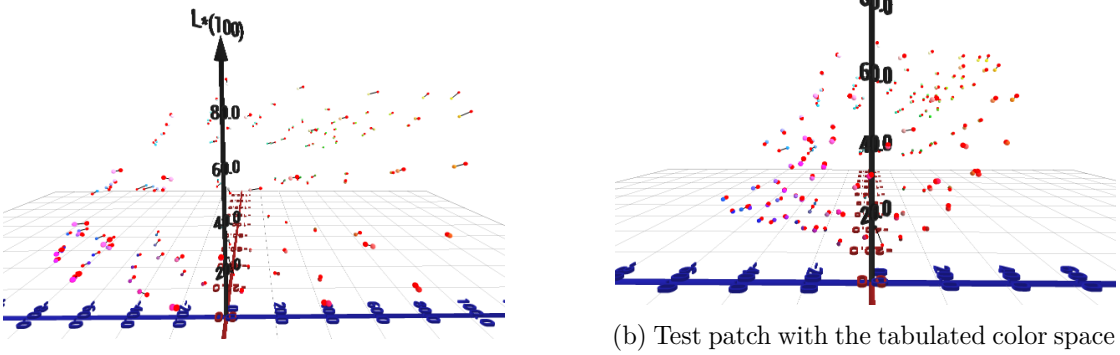

(a) Test patch errors with $CIELAB$.

(b) Test patch with the tabulated color space $CIELAB_{Tab00}$.

Figure 6.5: Test patch errors with $CIELAB$ and with the tabulated color space $CIELAB_{Tab00}$. The red spheres correspond to the colors estimated by the proposed forward model.

Gamut in $CIELAB$ and $CIELAB_{Tab00}$

This profile allows the computation of the 3D mesh corresponding to the gamut of the printer used in $CIELAB$ (see Figures 6.6a and 6.6b) as well as in the tabulated color space $CIELAB_{Tab00}$ (see Figures 6.6c and 6.6d), using a fine sampling of the RGB cube.

As shown in Figure 6.6 the gamut volume of the printer is smaller in the tabulated color space $CIELAB_{Tab00}$ than in $CIELAB$.

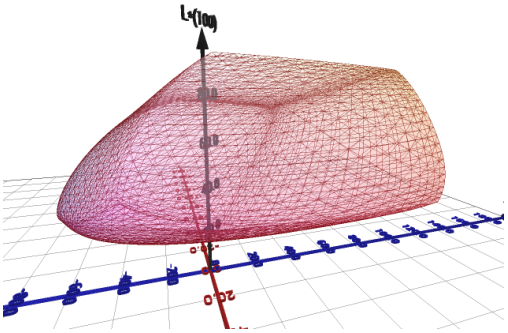

(a) Printer gamut in $CIELAB$ (first view)

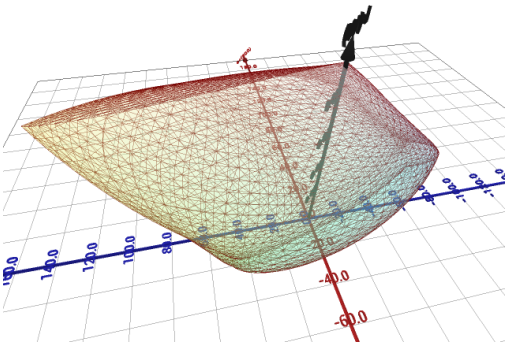

(b) Printer gamut in $CIELAB$ (second view)

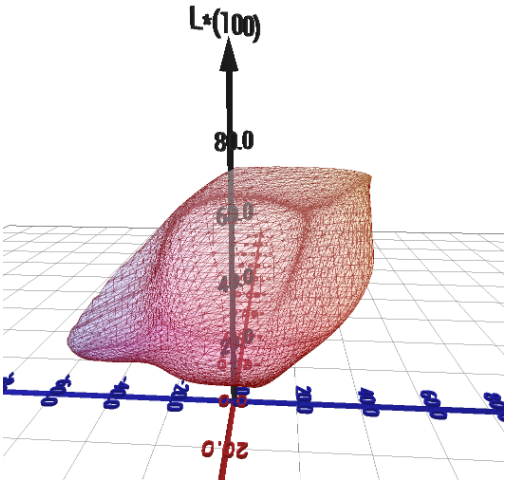

(c) Printer gamut in tabulated color space $CIELAB_{Tab00}$ (first view)

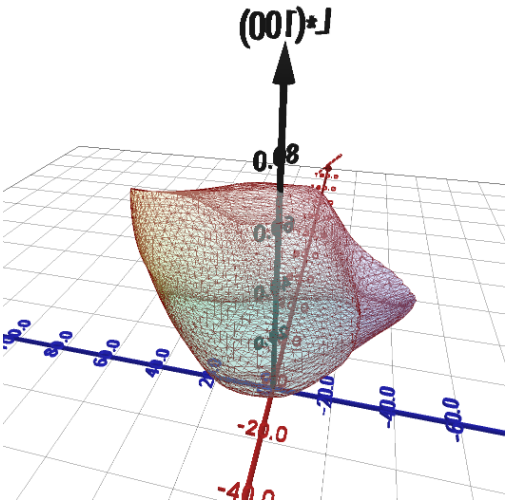

(d) Printer gamut in tabulated color space $CIELAB_{Tab00}$ (second view)

Figure 6.6: Printer gamut comparison in $CIELAB$ and $CIELAB_{Tab00}$

The fine sampling of the RGB cube is the same as the one used to generate the set of tetrahedra that we used for the forward model. This set of tetrahedra can also be used to determine if a $CIELAB$ and $CIELAB_{Tab00}$ triplet is within the gamut of the printer.

6.1.3 Selection of color reference patches

The methodologies detailed above provide both the colorimetric and color management tools needed to select the N reference colors required to create the targeted pairs of color samples. Since we chose to use the full color gamut of the printer to select the reference

patches, we opted for the most uniform sampling method available in the state of the art: the Kepler hexagonal stacking approach [191].

The Kepler hexagonal stack, also known as hexagonal, is particularly well-suited for discretizing a 3D space due to its optimal packing efficiency and geometric properties. This arrangement forms a highly regular and repetitive structure where each sphere is surrounded by 12 other spheres at equal distances, ensuring uniform distribution with maximum packing density.

To generate a set of colors centered on a reference color C, all spaced at a distance D within the $CIELAB$ color space or the tabulated color space $CIELAB_{Tab00}$, we used the algorithm described in the appendix of [190] (see Figure 6.7).

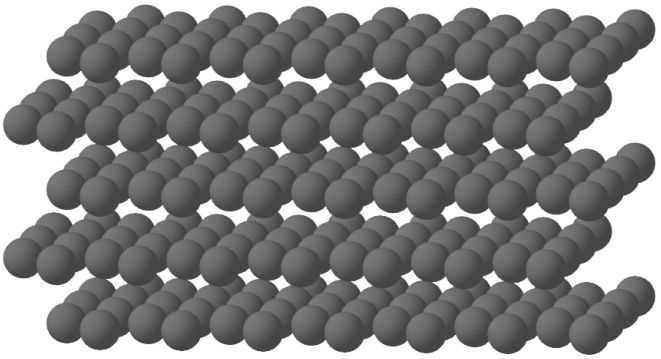

Figure 6.7: Kepler hexagonal stack

Since the printer can only reproduce colors that fall within its gamut, we set up a simple dichotomous algorithm to determine the distance D at which N colors from a Kepler stack remain within the printers gamut in the tabulated color space $CIELAB_{Tab00}$. To verify whether a color lies within the gamut, we used the tetrahedral structure created for the proposed backward model.

6.1.4 Experimental results for 20 reference patches

Figure 6.8 illustrates the results obtained when only 20 color patches are placed within the $CIELAB$ and $CIELAB_{Tab00}$ gamuts of the printer. When the reference patches are positioned in the $CIELAB_{Tab00}$ gamut the theoretical $\Delta_{E,00}$ color difference between adjacent reference colors is of 21.29.

To demonstrate the validity of the proposed methodology, we used the backward model to convert the 20 reference patch colors from the tabulated color space $CIELAB_{Tab00}$ into their corresponding RGB values. These RGB colors were then printed and measured. Figure 6.9 shows the measured colors in the tabulated color space $CIELAB_{Tab00}$ and the corresponding hexagonal grid. The average $\Delta_{E,00}$ distance within this grid is of 20.91 with a minimum distance of 18.16 and a maximum distance of 24.61.

These measured values show that despite the complexity of the different steps required to produce the reference patches, the proposed methodology successfully generates colors that are all equidistant within the gamut of the printer.

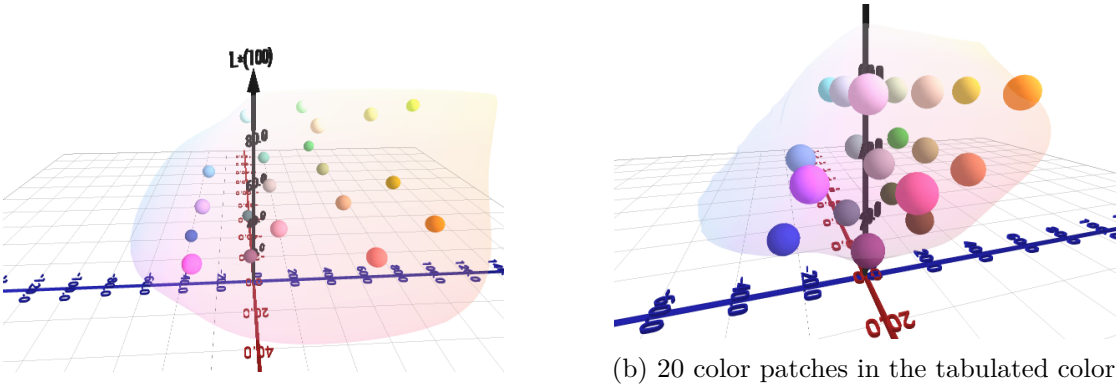

(a) 20 color patches in $CIELAB$

(b) 20 color patches in the tabulated color space $CIELAB_{Tab00}$.

Figure 6.8: Generated color patches in $CIELAB$ and the tabulated color space $CIELAB_{Tab00}$.

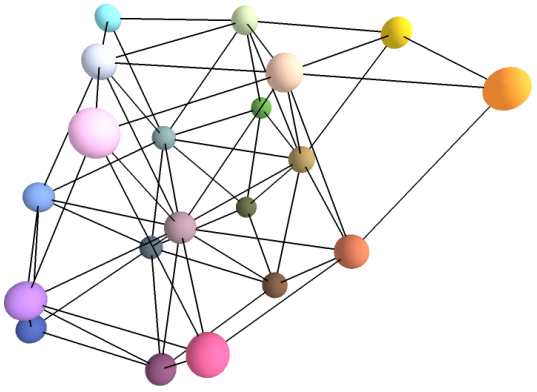

Figure 6.9: Measured grid (for 20 reference patches)

6.1.5 Generation of color pairs

We now propose to generate 10 color values for each reference color, with a normal distribution of ΔE_{00} color distance from each reference color, which will be paired and used in the discrimination experiment that we wish to perform in the next phase of this research.

The objective was to make a compromise between the number of pairs of test samples (20 reference colors $\times 10$ closely related colors) needed to perform a psychophysical experiment based on color discrimination and the duration of such an experiment.

Two main choices have been made in generating the color of these pairs of test patches: first, the perceptual lightness L^* was kept the same as the reference color; second, the equidistant colors were selected randomly in the neighbourhood of the corresponding reference color to avoid prioritizing any particular direction on the chromatic plane a^*b^*.

Since we are working in the tabulated color space $CIELAB_{Tab00}$, in this space the ΔE_{00} color distance is equivalent to the Euclidean distance.

To obtain a set of colors with a normal distribution of ΔE_{00} around the reference color, we simply sampled the tabulated color space $CIELAB_{Tab00}$ with a normal distribution of Euclidean distances to the reference colors. The direction in the a^*b^* plane was selected randomly using a uniform distribution.

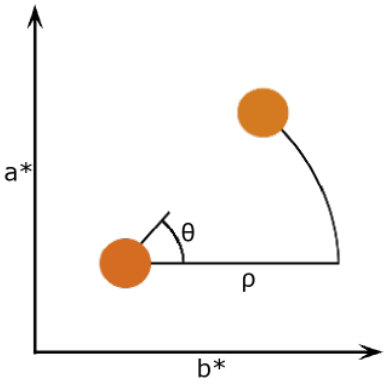

(a) Generation of equidistant colors.

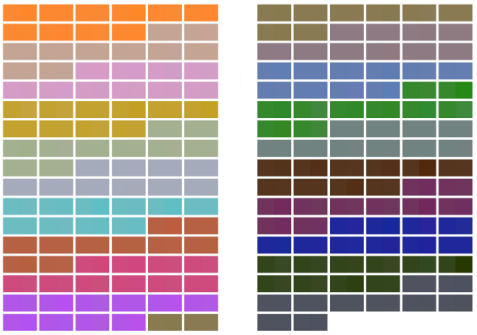

(b) The 200 pairs of square color samples printed (10 pairs per color, with the reference sample on the left).

Figure 6.10: Generation of color pairs.

For a reference color $(L^*_{ref}, a^*_{ref}, b^*_{ref})$, a closely related color (L^*, a^*, b^*) is obtained as follows:

$$\begin{cases} L^* = L^*_{ref} \\ a^* = a^*_{ref} + \rho * \sin\theta \\ b^* = b^*_{ref} + \rho * \cos\theta \end{cases} \tag{6.1}$$

with $\rho \sim \mathcal{N}(\mu, \sigma^2)$ and $\theta \sim \mathcal{U}(0, 2\pi)$. $\mathcal{N}$ and $\mathcal{U}$ are the normal and uniform distributions, respectively. The mean and standard deviation μ and σ were chosen to be set at 0.6 and 0.4 respectively in order to obtain colors that are close to but varied from the reference color (see Figure 6.10a).

The 200 pairs of samples (10 pairs of color per reference color, see Figure 6.10b) were printed on high quality paper at a size of $1.4cm \times 1.4cm$. They were then measured with a spectrophotometer. The spectrophotometer was set to perform three consecutive measurements for a given location and return the average. We made also five measurements at five different locations on each of the 400 patches (four in the corners and one in the middle), to optimize the accuracy of the measurements.

In Figure 6.11, we show the ΔE_{00} values for the 20 selected reference patches. The accuracy of the colors printed depends of the reference colors used (as an example, see color differences reference colors 5 and 15). If for a reference color all ΔE_{00} values are lower than 1 then we can consider that there is no noticeable difference between the

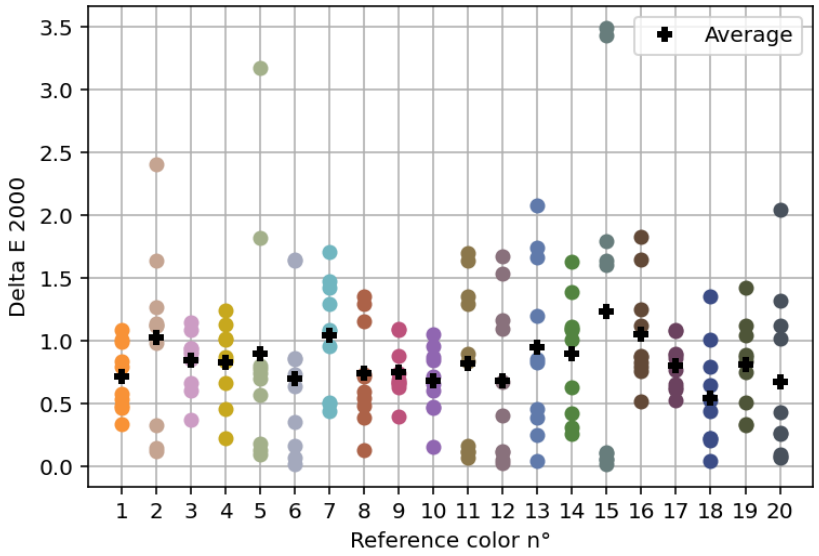

Figure 6.11: Distance between each printed color sample and the reference color.

reference color and the printed color patches which are then considered as equidistant to the reference color (e.g. reference colors 5 and 6). 66% of printed patches satisfied this criterion. If for a reference color a ΔE_{00} value is higher than 2 then we can consider that there is a significant difference between the reference color and the printed color patch (e.g. for reference colors 15 two color patches are concerned). Very few printed patches were concerned (3%), few more had a ΔE_{00} between 1.5 and 2 (8.5%). This demonstrates that the method proposed to print equidistant colors with small color differences is efficient and can be used to produce pairs of color patches that could be used to perform color discrimination experiment.

6.1.6 Printing stability

To assess the stability of the prints over time, we produced a page containing 20 color patches (one patch per reference color). After a drying period of one week, these patches were measured weekly over one month. No significant changes were observed in the measurements, all of which remained within the tolerance range of the spectrocolorimeter (with an average ΔE_{00} error of .2). However, we re-measured the color patches before starting psychophysical experiments.

6.2 Protocol proposed for the color discrimination experiment

The main constraint in designing this experiment was to ensure simplicity for future participants. The proposed protocol requires participants to observe a pair of color patches

and indicate whether they can distinguish between the two colors. Such an approach allows participants to focus solely on the task of color discrimination. By eliminating the need to pre-order the samples, the protocol significantly reduces the duration of the experiment and discard the need for a complex sample-feeding system. To achieve this, the color pairs are placed on a thick cardboard support covered with neutral grey paper for easy handling. In order to uniquely identify each color pair being examined by a participant, a ArUco marker is printed on the support. This type of marker can be easily detected using a camera and an example can be seen on Figure 6.13

The experimental setup was designed to be as simple as possible: a box containing all pairs of samples not yet examined; a holder for the pair currently under examination; and a box for discarding pairs that have already been examined. Additionally, a three-button keypad is connected to a computer equipped with a camera to read the ArUco markers, allowing the recording of participants' responses. This setup is illustrated in Figure 6.12.

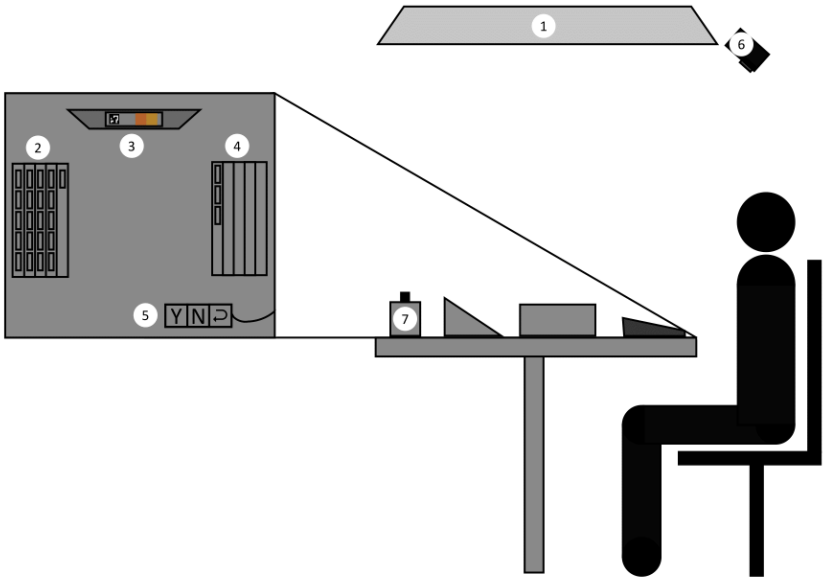

Figure 6.12: Experimental setup: (1) LED panel, (2) Box of samples not yet examined, (3) Sample support, (4) Box for discarded samples, (5) Three buttons keypad, (6) Camera, (7) Spectroradiometer.

6.2.1 Experiment samples

For simplicity of implementation of the protocol, the two patches constituting the pairs are squares of size $1.4cm \times 1.4cm$, which corresponds to a $2°$ angle of view at $40cm$. The paper used for printing the patches is a matte photo paper with a paper weight of $189g/m^2$, allowing for vibrant color as well as avoiding ripples of the paper due to the ink. The two patches of color are printed brought together and bonded with each other in order to avoid the contrast effect that would arise with a grey band between them. The color

Figure 6.13: An example of ArUco marker.

difference between adjacent patches should be small enough so that the Mach bands effect is negligible.

To simplify the task of handling the samples during the experiment, the color pairs are then glued to a thick cardboard support. This support is covered on all sides with the same neutral grey paper as the table. On one side, the location of the pair is marked with a cross to ensure that the position is the same for all pairs of patches, and on the other side, an ArUco marker is printed to automatically process the number of the sample being examined by the participant. The steps for the production of the experimental samples is shown in Figure 6.14. The choice of the ArUco was made after considering three options: numbers and Optical character recognition (OCR); QR codes; and ArUco markers. OCR was discarded to avoid any readable characters for the participant. The choice of ArUco over QR codes was made after several tests showing that ArUco is more robust at a further distance, at a given viewing angle, and with non-white paper.

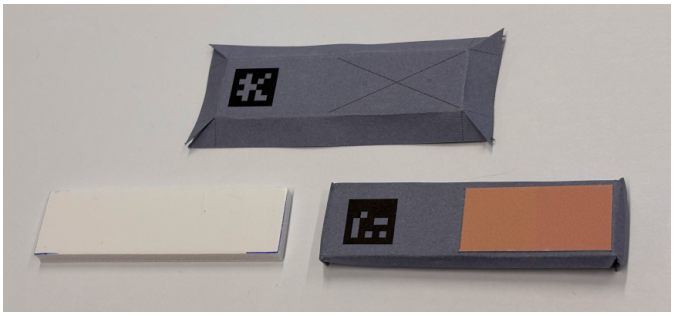

Figure 6.14: Production of the experimental samples

6.2.2 Experiment workflow

Before carrying out the experiment, several preliminary steps must be completed. First, participants must be screened for color vision deficiencies using an online Farnsworth-Munsell 100 hue test. Following this, instructions will be provided both orally and in written form. Participants will be shown two sample (not included in the actual experiment), one with a noticeable difference and one without, to familiarize them with the procedure and demonstrate proper handling to avoid touching the surface of the color patches. Afterward, participants will have an opportunity to ask any questions they may have.

The experiment workflow is managed by a series of Python scripts that coordinate the lighting system, the spectroradiometer used for light stabilization, the camera and the keypad used to record the responses of the participants.

This workflow is summarized in Figure 6.15.

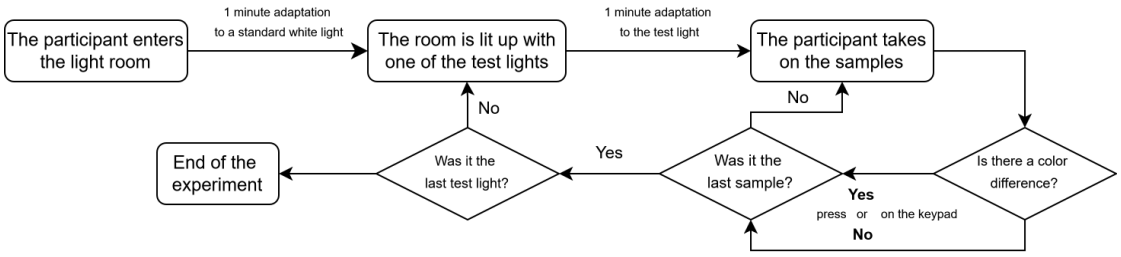

Figure 6.15: Experiment workflow.

6.3 Pilot Experiment

To validate the experimental protocol presented in this chapter and assess its effectiveness at evaluating a light sources ability to enhance color discrimination, a preliminary version of the experiment was conducted. For the sake of simplicity, this initial test was performed without simulation goggles.

The main objective of this initial study was to determine whether the protocol could reliably detect subtle differences in color discrimination between four light spectra with different color rendering characteristics. This first step serves both to evaluate the effectiveness of the method used and to identify any necessary adjustments before conducting the full-scale experiment which will be described in the following section. Special attention was given to the selection of the colored samples since it represented a key aspect of the experimental design.

This section first present the four light spectra that were selected for the experiment as well as the reason behind this choice, followed by a description of the experimental protocol that was employed. The results are then presented and discussed in order to draw some conclusions on this experiment's effectiveness.

6.3.1 Choice of spectra

This pilot experiment required different examples of spectra in order to be able to evaluate the performance of the experiment. Four different spectra were generated using the method presented in the previous chapter and are the results of exploring the full range of available spectra that the spectrally tunable LED system is able to generate. All four lights were designed to match 500 lux on the experiment table and match the chromaticity of the D65 standard illuminant.

The four lights used in this initial experiment are the following:

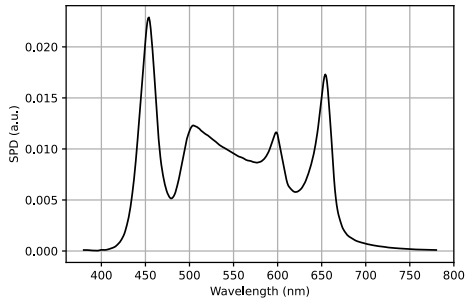

(a) SPD of Light 1.

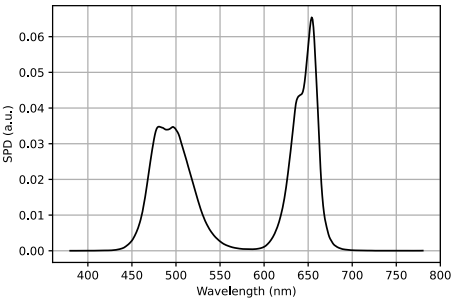

(b) SPD of Light 2.

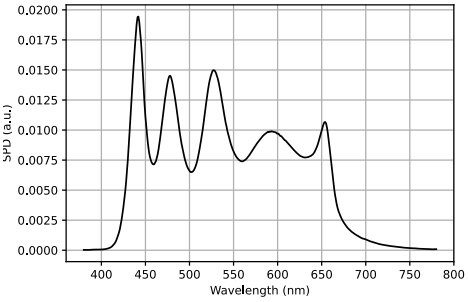

(c) SPD of Light 3.

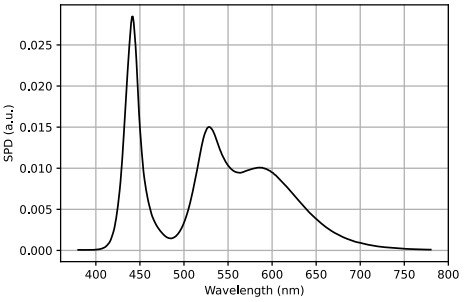

(d) SPD of Light 4.

Figure 6.16: The 4 SPD used in this preliminary experiment.

Light 1, best CIE R_a:
Light 1 was designed to have the highest achievable CRI using only 5 channels. It achieves a CIE R_a of 98. Its SPD is displayed in Figure 6.16a.

Light 2, worst CIE R_a:
In order to produce a light spectrum as different as possible to the previous one, it was decided to find the lowest CRI achievable. The SPD of the obtained light is presented in Figure 6.16b. It reaches a CIE R_a of -24. We can note that the Color Vector Graphic of the TM-30 report is particularly distorted in the direction of the cyan/red axis as displayed in Figure 6.17a

Light 3, best CIE R_f:
To generate a light with good color rendering while having a spectral composition distinct from Light 1, Light 3 was designed to maximize the CIE R_f. The resulting spectrum achieves a CIE R_f value of 94. Its spectral power distribution is displayed in Figure 6.16c.

Light 4, green/purple axis:
The final light chosen for this experiment was selected as an opposite to light 2 with

regards to the TM-30 color vector graphic. Light 2 displayed a strong distortion in the direction of the cyan/red axis, so this light was chosen to maximize the distortion in the perpendicular direction, the green/purple axis. Its SPD is displayed in Figure 6.16d and the color vector graphic comparison between Light 2 and 4 is presented in Figure 6.17.

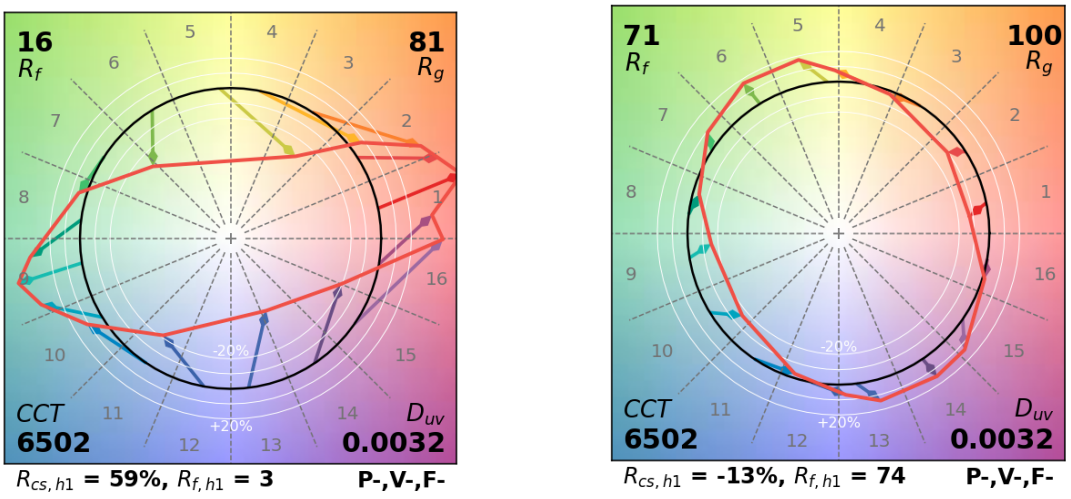

(a) Light 2.

(b) Light 4.

Figure 6.17: Comparison of the color vector graphics of the TM-30 report for lights 2 and 4.

The full TM-30 reports for the four lights are displayed in Appendix D.

6.3.2 Experimental protocol

Section 6.2.2 presented the general workflow of this experiment, the present section focuses on the practical details of its implementation.

The light booth was modified compared to the first experiment presented in Chapter 4: the platform used to raise the table closer to the LED panel was removed, no camera was employed to monitor participants, and the camera used to record the experimental results was positioned on the participants left side, over their shoulder, pointing toward the table.

The experiment table was positioned directly under the LED panel and was completely covered with gray cardboard. A touch screen placed parallel to the table was also covered with gray cardboard except for three regions corresponding to software buttons: a 'yes' button in the bottom left corner, a 'no' button in the bottom right corner, and a 'cancel' button in the top right corner. These buttons allowed participants to confirm that they perceived a color difference, deny it, or revert their previous response respectively. Distinct sounds were played to indicate that each response had been registered.

At the center of the screen, a support was installed to hold the samples in place while being viewed at a 45° angle relative to the table surface. The color difference of the 200 color pairs used in this pilot experiment are those presented in Figure 6.11. The samples

were stored in two 3D-printed white boxes, each containing 100 samples (Figure 6.18). During the experiment, one box at a time was positioned in the top left corner of the screen with the side featuring the colored part facing away from the participant.

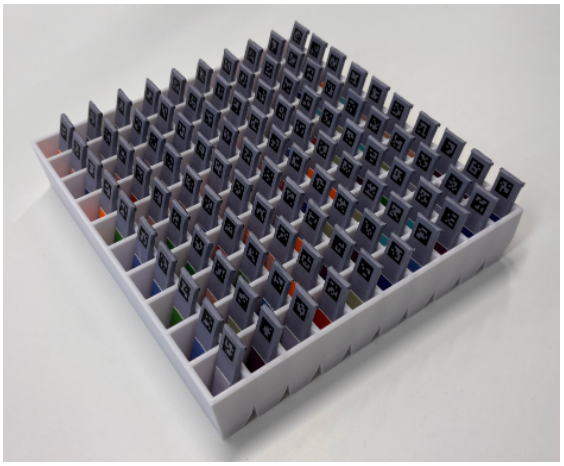

Figure 6.18: One of the 3D printed boxes with 100 experimental samples.

The spectroradiometer was equipped with a remote measuring head that uses a fiber optic cable, which allowed us to hide the device out of sight while still being able to measure the light close to the viewing area. During the complete session it is used with the light stabilization algorithm presented in Chapter 5 to ensure that the light condition do not change during the experiment. The disposition of the experimental table during this experiment is summarized by Figure 6.19.

Participants were first screened for color vision deficiencies in the same way as the first experiment described in Chapter 4. Then they entered the light booth and sat down on the chair in front of the experiment table. No experimental sample was visible before the experiment starts. The participants were given an explanation of the experiment and of the instructions. Two examples of experimental samples were made with colors not available in the experiment itself in order to give an example, one of them does not have any color difference while the other has a just visible color difference. The participants were then instructed with these examples to press "yes" if they could see a color difference and "no" if they could not or if they were not sure.

Participants were instructed to take a sample from the box, place it on the support, and answer the question: "Can you see a color difference between the two squares?" After selecting either "yes" or "no", they were asked to return the sample to the box one row ahead of its original position to prevent the risk of forgetting or repeating samples. Once all 100 samples from the first box had been evaluated, the experimenter entered the booth to replace it with the second box.

The 200 samples, while not being shuffled between sessions, were not presented in a particular order starting with any of the two boxes. The 4 lights tested in this preliminary experiment were presented in random order in succession. A 10 minutes break was done after the first two lights to split the experiment in two and reduce eye strain.

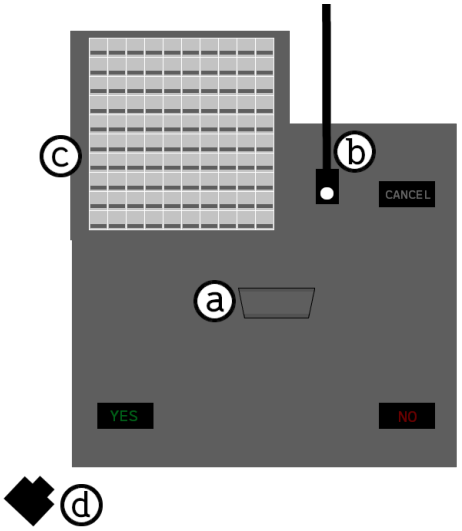

Figure 6.19: The setup of the experimental table during the pilot experiment (a: sample holder, b: spectroradiometer's remote measuring head, c: sample box with 100 color samples, d: camera).

6.3.3 Analysis of the results

A total of 10 participants completed this pilot experiment and each rated the 200 color pairs under the four different channels. All of the 200 color pairs presented a color difference, ranging from easily distinguishable to impossible to perceive. The participants did not have any prior knowledge about the goal of the experiment. The objective of this experiment was to determine if the four different lighting conditions had a meaningful influence on the ability of the observers to discriminate between closely related colors. This analysis focuses on comparing the results obtained under the different lighting conditions in order to assess potential perceptual performance differences.

In order to study if the four different lighting conditions affected differently color discrimination ability of the participants, we can compare the percentages of positive response rates depending on the light. On average, Light 1 received 39.1% positive responses, Light 2 received 44.5%, Light 3 received 39.8% and Light 4 received 42.1%.

To analyse statistically the significance of these differences in positive answer rates between the four lights, the positive response rate was computed for each participants under the four lights. This gives us four distributions that can be compared statistically. The positive answer rates are plotted in Figure 6.20, each color representing a unique participant. We can first observe on this figure that although the variance is high, there seems to be visually a clear trend.

A repeated-measures analysis of variance (ANOVA) which is type of ANOVA adapted to comparing dependent samples, was performed on these four distributions in order to reveal if there was a significant difference in results between the four lighting conditions. The obtained p-value is $4.71e-2$ which is lower than the selected threshold $\alpha = 0.05$

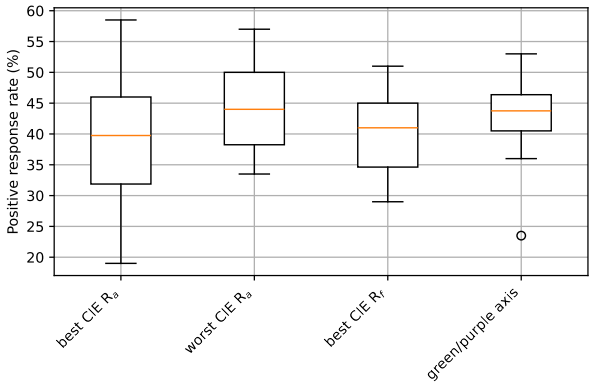

Figure 6.20: Percentage of positive responses for four lights per participant.

meaning that there is indeed a significant difference in results.

In order to check which lights showed significant differences, multiple paired t-test were performed in order to compare the four lights two by two. The results of this procedure are reported in Table 6.2. This statistical analysis reveals that overall Light 2 performed significantly better overall for color discrimination than Light 1 and Light 3.

	L1	L2	L3	L4
L1		2.5e-2	7.4e-1	2.5e-1
L2			9.6e-3	3.1e-1
L3				1.8e-1
L4				

Table 6.2: p-value of the individual paired t-tests tests between the 4 lights. p-values lower than the selected threshold $\alpha = 0.05$ are highlighted in green

The fact that no significant difference overall was found between the other lights, however does not mean that there are no local differences in color discrimination ability. To analyse this possibility, we can break down the positive response rates per hue. In this experiment, each hue features 10 different color pairs. Using the percentage of positive answers per hue gives us insight into which colors were more affected by the lighting conditions. Figure 6.21 shows the breakdown of positive answers per hues.

To identify local differences in color discrimination ability, first, repeated-measures ANOVA were performed on the distributions obtained by breaking down the results per hue. This allows us to check which hues had difference performances depending on the lighting conditions. If the obtained p-values were lower than the threshold $\alpha = 0.05$, multiple paired t-tests were done to check which lights showed significant differences. This statistical analysis is reported in Table 6.3. The grayed lines correspond to hues were the

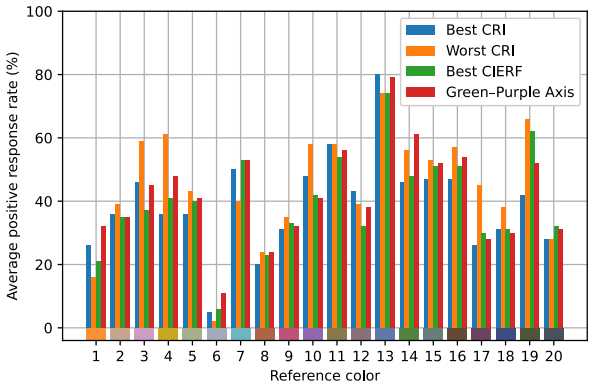

Figure 6.21: Average positive response rate for the twenty hues under the four lights.

ANOVA could not reject the null hypothesis. For the other lines, the green cells correspond to a paired t-test rejection of the null hypothesis with a p-value lower than the threshold of rejection $\alpha = 0.05$, on the contrary red cells correspond to p-values that fail to reject the null hypothesis.

The first observation that can be made is that among the 20 hues tested, 12 showed no significant differences in color discrimination performance. Light 2 stands out as the most distinct from the other three lights, showing the greatest number of local variations in color discrimination performance. Finally, we can observe that smaller local differences were also detected between other lighting conditions, suggesting that all lights influence color discrimination to some extent.

The most pronounced effects were observed between Lights 1 and 2, with six hues showing significant difference. Light 1 only outperforms Light 2 for the cyan hue (07). These two lights also represent the extremes in terms of color rendering quality, having respectively the highest and lowest CRI R_a values.

The two most similar light sources are Light 1 and Light 3, corresponding respectively to the spectra with the highest R_a and R_f values. The only significant difference between them occurs for hue 19 corresponding to dark green, where Light 3 shows a 20% higher rate of positive responses on average.

6.3.4 Discussion and evaluation of the experiment

The experiment described in this section and the results that were obtained from it provide us a basis for evaluating how effectively it can assess the performance of different lighting conditions in terms of color discrimination ability.

As previously noted, certain hues did not reveal significant differences in color discrimination performance across the four lighting conditions. This may be attributed to the fact that these hues are not affected differently by the spectral characteristics of the selected lights. However, closer examination of the results reveal for example that hue 06 displays extremely low positive responses rates (≤ 11), while on the contrary, hue 13 shows particularly high rates (≥ 74). This suggests that at least some of the hues show

	L1/L2	L1/L3	L1/L4	L2/L3	L2/L4	L3/L4
01	9.57×10^{-2}	1.38×10^{-1}	4.34×10^{-1}	3.43×10^{-1}	1.07×10^{-2}	9.32×10^{-2}
02	6.56×10^{-1}	8.53×10^{-1}	8.72×10^{-1}	4.94×10^{-1}	5.65×10^{-1}	1.00×10^{0}
03	6.26×10^{-3}	1.34×10^{-1}	8.64×10^{-1}	3.10×10^{-4}	1.28×10^{-2}	1.04×10^{-1}
04	4.55×10^{-2}	6.14×10^{-1}	1.40×10^{-1}	1.15×10^{-2}	1.86×10^{-1}	1.91×10^{-1}
05	1.53×10^{-1}	4.79×10^{-1}	3.97×10^{-1}	5.41×10^{-1}	7.80×10^{-1}	8.11×10^{-1}
06	2.79×10^{-1}	7.80×10^{-1}	5.10×10^{-2}	3.09×10^{-1}	9.99×10^{-3}	2.44×10^{-1}
07	4.18×10^{-2}	5.91×10^{-1}	2.79×10^{-1}	3.73×10^{-3}	6.26×10^{-3}	1.00×10^{0}
08	5.09×10^{-1}	1.93×10^{-1}	2.23×10^{-1}	8.95×10^{-1}	1.00×10^{0}	7.58×10^{-1}
09	5.34×10^{-1}	6.93×10^{-1}	8.85×10^{-1}	7.64×10^{-1}	3.94×10^{-1}	8.79×10^{-1}
10	2.04×10^{-1}	1.93×10^{-1}	1.91×10^{-1}	1.61×10^{-2}	1.65×10^{-2}	8.11×10^{-1}
11	1.00×10^{0}	2.69×10^{-1}	5.09×10^{-1}	2.23×10^{-1}	4.43×10^{-1}	5.55×10^{-1}
12	4.23×10^{-1}	3.99×10^{-2}	4.27×10^{-1}	1.11×10^{-1}	8.47×10^{-1}	2.39×10^{-1}
13	1.11×10^{-1}	5.10×10^{-2}	7.98×10^{-1}	1.00×10^{0}	2.73×10^{-1}	1.38×10^{-1}
14	3.19×10^{-2}	7.05×10^{-1}	6.69×10^{-3}	6.97×10^{-2}	2.13×10^{-1}	9.46×10^{-3}
15	2.39×10^{-2}	1.04×10^{-1}	1.50×10^{-2}	3.43×10^{-1}	3.43×10^{-1}	5.91×10^{-1}
16	8.48×10^{-2}	5.34×10^{-1}	2.42×10^{-1}	3.43×10^{-1}	6.47×10^{-1}	4.96×10^{-1}
17	1.03×10^{-1}	6.70×10^{-1}	6.78×10^{-1}	1.15×10^{-1}	6.72×10^{-2}	7.85×10^{-1}
18	1.32×10^{-1}	1.00×10^{0}	8.72×10^{-1}	2.09×10^{-1}	1.21×10^{-1}	8.53×10^{-1}
19	3.25×10^{-4}	4.76×10^{-3}	1.48×10^{-1}	3.73×10^{-1}	3.43×10^{-2}	8.47×10^{-3}
20	1.00×10^{0}	4.79×10^{-1}	5.76×10^{-1}	3.73×10^{-1}	5.41×10^{-1}	7.58×10^{-1}

Table 6.3: p-value of the individual t-tests comparing the 4 lights for the 20 different hues.

inconsistencies in the selection or spacing of the color pairs, even though the measured $\Delta_{E,00}$ corresponded to the intended differences.

Of the four selected lights, the most different SPD which was supposed to induce the strongest color shifts was supposed to be Light 2, which was correctly detected by the experiment. Light 1 and Light 3 on the other hand, which are respectively the best CIE R_a and best CIE R_f showed overall particularly similar results which is consistent with the fact that they display similar spectral and color rendering characteristics.

Furthermore, this experiment illustrates that good color rendering, such as provided by lights L1 and L3, does not necessarily correspond to the highest color discrimination ability. Although this trend is not verified for all hues, the light with the lowest achievable CRI showed a significant improvement in the ability of observers to discriminate between certain colors. This further supports the idea that it can be possible to design light spectra that enhance color discrimination performance, at least for specific hue regions.

To conclude, this pilot experiment successfully demonstrated its ability to evaluate the performance of different lighting conditions in terms of color discrimination. The experiment also proved to be able to analyse color discrimination capabilities for specific hue ranges. The simplicity of the discrimination task facilitated participant understanding, allowing each to complete the evaluation of approximately 200 color pairs in about 20 minutes. However, letting the participant handle the physical samples introduced variability in observation time across participants and extended the overall duration of the experiment. Moreover, the selection of color pairs proved to be a critical factor and should be carefully examined prior to testing, as the $\Delta_{E,00}$ values alone are insufficient to ensure a consistent

and well balanced set of colored pairs. These observation are the basis to the full-scale experiment that will be described in the next section.

6.4 Color discrimination experiment in simulated low vision conditions

The experiment presented in Chapter 4 examined how color discrimination performance varies depending on the wavelength of the individual LED channels. Building on these results, the experiment introduced and validated in the previous section allows us to investigate the possibility of designing optimized lighting spectra to improve color discrimination under low vision conditions.

However, because the simulation goggles substantially increase the difficulty of the discrimination task, several adjustments were made to ensure that it could produce meaningful results.

This section describes the final experiment aimed at investigating different lighting conditions under simulated low vision, detailing the modifications made from the pilot study in color pair selection, lighting setup, and practical adjustments to reduce experiment duration. The resulting data are then presented and analyzed in details.

6.4.1 Low vision simulation groups

The most important change compared to the pilot experiment is the introduction of low vision simulation goggles. In the experiment described in Chapter 4, 4 groups were formed: control group, blurry vision, central scotoma and tunnel vision. In this final experiment, only two groups were retained.

Preliminary testing has shown that it was not feasible to design a single protocol that would provide meaningful data for both participants wearing simulation goggles and participants without. Under white light, discrimination tasks that were appropriately challenging for participants wearing the goggles proved too easy for those without them, and vice versa. Therefore no control group was included in this experiment.

Moreover, the color discrimination experiment conducted under monochromatic LED lighting revealed no meaningful differences between participants wearing blurry vision goggles and those wearing tunnel vision goggles. Therefore, only the blurry vision condition was retained. This allowed us to concentrate on two groups in the final experiment: participants wearing blurry vision goggles and participants wearing central scotoma goggles.

6.4.2 Color sample selection

In the pilot experiment, the selection of color pairs was obtained by randomly generating color differences around a fixed average $\Delta_{E,00}$ value. However, as was explained in Subsection 6.3.4, this approach did not provide a balanced level of difficulty for all hues: some hues had color pairs consistently easier or harder to discriminate than others. Furthermore, since the simulation goggles were used in this experiment, $\Delta_{E,00}$ can no longer be used as a meaningful indicator of color discrimination difficulty. No metric

currently exists that characterizes color difference under non-standard conditions such as low vision.

To solve this issue, the same reference colors used in the pilot experiment were kept, but a different method was used to select the comparison samples in order to produce a balanced distribution of difficulty. A large set of printed samples was generated at different $\Delta_{E,00}$ distances from each reference color. These samples were then viewed individually while wearing the blurry vision goggles, and the final set of color pairs was selected manually to ensure a balanced distribution of task difficulty, from easily distinguishable differences to color differences that were nearly impossible to detect.

The resulting distribution of selected color pairs is shown in Figure 6.22. As the figure illustrates, achieving a balanced discrimination task required assigning different $\Delta_{E,00}$ values depending on the hue, confirming that standard color-difference metrics do not translate uniformly under the simulated low vision viewing conditions used in this study.

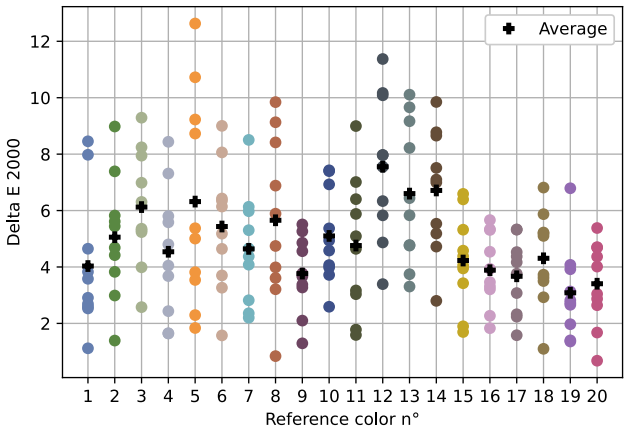

Figure 6.22: Color distance between each printed reference and comparison color samples.

6.4.3 Selection of the lights

Since this experiment focused on two types of simulated low vision, three lighting conditions were chosen: one control white light and two additional lights derived from the results of the experiment presented in Chapter 4. To ensure that the resulting spectra would remain practical to reproduce while still offering meaningful spectral variation, the design of each light was constrained to use a maximum of five LED channels.

In order to evaluate specifically the influence of spectral composition of the light, all three spectra were designed using the algorithms introduced in Chapter 5, to match the chromaticity of a standard office lighting at 4000 Kelvin and an illuminance of 500 lux on the viewing area.

Light 1, standard LED lighting:

The first light selected was a control light, used to represent standard LED lighting conditions and is a standard office LED light at a CCT of 4000 kelvin. The spectral power distribution of this light is presented in Figure 6.23a.

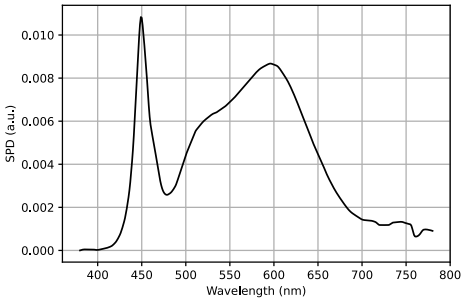

(a) SPD of Light 1.

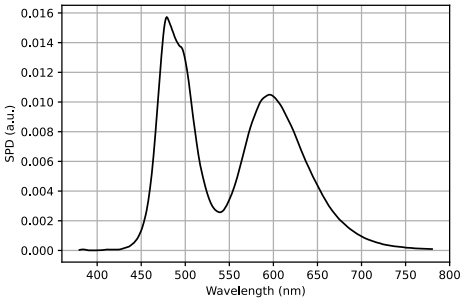

(b) SPD of Light 2.

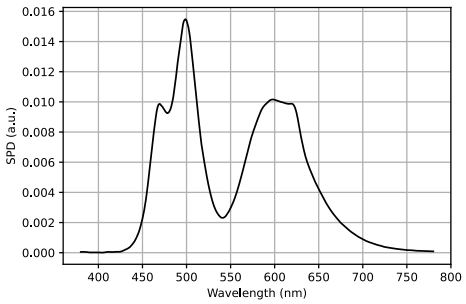

(c) SPD of Light 3.

Figure 6.23: The 3 SPD used in this experiment.

The two additional lights were selected based on the performance of the blurry vision and central scotoma groups in the experiment conducted on the individual channels.

To determine these lights, all possible combinations of five LED channels were first evaluated using the light mixing algorithm presented in Chapter 5 to identify which combinations had the ability to reproduce the same chromaticity as L1. The channel combinations were then ranked according to the experimental results from Chapter 4. Specifically, the goal was to select the combination channels that provided the best possible coverage of the entire hue circle, achieved by minimizing the quantity defined in Equation 6.2.

$$\min_{c_1,\ldots,c_5} \sum_{i=1}^{28} \min\left(S_{c_1}(i), \ldots, S_{c_1}(i)\right) \tag{6.2}$$

with $S_{c_k}(i)$ the average score obtained for sample i under the monochromatic LED corresponding to channel c_k.

After applying this procedure separately to the two groups, two distinct sets of five LED channels were identified, one optimized for the blurry vision group and one for the central scotoma group. These channel sets were then used to compute all spectra that matched the chromaticity of L1. Among the resulting metameric spectra, the one selected for each group was the spectrum that maximized the drive level of the channels associated with the lowest total error scores in the monochromatic color discrimination experiment.

Light 2, blurry vision light:
When applied to the results obtained for the group with the blurry vision goggles, the resulting spectrum selected is shown in Figure 6.23b. To produce this spectrum, the channels B2, C, G2, L and PC-A are used, with peaks at respectively wavelengths 478, 500, 528, 544 and 594 nm.

Light 3, central scotoma light:
When applied to the results obtained for the group with the central scotoma goggles, the resulting spectrum selected is shown in Figure 6.23c. To produce this spectrum, the channels B1, C, L, PC-A and R1 are used, with peaks at respectively wavelengths 468, 500, 544, 594 and 636 nm.

The full TM-30 report of the three lights are available in Appendix E.

6.4.4 Practical modifications

The general experimental workflow followed the same structure as described in Subsection 6.2.2. However, several practical adjustments were made compared to the pilot experiment in order to take into account the use of low vision simulation goggles and to improve the duration of the experiment.

In the pilot experiment, participants manipulated the color samples themselves and handled placing and removing them from the sample holder. However, testing showed that this task became much more difficult when wearing the simulation goggles. To ensure smooth execution and reduce participant strain, it was decided that the experimenter would stay inside the light booth and handle the cycling of samples. This adjustment resulted in faster and more consistent duration of presentation of the samples.

Additionally, the touch screen interface used in the pilot experiment to record the answers of the participants was found to be inefficient and difficult to use for some participants. Moreover, under simulated low vision conditions, a solution with a tactile response system was found to be more suitable. In place of the touchs creen, a numpad was used, where the key 0 was marked with a green sticker (indicating "yes") and the Enter key with a red sticker (indicating "no"). This provided clearer physical feedback and made it easier and quicker for the participants to give their answer.

To allow to cycle samples efficiently, the experimenter was positioned directly in front of the participant. A monitor set to minimum brightness was also placed facing away from the participant to provide visual feedback to the experimenter without influencing the lighting environment. Because the simulation goggles substantially restrict the field

of view, the participant could not see either the experimenter, screen or numpad while viewing the colored samples ensuring no interference with the task. The setup used is illustrated by Figure 6.24.

Finally, as the experiment involved testing only three lighting conditions, participants were given a short break of approximately five minutes between lighting conditions to reduce fatigue. In total, the experiment took less than an hour with about 15 to 20 minutes per light tested. The three lights were presented in random order.

Figure 6.24: The setup of the light booth for this experiment.

6.4.5 Analysis and discussion of the results

In total, 20 observers participated in the experiment. They were divided into two groups each containing 10 participants, one wearing the blurry vision goggles and one wearing the central scotoma goggles.

The overall positive response rates for the participants in the blurry vision group under the three lighting conditions are shown in Figure 6.25a. On average, the proportion of positive responses remains close to 50% for all three lights, indicating no improvement or deterioration in color discrimination performance at the group level.

However, examining the individual results reveals that most participants do exhibit variations in performance across lighting conditions, though they do not consistently favor any specific light. This observation is supported by a repeated-measures ANOVA, which gives a p-value of 7.8×10^{-1}, which is above the significance threshold $\alpha = 0.05$, confirming that the observed differences are not statistically significant at the group level.

The overall positive response rates for the participants in the central scotoma groups under the three lighting conditions are displayed in Figure 6.25b. The same observations can be made, the repeated-measures ANOVA returns a p-value higher than the threshold $\alpha = 0.05$ with a p-value of $5.0e - 1$, failing to reject the null hypothesis.

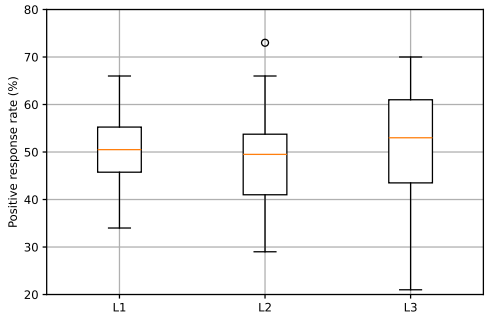

(a) Average positive answer rate for the blurry vision group for the three lights.

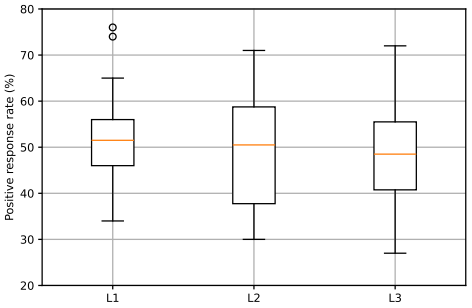

(b) Average positive answer rate for the central scotoma group for the three selected lighting conditions.

Figure 6.25: Positive answer rate for both groups under the three lights.

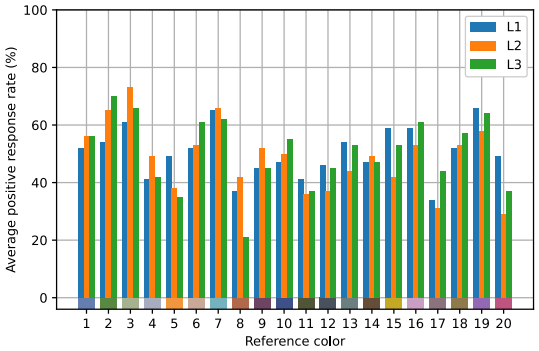

Figure 6.26: Percentages of positive answers for the 20 hues under each light for the blurry vision group.

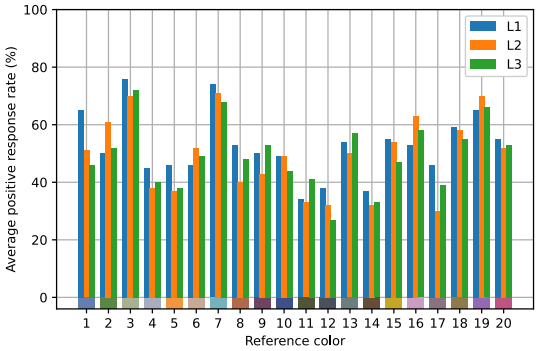

Figure 6.27: Percentages of positive answers for the 20 hues under each light for the central scotoma group.

To investigate whether specific hues were affected differently by the lighting conditions, the average positive response rates for each hue are reported in Table 6.26 for the blurry vision group and in Table 6.27 for the central scotoma group. As shown in both tables, the distribution of response rates is more balanced than in the pilot experiment. Under the control light, most hues show positive response rates close to the 50% positive response level, with only a few hues showing lower values in the 30% range or higher values in the 70% range. This confirms that the selection of color pairs in the final experiment resulted in a more balanced difficulty.

Compared to what was observed in the pilot experiment, the differences in positive response rates between the lighting conditions are more uniform for both groups. To determine whether any localized differences in color discrimination were significant, repeated-measures ANOVAs followed by pairwise t-tests were conducted for each hue in both groups. The results of these analyses are presented in Table 6.4 for the blurry vision group and in Table 6.5 for the central scotoma group. As shown in the tables, only a small number of hues exhibit statistically significant differences between the lighting conditions: three hues for the blurry vision group and a single hue for the central scotoma group. This indicates that the lighting variations produced minimal localized effects on positive response rates at the group level.

	L1/L2	L1/L3	L2/L3
01	5.91×10^{-1}	6.62×10^{-1}	1.00×10^{0}
02	3.18×10^{-2}	1.07×10^{-2}	3.97×10^{-1}
03	9.63×10^{-2}	3.63×10^{-1}	8.86×10^{-2}
04	1.53×10^{-1}	8.47×10^{-1}	2.42×10^{-1}
05	3.99×10^{-2}	6.62×10^{-2}	5.76×10^{-1}
06	8.91×10^{-1}	2.25×10^{-1}	1.96×10^{-1}
07	8.68×10^{-1}	5.20×10^{-1}	5.34×10^{-1}
08	6.10×10^{-1}	1.21×10^{-1}	9.53×10^{-3}
09	3.10×10^{-1}	1.00×10^{0}	1.91×10^{-1}
10	7.13×10^{-1}	3.93×10^{-1}	3.81×10^{-1}
11	5.81×10^{-1}	5.22×10^{-1}	8.40×10^{-1}
12	1.47×10^{-1}	9.12×10^{-1}	2.35×10^{-1}
13	1.17×10^{-1}	8.32×10^{-1}	1.08×10^{-1}
14	7.05×10^{-1}	1.00×10^{0}	8.14×10^{-1}
15	1.65×10^{-2}	3.29×10^{-1}	9.32×10^{-2}
16	4.25×10^{-1}	7.05×10^{-1}	1.82×10^{-1}
17	6.71×10^{-1}	2.37×10^{-1}	7.03×10^{-2}
18	8.95×10^{-1}	5.44×10^{-1}	5.83×10^{-1}
19	1.37×10^{-1}	6.62×10^{-1}	1.11×10^{-1}
20	4.76×10^{-3}	1.93×10^{-1}	1.37×10^{-1}

Table 6.4: p-value of the individual t-tests comparing the 3 lights for the 20 different hues.

	L1/L2	L1/L3	L2/L3
01	1.27×10^{-1}	3.24×10^{-2}	4.27×10^{-1}
02	1.62×10^{-1}	7.94×10^{-1}	2.95×10^{-1}
03	3.70×10^{-1}	4.62×10^{-1}	7.35×10^{-1}
04	1.53×10^{-1}	9.57×10^{-2}	6.93×10^{-1}
05	1.34×10^{-1}	1.21×10^{-1}	9.06×10^{-1}
06	4.60×10^{-1}	6.64×10^{-1}	7.58×10^{-1}
07	5.60×10^{-1}	3.82×10^{-1}	4.34×10^{-1}
08	4.50×10^{-2}	5.63×10^{-1}	3.18×10^{-1}
09	2.85×10^{-1}	6.27×10^{-1}	1.38×10^{-1}
10	1.00×10^{0}	2.99×10^{-1}	5.13×10^{-1}
11	8.23×10^{-1}	1.73×10^{-1}	1.37×10^{-1}
12	3.82×10^{-1}	1.20×10^{-1}	3.43×10^{-1}
13	6.37×10^{-1}	7.18×10^{-1}	2.26×10^{-1}
14	1.77×10^{-1}	2.23×10^{-1}	7.80×10^{-1}
15	9.03×10^{-1}	1.53×10^{-1}	3.54×10^{-1}
16	1.77×10^{-1}	3.81×10^{-1}	4.53×10^{-1}
17	1.53×10^{-1}	4.35×10^{-1}	3.31×10^{-1}
18	9.15×10^{-1}	6.42×10^{-1}	7.08×10^{-1}
19	5.21×10^{-1}	9.15×10^{-1}	6.99×10^{-1}
20	7.85×10^{-1}	8.30×10^{-1}	9.09×10^{-1}

Table 6.5: p-value of the individual t-tests comparing the 3 lights for the 20 different hues.

6.4.6 Discussion of the results

The results presented in the previous subsection indicate that no significant differences in color discrimination performance were observed between the three lighting conditions. Overall, the average proportion of positive responses across all participants remained close to 50% for each light, suggesting no consistent improvement or deterioration of performance at the group level. Furthermore, when examining the hue-by-hue results, only a small number of localized differences were statistically significant.

However, the three lights differed in their properties, with the most important differences observed between L1 and the other two lights. Based on the results of the pilot experiment, these differences should have been detectable. The main difference between the pilot experiment and the present one is the fact that the experiment was conducted with the low vision simulation goggles. Discussions with participants after the experiment, as well as observation of performance patterns, suggest that the goggles might have introduced a bias that likely influenced the outcomes.

The use of simulation goggles greatly increased inter-individual variability. Either meaning that low vision conditions exacerbate the variability in performance between individuals or that participants adapted differently to the restricted vision. Some participants reported during the experiment seeing improvement in their ability to perceive the color differences as the session progressed, while on the contrary others reported increasing visual fatigue and reduced color discrimination performance over time. We hypothesize that this disparity in adaptation to the visual conditions might be one of the reasons why the effect of lighting is masked in the results of the experiment.

Moreover, contrary to the experiment presented in Chapter 4, the nature of the task in this experiment makes it particularly sensitive to such adaptation effects. Unlike the arrangement experiment performed under monochromatic LED channels, this experiment relies on the detection of the color discrimination threshold through a simple yes or no question. Because the simulation goggles imposed unusual and visually demanding viewing conditions, making it difficult for participants to draw a clear line between perceiving a color difference or not. As a result, even minor fluctuations in adaptation to the visual environment or differences in the confidence they have in their responses can have a disproportionate effect on the measured discrimination thresholds.

These factors could provide a plausible explanation for why the differences observed in the pilot experiment did not replicate under simulated low vision. They also highlight a more general limitation of using low vision simulation goggles for studying precisely perceptual phenomena such as color discrimination. While such goggles can simulate certain visual impairments, they do not reproduce the long-term neural and perceptual adaptations that occur for individuals with long term low vision.

These observations point toward two important considerations. First, to meaningfully assess the potential of optimized lighting to improve color discrimination in low-vision contexts using this protocol, additional parameters, such as alternative color-pair sets or varied lighting conditions, should be explored. Second, the study would be strengthened by involving panels of real low-vision participants who are already adapted to their visual condition.

6.5 Chapter Summary

This chapter presented a new psychophysical experiment designed to investigate color discrimination capabilities of different white light spectra. To achieve this goal, a method for generating customized sets of color pairs was first developed. Using a calibrated inkjet printer, a sampling method based on the gamut of the printer was implemented to produce a range of reference colors. By tabulating the CIELAB color space to the $\Delta_{E,00}$ color difference metric, color pairs were generated with controlled distributions of color differences around a fixed average value. Furthermore, because participants were required to assess subtle color differences, the light spectra produced by the tunable LED system were stabilized in real time using the algorithm introduced in Chapter 5.

A dedicated experimental protocol was then established to use these color pairs. Each color pair was glued a gray cardboard support featuring an ArUco code, which allowed automatic recording of participant responses using a simple camera but also permitted randomized presentation of the samples. The entire experiment was supported by a specifically developed software optimized participant usability, ensuring that system performance did not interfere with the accuracy or smoothness of the experiment.

To validate this new protocol, a pilot study was first conducted without the use of low vision simulation goggles. This pilot experiment served to verify both that the experiment was sensitive enough to highlight subtle variations in color discrimination, but also identify aspects of the procedure that could be improved. Four white light sources with distinct spectral power distributions but identical chromaticity coordinates were tested with ten participants. The analysis revealed clear differences in color discrimination performance across lighting conditions, even though inter-observer variability was particularly high. The light source with the lowest CRI produced an average 5% increase in positive response rate compared with those having CIE R_a values above 97, demonstrating that a high CRI does not necessarily correlate with improved color discrimination.

Several adjustments were made prior to conducting the full-scale experiment with low vision simulation goggles. First, it was observed that some hues consistently resulted in either extremely low or extremely high correct response rates, regardless of the lighting condition, indicating that the $\Delta_{E,00}$ metric alone is not sufficient to ensure balanced difficulty in a color discrimination experiment. Additionally, while the pilot study used a touchscreen interface for responses, this proved impractical for participants wearing simulation goggles due to the lack of tactile feedback. In the pilot experiment, the participants handled the colored samples autonomously, however it was found to be too difficult under low vision conditions. Consequently, for the full scale experiment, a numpad was introduced for participants to input their responses, and the experimenter handled the cycling of the samples. These modifications improved both consistency for the viewing of the samples and overall duration of the experiment.

The full scale experiment was then conducted with two types of low vision simulation goggles: one simulating blurry vision and the other central scotoma. Twenty participants took part in this experiment, evenly distributed between the two types of simulation goggles. Three lighting environments were evaluated, a control standard office white light and two additional spectra derived from the findings of the experiment presented in Chapter 4. Although no significant trends were observed among the three lighting conditions, analysis

of the results and post-experiment discussions with participants highlighted factors that may have influenced performance. Because the task evaluated a color-discrimination threshold using a simple yes/no response, it could make it particularly sensitive to short-term adaptation effects. The use of simulation goggles may have introduced adaptation effects as some participants reported gradually adapting to the simulated low vision condition and perceiving finer color differences over time, while others experienced increasing visual fatigue that made the task more challenging.

Based on these observations, a promising direction for future improvement would be to refine the experimental design to better consider adaptation dynamics. This may include implementing structured adaptation periods before the task, revising the selection and configuration of color samples, or complementing simulation-based assessments with data collected from actual low-vision participants. Such adjustments would help to improve the evaluation of color-discrimination thresholds that reflect stable perceptual performance rather than transient adaptation effects.

Chapter 7

Conclusion and Perspectives

7.1 Main Findings and Contributions

This thesis explored the potential of lighting to improve visual performance for individuals with low vision by designing light spectra specifically optimized for certain types of visual impairments. Since colorimetry has been developed without considering the specific characteristics of low vision, this research relied heavily on psychophysical experiments specifically prepared for the objectives of this study. The results demonstrated that lighting can indeed serve as a potential aid, as its spectral properties can be adjusted to enhance color contrast in order to improve residual vision for low vision people.

The first part of this work focused on the technical details required to conduct this study and highlighted both the capabilities and challenges associated with the use of LEDs (**see Chapter 2**). A comprehensive procedure was developed to fully control and characterize the experimental environment (**contribution 1**). An investigation of different simulation methods available was carried out, revealing that while augmented or mixed reality systems are promising, their current technical limitations make them unsuitable for reliably simulating low vision conditions in psychophysical experiments studying color vision.

The following chapter presented an overview of existing methods used to study low vision, as well as current lighting research and recommendations (**see Chapter 3**). There have been many studies done to optimize lighting for a variety of characteristics, however there is a clear gap in the literature: most lighting studies focus exclusively on normal vision. Moreover, since most commonly used metrics are not adapted to low vision observers, this highlighted the necessity of conducting experiments specifically made for low vision conditions.

Following these observations, a first psychophysical experiment was conducted with 57 participants divided into four groups: a control group and three groups simulating different types of visual impairment, blurry vision, tunnel vision, and central scotoma (**see Chapter 4**). The experiment aimed to assess if different types of visual impairments had a significant influence on color discrimination ability depending on the LED channels used. Using a modified version of the FarnsworthMunsell 100 Hue Test, color discrimination was

evaluated across the full chromatic circle (**contribution 2**). Statistical results revealed significant differences between the control group and all simulated visual impairments. In this study, we paid particular attention to the statistical tests used given the parametric dependence of several study factors (**contribution 3**).

Participants with central scotoma performed significantly worse than those with blurry or tunnel vision, which produced relatively similar outcomes. These findings indicate that the type of visual impairment, at least simulated visual impairments, influences color discrimination depending on the LED wavelength. An additional contribution of this study was the development of a fully automated method for recording experimental results using only a consumer-grade camera. These findings were first presented at the 2025 ENVISION conference and are currently under publication process.

Based on these preliminary results, it became necessary to determine the full range of spectral capabilities of the LED panel used in the experiments. Since this study focused on the influence of spectral composition on color discrimination, comparisons had to be made between lights of similar chromaticity. To do this, the spectra produced by the LED panel and those corresponding to the selected chromaticity were identified. Two versions of the metamer generation algorithm proposed by Finlayson et al. were successfully implemented and tested (**see Chapter 5**). Observations revealed that LED spectral drift due to temperature variations was both significant and perceptible. Therefore, a spectral matching algorithm was developed, requiring only a brief characterization procedure involving a single measurement per channel (**contribution 4**). This method estimates the intensity reduction and spectral shift caused by rising junction temperatures, enabling real-time correction of the panels spectral output. The combination of this algorithm with Finlaysons approach proved to be an effective way to produce light spectra with both accurate spectral and chromaticity matching. The proposed spectral matching and stabilization algorithm was presented at the Computational Color Imaging Workshop (CCIW) in Milan.

Using this combination of algorithms, we conduct a new experiment under white stabilized light (**see Chapter 6**). Therefore, a new experiment was designed, using a method to calibrate an inkjet to produce custom color sample sets (**contribution 5**). First a pilot experiment was conducted to verify that the experiment was indeed capable of evaluating differences of color discrimination ability under different lights and identify certain flaws in the design of the experiment. This pilot experiment proved that the method employed was suitable to evaluate color discrimination differences between different lighting conditions. It also proved that good color rendering does not equate to better color discrimination capabilities and that a light without good CRI could be even better. A final experiment was conducted from the data obtained in **Chapter 4**, with two types of simulation goggles blurry vision and central scotoma. The outcomes highlighted the influence of short-term adaptation and, for some participants, visual fatigue when using the goggles. In this type of psychophysical experiment, where determining a precise color-discrimination threshold is essential, such effects can influence performance. These observations illustrate the practical limitations of simulation-based approaches in studies of this kind while also pointing toward useful refinements for future protocols. The original design and protocol of the experiment were published in the Journal of Imaging as an extended version of the paper originally presented at the Computational Color Imaging Workshop (CCIW).

Another major contribution of this work lies in the extensive effort that was dedicated to ensure a seamless experimental experience for participants (**contribution 6**). This was achieved through careful optimization of the experimental software developed specifically for this study, in order to improve latency, therefore reducing participant strain, enhancing consistency across trials, and ultimately improving the reproducibility of the results. This aspect was particularly crucial given the technical complexity of the experimental setup, which relied on the integration of multiple devices, including various cameras or the implementation of a real-time feedback loop to continuously correct lighting conditions. To support this level of coordination, dedicated software applications were developed to manage and synchronize all components necessary to the experiments with high reliability and precision.

Overall, this work demonstrated that lighting can play a significant role in enhancing visual performance for individuals with low vision, more specifically for tasks involving color discrimination. It also highlighted the limitations of traditional colorimetry, which fails to account for the perceptual specificities of low vision observers. The first experiment revealed that different types of visual impairments lead to different performance in terms of color discrimination, suggesting that different types of low vision could benefit from different lighting conditions. Significant efforts were made to ensure the reliability and precision of the experimental setup: the light booth was thoroughly characterized, from the spectral properties of its LED panel to the reflectance of its interior surfaces. Considerable programming work was also carried out to allow the psychophysical experiments to be conducted faster, allowing to minimize observer fatigue. The integration and synchronization of multiple devices posed significant challenges, particularly in the second experiment, where a custom program was developed to automatically record participant responses and ensure consistent data collection while stabilizing the lighting system.

7.2 Discussion and Perspectives

The findings presented in this thesis highlighted the significant influence of lighting on color discrimination ability and its potential application as an aid for individuals with low vision. To build upon these findings, several key directions for future investigation can be proposed.

First and most importantly, this work revealed that simulation goggles are not reliable for experiments that require the evaluation of color discrimination threshold, as seen in the final study. The inconsistencies found likely come from visual adaptation or fatigue effects. This highlights the need for future experiments involving actual low vision participants, who are already used to their condition.

Furthermore, all experiments conducted during this thesis also showed significant inter-individual variability in color discrimination performance, which was even more important for the groups with low vision simulation goggles. This represents a major challenge for designing universally effective lighting solutions an suggests that future research should explore the possibility of personalized lighting optimization customized to match the needs of specific individuals.

Additionally, the findings in this work indicate that lighting conditions can influence

specific localized color regions. This suggests the possibility of optimizing lighting environments to enhance color discrimination for targeted applications, particularly in contexts where accurate differentiation of certain color ranges is critical.

Another key finding is that, although the experiments conducted in this study were primarily aimed at optimizing lighting conditions for individuals with low vision, the results also demonstrate that light can also be optimized for individuals with normal vision. This is particularly relevant in contexts where accurate color evaluation is critical, such as in quality control processes or medical diagnostics.

More spectral diversity of lighting conditions should also be considered, in the final part of this study experiments were conducted under white lighting conditions with identical chromaticity coordinates. This approach made it possible to analyze the specific influence of the spectral composition of a light source spectral on color discrimination. However, this method relied on the computation of all spectra with a perfect colorimetric match, which significantly limited the range of spectral diversity examined and failed to account for uncertainties both in measurement accuracy and in inter-observer variability of perception. A more recent approach proposed by Morovič et al. [192] addresses these limitations by representing colors not as single points in a color space but as probabilistic distributions, and therefore incorporating uncertainty. Such a framework would allow the exploration of a wider set of lighting conditions that are still perceptually similar in color.

Finally, while the experiments were conducted in a highly controlled environment to ensure accuracy and repeatability, real-world conditions may give different outcomes. Although preliminary simulations were performed out to assess the influence of environmental variations on illumination, further research is required to evaluate the effectiveness of these optimized lighting conditions in practical, everyday contexts and to fully determine their potential impact on real visual performance.

Bibliography

[1] Sofiane Vernet et al. “Stabilization of the spectral power distribution of a tunable multichannel led lighting system”. In: *International Workshop on Computational Color Imaging*. Springer. 2024, pp. 93–104.

[2] Sofiane Vernet et al. “Experimental Protocol for Color Difference Evaluation Under Stabilized LED Light”. In: *Journal of Imaging* 11.1 (2024), p. 4.

[3] Miquel Perello Nieto. CC BY-SA 4.0 <https://creativecommons.org/licenses/by-sa/4.0>. URL: https://www.researchgate.net/publication/338137873_Convolutional_Neural_Networks_A_Binocular_Vision_Perspective.

[4] Rhcastilhos. and Jmarchn. CC BY-NC-ND 4.0 (http://creativecommons.org/licenses/by-nc-nd/4.0/). URL: https://www.ncbi.nlm.nih.gov/books/NBK470322/figure/article-21504.image.f1/.

[5] Huyen TT Tran et al. “Impacts of retina-related zones on quality perception of omnidirectional image”. In: *IEEE Access* 7 (2019). CC BY 4.0 <https://creativecommons.org/licenses/by/4.0>, pp. 166997–167009.

[6] Helga Kolb. *Facts and Figures Concerning the Human Retina*. University of Utah Health Sciences Center, Salt Lake City (UT), 1995.

[7] Austin Roorda and David R. Williams. “The arrangement of the three cone classes in the living human eye”. en. In: *Nature* 397.6719 (Feb. 1999). Publisher: Nature Publishing Group, pp. 520–522. ISSN: 1476-4687. DOI: 10.1038/17383.

[8] E. Bruce Goldstein, ed. *Blackwell Handbook of Sensation and Perception*. en. 1st ed. Wiley, Feb. 2008. ISBN: 978-0-631-20684-2 978-0-470-75347-7. DOI: 10.1002/9780470753477.

[9] Zhaoping Li. *Understanding vision: theory, models, and data*. Oxford University Press, 2014.

[10] Peter DeSaix et al. *Anatomy & Physiology (OpenStax)*. CC BY 4.0 <https://creativecommons.org/licenses/by/4.0/>. 2013.

[11] A.K. Roy Choudhury. “Chromatic adaptation and colour constancy”. en. In: *Principles of Colour and Appearance Measurement*. Elsevier, 2015, pp. 214–264. ISBN: 978-1-78242-367-6. DOI: 10.1533/9781782423881.214.

[12] *Colorimétrie Partie 3: Composantes trichromatiques CIE | CIE*.

[13] Michael Vollmer. “Physics of the electromagnetic spectrum”. In: *Electromagnetic technologies in food science* (2021), pp. 1–32.

[14] Edward F Zalewski. “Radiometry and photometry”. In: *Handbook of optics* 2 (1995), pp. 24–1.

[15] William Ross McCluney. *Introduction to radiometry and photometry*. Artech House, 2014.

[16] D Durmus. “Correlated color temperature: Use and limitations”. In: *Lighting Research & Technology* 54.4 (2022), pp. 363–375. DOI: 10.1177/14771535211034330.

[17] Kevin A. G. Smet. “Tutorial: The LuxPy Python Toolbox for Lighting and Color Science”. In: *LEUKOS* 16.3 (July 2020), pp. 179–201.

[18] Richard L Alfvin and Mark D Fairchild. “Observer variability in metameric color matches using color reproduction media”. In: *Color Research & Application* 22.3 (1997), pp. 174–188.

[19] Johannes J Vos. “Colorimetric and photometric properties of a 2 fundamental observer”. In: *Color Research & Application* 3.3 (1978), pp. 125–128.

[20] Walter Stanley Stiles and Jennifer M Burch. “NPL colour-matching investigation: final report (1958)”. In: *Optica Acta: International Journal of Optics* 6.1 (1959), pp. 1–26.

[21] Anders Hård and Lars Sivik. “NCS-Natural Color System: A Swedish Standard for Color Notation”. en. In: *Color Research & Application* 6.3 (1981). _eprint: https://onlinelibrary.wiley.com/doi/pdf/10.1002/col.5080060303, pp. 129–138. ISSN: 1520-6378. DOI: 10.1002/col.5080060303.

[22] Gaurav Sharma, Wencheng Wu, and Edul N. Dalal. “The CIEDE2000 color-difference formula: Implementation notes, supplementary test data, and mathematical observations”. In: *Color Research & Application* 30.1 (2005), pp. 21–30. DOI: https://doi.org/10.1002/col.20070.

[23] Cheng Gao et al. “The von Kries chromatic adaptation transform and its generalization”. In: *Chinese Optics Letters* 18.3 (2020), p. 033301.

[24] MP Royer, KW Houser, and AM Wilkerson. “Color discrimination capability under highly structured spectra”. In: *Color Research & Application* 37.6 (2012), pp. 441–449.

[25] Changjun Li et al. “CMC 2000 chromatic adaptation transform: CMCCAT2000”. In: *Color Research & Application* 27.1 (2002), pp. 49–58.

[26] Wendy Davis and Yoshihiro Ohno. “Color quality scale”. In: *Optical Engineering* 49.3 (Mar. 2010). Publisher: SPIE, p. 033602. ISSN: 0091-3286, 1560-2303. DOI: 10.1117/1.3360335.

[27] W. A. Thornton. “Color-Discrimination Index”. EN. In: *JOSA* 62.2 (Feb. 1972). Publisher: Optica Publishing Group, pp. 191–194. DOI: 10.1364/JOSA.62.000191.

[28] Mark S. Rea and Jean P. Freyssinier-Nova. "Color rendering: A tale of two metrics". en. In: *Color Research & Application* 33.3 (2008). _eprint: https://onlinelibrary.wiley.com/doi/pdf/10.1002/col.20399, pp. 192–202. ISSN: 1520-6378. DOI: 10.1002/col.20399.

[29] Michael P. Royer. "Tutorial: Background and Guidance for Using the ANSI/IES TM-30 Method for Evaluating Light Source Color Rendition". In: *LEUKOS* 18.2 (Apr. 2022). Publisher: Taylor & Francis _eprint: https://doi.org/10.1080/15502724.2020.1860771, pp. 191–231. ISSN: 1550-2724. DOI: 10.1080/15502724.2020.1860771.

[30] Pedro Bustamante et al. "Assessment of color discrimination of different light sources". In: *Buildings* 11.11 (2021), p. 527.

[31] Ai-Hong Chen, Fazrin Mazlan, and Saiful-Azlan Rosli. "Colour Discrimination Ability under Fluorescent and Light Emitting Diode". In: *Pertanika J Sci Technol* 25.S8 (2017), pp. 151–162.

[32] Matteo Meneghini et al. "A Review on the Reliability of GaN-Based LEDs". In: *IEEE Transactions on Device and Materials Reliability* 8.2 (June 2008). Conference Name: IEEE Transactions on Device and Materials Reliability, pp. 323–331. ISSN: 1558-2574. DOI: 10.1109/TDMR.2008.921527.

[33] Pradip Dalapati, Nabin Baran Manik, and Asok Nath Basu. "Influence of temperature on the performance of high power AlGaInP based red light emitting diode". en. In: *Optical and Quantum Electronics* 47.5 (May 2015), pp. 1227–1238. ISSN: 1572-817X. DOI: 10.1007/s11082-014-9980-5.

[34] TIFAC - CORE, New Delhi 110016, India et al. "A Review on Effect of The rmal Factors on Performance of High Power Light Emitting Diode (HPLED)". en. In: *Journal of Engineering Science and Technology Review* 9.4 (Aug. 2016), pp. 165–176. ISSN: 17919320, 17912377. DOI: 10.25103/jestr.094.24.

[35] S. Chhajed et al. "Influence of junction temperature on chromaticity and color-rendering properties of trichromatic white-light sources based on light-emitting diodes". In: *Journal of Applied Physics* 97.5 (Feb. 2005), p. 054506. ISSN: 0021-8979. DOI: 10.1063/1.1852073.

[36] Wenzel Jakob et al. *Mitsuba 3 renderer*. Version 3.0.1. https://mitsuba-renderer.org. 2022.

[37] Valeria Acevedo et al. "Real-time low vision simulation in mixed reality". In: *2022 16th International Conference on Signal-Image Technology & Internet-Based Systems (SITIS)*. IEEE. 2022, pp. 354–361.

[38] *Fork in the Road*. https://www.lowvisionsimulators.com/.

[39] Hassan Hashemi et al. "Contrast Sensitivity Evaluation in a Population-Based Study in Shahroud, Iran". In: *Ophthalmology* 119.3 (2012), pp. 541–546. ISSN: 0161-6420. DOI: https://doi.org/10.1016/j.ophtha.2011.08.030.

[40] C Kniestedt and R Stamper. "Visual acuity and its measurement". en. In: *Ophthalmology Clinics of North America* 16.2 (June 2003), pp. 155–170. ISSN: 08961549. DOI: 10.1016/S0896-1549(03)00013-0.

[41] Michael Kalloniatis and Charles Luu. "Visual acuity". In: *Webvision: The Organization of the Retina and Visual System [Internet]* (2007).

[42] M.H. PIRENNE. "CHAPTER 9 - Visual Acuity". In: *The Visual Process*. Ed. by HUGH DAVSON. Academic Press, 1962, pp. 175–195. ISBN: 978-1-4832-3089-4. DOI: https://doi.org/10.1016/B978-1-4832-3089-4.50018-2.

[43] De Jong and Paulus T. V. M. "A history of visual acuity testing and optotypes". en. In: *Eye* 38.1 (Jan. 2024). Publisher: Nature Publishing Group, pp. 13–24. ISSN: 1476-5454. DOI: 10.1038/s41433-022-02180-6.

[44] Herman Snellen. *Probebuchstaben zur bestimmung der sehschärfe*. H. Peters, 1873.

[45] F Monoyer. "Echelle typographique décimale pour mésurer l'acuité de la vue". In: *Acad des Sc Compt rend* 80 (1875), pp. 1137–1138.

[46] Ian L Bailey and Jan E Lovie. "New design principles for visual acuity letter charts". In: *Optometry and Vision Science* 53.11 (1976), pp. 740–745.

[47] Frederick L Ferris III et al. "New visual acuity charts for clinical research". In: *American journal of ophthalmology* 94.1 (1982), pp. 91–96.

[48] Edmund Landolt. "Methode optometrique simple". In: *Bull Mem Soc Fran Ophtalmol* 6 (1888), pp. 213–4.

[49] *ISO 8596:2017*. en.

[50] Public domain. URL: https://commons.wikimedia.org/wiki/File:Snellen06.png.

[51] URL: https://precision-vision.com/products/visual-acuity-reading-charts/letter-symbol/charts-for-cabinets/charts-for-small-cabinets/landolt-c/logarithmic-landolt-c-eye-chart/.

[52] Robert H Spector. "Visual fields". In: *Clinical methods: The history, physical, and laboratory examinations* 3 (1990), pp. 565–572.

[53] Ranjeet J Pandit, Kevin Gales, and Philip G Griffiths. "Effectiveness of testing visual fields by confrontation". In: *The Lancet* 358.9290 (2001), pp. 1339–1340.

[54] Lenworth N Johnson and Frank G Baloh. "The accuracy of confrontation visual field test in comparison with automated perimetry". In: *Journal of the national medical association* 83.10 (1991), p. 895.

[55] Chris A Johnson, Michael Wall, and H Stanley Thompson. "A history of perimetry and visual field testing". In: *Optometry and Vision Science* 88.1 (2011), E8–E15.

[56] Molly L Fuller et al. "Tangent screen perimetry in the evaluation of visual field defects associated with ptosis and dermatochalasis". In: *PLoS One* 12.3 (2017), e0174607.

[57] URL: https://www.ophthalmic.com.sg/product/tangent-screen/.

[58] Hans Goldmann. "Ein selbstregistrierendes projektionskugelperimeter". In: *Ophthalmologica* 109.2-3 (1945), pp. 71–79.

[59] RobertB3009. CC BY-SA 4.0 <https://creativecommons.org/licenses/by-sa/4.0>, via Wikimedia Commons. URL: https://commons.wikimedia.org/wiki/File:PatientviewGoldmannperimeter.jpg.

[60] URL: https://www.ebc-europe.com/produit/octopus-900/.

[61] Jesse Richman, George L. Spaeth, and Barbara Wirostko. "Contrast sensitivity basics and a critique of currently available tests". en. In: *Journal of Cataract and Refractive Surgery* 39.7 (July 2013), pp. 1100–1106. ISSN: 0886-3350. DOI: 10.1016/j.jcrs.2013.05.001.

[62] David B Elliott, Kay Sanderson, and Alison Conkey. "The reliability of the Pelli-Robson contrast sensitivity chart". In: *Ophthalmic and Physiological Optics* 10.1 (1990), pp. 21–24.

[63] DEBORAH C SPELLMAN et al. "Letter contrast sensitivity in retinitis pigmentosa patients assessed by Regan charts". In: *Retina* 9.4 (1989), pp. 287–291.

[64] URL: https://precision-vision.com/products/contrast-sensitivity-tests/peak-contrast-sensitivity/pelli-robson/pelli-robson-contrast-sensitivity-chart/.

[65] Vistech Consultants. 1988.

[66] Shinobu Ishihara. "Test for color blindness". In: (1917).

[67] Alex Melamud, Stephanie Hagstrom, and Elias Traboulsi. "Color vision testing". In: *Ophthalmic Genetics* 25.3 (2004), pp. 159–187.

[68] Barry L Cole, Ka-yee Lian, and Carol Lakkis. "The new Richmond HRR pseudoisochromatic test for colour vision is better than the Ishihara test". In: *Clinical and Experimental Optometry* 89.2 (2006), pp. 73–80.

[69] M Shiva Ram and Rishi Bhardwaj. "To assess the effect of lighting on identifying the ishihara colour vision plates in trichromats". In: *Ophthalmology Research: An International Journal* 7.1 (2017), pp. 1–6.

[70] Shinobu Ishihara. Public domain, via Wikimedia Commons.

[71] URL: https://www.xrite.com/fr-fr/service-support/product-support/visual-assessment-tools/fm-100-hue-test.

[72] URL: https://www.xrite.com/pl-pl/categories/visual-assessment-tools/fm-dichotomous-d15-test.

[73] Dean Farnsworth. "The Farnsworth-Munsell 100-Hue and Dichotomous Tests for Color Vision*". EN. In: *JOSA* 33.10 (Oct. 1943). Publisher: Optica Publishing Group, pp. 568–578. DOI: 10.1364/JOSA.33.000568.

[74] Jason S Ng and Sophia C Liem. "Can the Farnsworth D15 color vision test be defeated through practice?" In: *Optometry and Vision Science* 95.5 (2018), pp. 452–456.

[75] URL: https://www.color-blind-test.com/anomaloscope-more.

[76] Stephen J Dain and Jeffery K Hovis. "Recommendations and requirements for the wavelengths in Rayleigh equation anomaloscopes". In: *Journal of the Optical Society of America A* 40.3 (2023), A121–A129.

[77] J.D. MORELAND. "Moreland match revisited". In: *Visual Neuroscience* 21.3 (2004), pp. 471–476. DOI: 10.1017/S0952523804213438.

[78] Rachel A Murphy. "Comparing Color Vision Testing Using the Farnsworth-Munsell 100-Hue, Ishihara Compatible, and Digital TCV Software". In: *College of Optometry* 9 (2015).

[79] Alvaro Fanlo-Zarazaga et al. "Validation of a New Digital and Automated Color Perception Test". In: *Diagnostics* 14.4 (2024). ISSN: 2075-4418. DOI: 10.3390/diagnostics14040396.

[80] Omar K Ozgur et al. "Validity and acceptance of color vision testing on smartphones". In: *Journal of Neuro-ophthalmology* 38.1 (2018), pp. 13–16.

[81] Ali Almustanyir, Jeffery Hovis, and Mackenzie G. Glaholt. "Predicting the Farnsworth–Munsell D15 and Holmes–Wright-A lantern outcomes with computer-based color vision tests". In: *J. Opt. Soc. Am. A* 37.4 (May 2020), A1–A10. DOI: 10.1364/JOSAA.381305.

[82] JD Mollon and BC Regan. "Cambridge colour test handbook". In: *Cambridge: Cambridge Research Systems* (2000).

[83] Galina V. Paramei. "Color discrimination across four life decades assessed by the Cambridge Colour Test". In: *J. Opt. Soc. Am. A* 29.2 (Feb. 2012), A290–A297. DOI: 10.1364/JOSAA.29.00A290.

[84] Jayasree Seshadri et al. "Evaluation of the new web-based Colour Assessment and Diagnosis test". In: *Optometry and vision science* 82.10 (2005), pp. 882–885.

[85] J Stephen Mansfield, Gordon E Legge, and Mark C Bane. "Psychophysics of reading. XV: Font effects in normal and low vision." In: *Investigative ophthalmology & visual science* 37.8 (1996), pp. 1492–1501.

[86] Keith Bright and Veronika Egger. "Using visual contrast for effective, inclusive environments". In: *Information Design Journal* 16.3 (2008), pp. 178–189.

[87] URL: https://japanupclose.web-japan.org/tech/t20211008_1.html.

[88] Paula Baptista Eliseo da Silva, Ariadne Stavare Leal, and Nvea Nunes Ferraz. "Usability of smartphone apps as reading aids for low vision patients". In: *Disability and Rehabilitation: Assistive Technology* 17.7 (2022), pp. 848–852.

[89] Natalina Martiniello et al. "Exploring the use of smartphones and tablets among people with visual impairments: Are mainstream devices replacing the use of traditional visual aids?" In: *Assistive Technology* 34.1 (2022), pp. 34–45.

[90] MD Bharat Gurnani. CC BY-NC-ND 4.0, (http://creativecommons.org/licenses/by-nc-nd/4.0/), StatPearls Publishing LLC. URL: https://www.ncbi.nlm.nih.gov/sites/books/NBK585124/figure/article-145084.image.f1/?report=objectonly.

[91] Haifa Ammar Zeineddin et al. "PERCEVO: AI-powered Smart Cane with Dynamic Object Recognition to Support People with Disabilities". In: *2025 Eighth International Women in Data Science Conference at Prince Sultan University (WiDS PSU)*. IEEE. 2025, pp. 85–90.

[92] Qingtian Chen et al. "CCNY smart cane". In: *2017 IEEE 7th Annual International Conference on CYBER Technology in Automation, Control, and Intelligent Systems (CYBER)*. IEEE. 2017, pp. 1246–1251.

[93] Tushar Sharma et al. "Smart cane: Better walking experience for blind people". In: *2017 3rd International Conference on Computational Intelligence and Networks (CINE)*. IEEE. 2017, pp. 22–26.

[94] T Lavanya Narayani et al. "Design of Smart Cane with integrated camera module for visually impaired people". In: *2021 International Conference on Artificial Intelligence and Smart Systems (ICAIS)*. IEEE. 2021, pp. 999–1004.

[95] Sankari Subbiah et al. "Smart cane for visually impaired based on IOT". In: *2019 3rd International Conference on Computing and Communications Technologies (ICCCT)*. IEEE. 2019, pp. 50–53.

[96] Aya Dernayka et al. "Tom Pouce III, an electronic white cane for blind people: Ability to detect obstacles and mobility performances". In: *Sensors* 21.20 (2021), p. 6854.

[97] Chunming Mai et al. "A smart cane based on 2d lidar and rgb-d camera sensor-realizing navigation and obstacle recognition". In: *Sensors* 24.3 (2024), p. 870.

[98] Emanuele Cardillo, Changzhi Li, and Alina Caddemi. "Millimeter-wave radar cane: A blind people aid with moving human recognition capabilities". In: *IEEE Journal of Electromagnetics, RF and Microwaves in Medicine and Biology* 6.2 (2021), pp. 204–211.

[99] Ahmad Abusukhon. "IOT bracelets for guiding blind people in an indoor environment". In: *Journal of Communications Software and Systems* 19.2 (2023), pp. 114–125.

[100] Jessica Tipantuña et al. "Electronic bracelet with artificial vision for assisting blind people". In: *International Conference on Computer Science, Electronics and Industrial Engineering (CSEI)*. Springer. 2022, pp. 366–379.

[101] Rakesh Chandra Joshi et al. "AI-SenseVision: a low-cost artificial-intelligence-based robust and real-time assistance for visually impaired people". In: *IEEE Transactions on Human-Machine Systems* 54.3 (2024), pp. 325–336.

[102] Erick Javier Argüello Prada and Lina Mara Santacruz Forero. "A belt-like assistive device for visually impaired people: Toward a more collaborative approach". In: *Cogent Engineering* 9.1 (2022), p. 2048440.

[103] Shripad Bhatlawande et al. "Electronic bracelet and vision-enabled waist-belt for mobility of visually impaired people". In: *Assistive Technology* 26.4 (2014), pp. 186–195.

[104] Seyed Ali Cheraghi, Vinod Namboodiri, and Laura Walker. "GuideBeacon: Beacon-based indoor wayfinding for the blind, visually impaired, and disoriented". In: *2017 IEEE International Conference on Pervasive Computing and Communications (PerCom)*. IEEE. 2017, pp. 121–130.

[105] Madhura Gharat, Rizwan Patanwala, and Adithi Ganaparthi. "Audio guidance system for blind". In: *2017 International conference of Electronics, Communication and Aerospace Technology (ICECA)*. Vol. 1. IEEE. 2017, pp. 381–384.

[106] Maria Rosiak, Mateusz Kawulok, and Micha Makowski. "The effectiveness of UWB-based indoor positioning systems for the navigation of visually impaired individuals". In: *Applied Sciences* 14.13 (2024), p. 5646.

[107] Xinrui Yu and Jafar Saniie. "Visual impairment spatial awareness system for indoor navigation and daily activities". In: *Journal of Imaging* 11.1 (2025), p. 9.

[108] Paniz Sedighi, Mohammad Hesam Norouzi, and Mehdi Delrobaei. "An RFID-based assistive glove to help the visually impaired". In: *IEEE Transactions on Instrumentation and Measurement* 70 (2021), pp. 1–9.

[109] Yunjin Zhang et al. "Color contrast enhanced rendering for optical see-through head-mounted displays". In: *IEEE Transactions on Visualization and Computer Graphics* 28.12 (2021), pp. 4490–4502.

[110] Benoit Froissard. "Assistance visuelle des malvoyants par traitement dimages adaptatif". PhD thesis. Université Jean Monnet-Saint-Etienne, 2014.

[111] Yuhang Zhao et al. "Designing and evaluating a customizable head-mounted vision enhancement system for people with low vision". In: *ACM Transactions on Accessible Computing (TACCESS)* 12.4 (2019), pp. 1–46.

[112] Marie-Céline Lorenzini, Anni M Hämäläinen, and Walter Wittich. "Factors related to the use of a head-mounted display for individuals with low vision". In: *Disability and Rehabilitation* 43.17 (2021), pp. 2472–2486.

[113] Yuhang Zhao et al. "CueSee: exploring visual cues for people with low vision to facilitate a visual search task". In: *Proceedings of the 2016 ACM International Joint Conference on Pervasive and Ubiquitous Computing*. 2016, pp. 73–84.

[114] Lior Maman and Sarit FA Szpiro. "Enhancing Obstacle Visibility with Augmented Reality Improves Mobility in People with Low Vision". In: *IEEE Transactions on Visualization and Computer Graphics* (2025).

[115] Dylan R Fox et al. "Using augmented reality to cue obstacles for people with low vision". In: *Optics express* 31.4 (2023), pp. 6827–6848.

[116] Yuhang Zhao et al. "The Effectiveness of Visual and Audio Wayfinding Guidance on Smartglasses for People with Low Vision". In: *Proceedings of the 2020 CHI Conference on Human Factors in Computing Systems*. CHI '20. Honolulu, HI, USA: Association for Computing Machinery, 2020, pp. 1–14. ISBN: 9781450367080. DOI: 10.1145/3313831.3376516.

[117] URL: https://www.ray-ban.com/france/electronics/RW4006ray-ban%2020%7C%2020meta%2020wayfarer-noir/8056597988377.

[118] Samrat Raj Sharma et al. "Smart Glasses for Blind People Using Obstacles Detection". In: *2023 International Conference on Sustainable Emerging Innovations in Engineering and Technology (ICSEIET)*. IEEE. 2023, pp. 891–894.

[119] K Makanyadevi et al. “AI-Powered Smart Glasses and Shoes for the Visually Impaired”. In: *2025 6th International Conference on Mobile Computing and Sustainable Informatics (ICMCSI)*. IEEE. 2025, pp. 1595–1603.

[120] H Burkhard Dick and Ronald D Gerste. “Future intraocular lens technologies”. In: *Ophthalmology* 128.11 (2021), e206–e213.

[121] Jorge L Alió et al. “Intraocular telescopic lens evaluation in patients with age-related macular degeneration”. In: *Journal of Cataract & Refractive Surgery* 30.6 (2004), pp. 1177–1189.

[122] Cihun-Siyong Gong. “Advances in Electrode Design and Physiological Considerations for Retinal Implants”. In: *Micromachines* 16.5 (2025), p. 598.

[123] Amy Nau, Michael Bach, and Christopher Fisher. “Clinical tests of ultra-low vision used to evaluate rudimentary visual perceptions enabled by the BrainPort vision device”. In: *Translational vision science & technology* 2.3 (2013), pp. 1–1.

[124] Fatima Zahid and Devi Mohan Lal. “Influence of Low Vision Assistive Technology on Mobility Among Visually Impaired Individuals”. In: *Journal of Health, Wellness and Community Research* (2025), e630–e630.

[125] Carl Halladay Abraham, Diane van Staden, and Nishanee Rampersad. “Barriers and enablers to low vision care and rehabilitation in sub-Saharan Africa within a global context”. In: *Clinical and Experimental Optometry* 107.1 (2024), pp. 3–13.

[126] Priya Sivakumar et al. “Barriers in utilisation of low vision assistive products”. In: *Eye* 34.2 (2020), pp. 344–351.

[127] Hein Min Htike et al. “Ability of head-mounted display technology to improve mobility in people with low vision: A systematic review”. In: *Translational Vision Science & Technology* 9.10 (2020), pp. 26–26.

[128] Anne Macnamara et al. “Low vision devices for age-related macular degeneration: a systematic review”. In: *Disability and Rehabilitation: Assistive Technology* 18.7 (2023), pp. 998–1010.

[129] Eugenie Golubova et al. “Design considerations for the ideal low vision aid: insights from de-brief interviews following a real-world recording study”. In: *Ophthalmic and Physiological Optics* 41.2 (2021), pp. 266–280.

[130] Karima S Khimani et al. “Barriers to low-vision rehabilitation services for visually impaired patients in a multidisciplinary ophthalmology outpatient practice”. In: *Journal of Ophthalmology* 2021.1 (2021), p. 6122246.

[131] Georges M Durr and Iqbal Ike K Ahmed. “Intraocular lens complications: decentration, uveitis–glaucoma–hyphema syndrome, opacification, and refractive surprises”. In: *Ophthalmology* 128.11 (2021), e186–e194.

[132] British Standard. “Light and lighting: Lighting of work places: Part 1: Indoor work places”. In: *Indoor work places.* (2011).

[133] ANSI/IES. *Design guide: recommended practice for office lighting*. 2012.

[134] Mary Butler, Keri McMullan, and Susan E Ryan. “Lighting prescriptions for low vision”. In: *Journal of Housing for the Elderly* 33.2 (2019), pp. 189–203.

[135] Karyono Karyono et al. “A novel adaptive lighting system which considers behavioral adaptation aspects for visually impaired people”. In: *Buildings* 10.9 (2020), p. 168.

[136] Rebecca Henry, Josée Duquette, and Walter Wittich. “Comparison of two lighting assessment methods when reading with low vision”. In: *Optometry and Vision Science* 97.4 (2020), pp. 257–264.

[137] Yukio Akashi et al. *CIE 227:2017 Lighting for Older People and People with Visual Impairment in Buildings*. Jan. 2017. DOI: 10.25039/TR.227.2017.

[138] Nicolaas Prins et al. *Psychophysics: a practical introduction*. Academic Press, 2016.

[139] Daisuke Saito et al. “A study on visibility estimation of web-safe colors using paired comparison and discriminant analysis”. In: *Electrical Engineering in Japan* 157.2 (2006), pp. 32–39.

[140] Min Huang et al. “Colorimetric Observer Categories for Young and Aged Using Paired-Comparison Experiments”. In: *IEEE Access* 8 (2020), pp. 219473–219482. DOI: 10.1109/ACCESS.2020.3042817.

[141] Fereshteh Mirjalili et al. “Color-difference formula for evaluating color pairs with no separation: ENS”. In: *Journal of the Optical Society of America A* 36.5 (May 2019), p. 789. ISSN: 1520-8532. DOI: 10.1364/josaa.36.000789.

[142] Ethan D. Montag and David C. Wilber. “A comparison of constant stimuli and gray-scale methods of color difference scaling”. In: *Color Research & Application* 28.1 (2003), pp. 36–44. DOI: https://doi.org/10.1002/col.10112.

[143] Min Huang et al. “Testing uniform colour spaces and colour-difference formulae using printed samples”. In: *Color Research & Application* 37.5 (2012), pp. 326–335. DOI: https://doi.org/10.1002/col.20689.

[144] Ting Xu et al. “Effect of Printed Color Sample Separation and Color-Difference Magnitude on Perceived Color Difference”. In: *Advances in Graphic Communication, Printing and Packaging*. Ed. by Pengfei Zhao et al. Singapore: Springer Singapore, 2019, pp. 87–92. ISBN: 978-981-13-3663-8.

[145] Yuta Asano et al. “Color matching experiment for highlighting interobserver variability”. en. In: *Color Research & Application* 41.5 (2016). _eprint: https://onlinelibrary.wiley.com/doi/pdf/10.1002/col.21975, pp. 530–539. ISSN: 1520-6378. DOI: 10.1002/col.21975.

[146] Jorge Vila-Tomás, Pablo Hernández-Cámara, and Jesús Malo. “Artificial psychophysics questions classical hue cancellation experiments”. In: *Frontiers in Neuroscience* 17 (2023), p. 1208882.

[147] Sang Wook Hong and Randolph Blake. “Early visual mechanisms do not contribute to synesthetic color experience”. In: *Vision Research* 48.8 (2008), pp. 1018–1026. ISSN: 0042-6989. DOI: https://doi.org/10.1016/j.visres.2008.01.024.

[148] Benediktus Anindito et al. “Indoor Agriculture: Measurement of The Intensity of LED for Optimum Photosynthetic Recovery”. In: *2018 5th International Conference on Electrical Engineering, Computer Science and Informatics (EECSI)*. IEEE. 2018, pp. 356–361.

[149] S-kei. CC BY-SA 2.5 <https://creativecommons.org/licenses/by-sa/2.5>, via Wikimedia Commons. URL: https://commons.wikimedia.org/wiki/File:PnJunction-LED-E.svg.

[150] Russell D Dupuis and Michael R Krames. "History, development, and applications of high-brightness visible light-emitting diodes". In: *Journal of lightwave technology* 26.9 (2008), pp. 1154–1171.

[151] Jaehee Cho et al. "White light-emitting diodes: history, progress, and future". In: *Laser & photonics reviews* 11.2 (2017), p. 1600147.

[152] Clay Elliott and Kyung Lee. *Adoption of light-emitting diodes in common lighting applications*. Tech. rep. Guidehouse, Inc., Washington, DC (United States), 2020.

[153] Georges Zissis, Paolo Bertoldi, SERRENHO Tiago RIBEIRO, et al. "Update on the Status of LED-Lighting world market since 2018". In: (2021).

[154] Francisco J Burgos-Fernandez et al. "Spectrally tunable light source based on light-emitting diodes for custom lighting solutions". In: *Optica Applicata* 46.1 (2016), pp. 117–129.

[155] Guoxing He, Lihong Zheng, and Huafeng Yan. "LED white lights with high CRI and high luminous efficacy". In: *LED and Display Technologies*. Vol. 7852. SPIE. 2010, pp. 58–66.

[156] Licai Xiao et al. "Spectral optimization of phosphor-coated white LED for road lighting based on the mesopic limited luminous efficacy and IES color fidelity index". In: *Applied Optics* 57.4 (2018), pp. 931–936.

[157] Guoxing He and Ju Tang. "Spectral optimization of phosphor-coated white LEDs for color rendering and luminous efficacy". In: *IEEE Photonics Technology Letters* 26.14 (2014), pp. 1450–1453.

[158] J.J. Zhang et al. "Spectral optimization based simultaneously on color-rendering index and color quality scale for white LED illumination". In: *Optics & Laser Technology* 88 (2017), pp. 161–165. ISSN: 0030-3992. DOI: https://doi.org/10.1016/j.optlastec.2016.08.006.

[159] Snjezana Soltic and Andrew Chalmers. "Optimization of LED Lighting for Clinical Settings". In: *Journal of Healthcare Engineering* 2019.1 (2019), p. 5016013. DOI: https://doi.org/10.1155/2019/5016013.

[160] Yi Jiau Saw, Vineetha Kalavally, and Chee Pin Tan. "The Spectral Optimization of a Commercializable Multi-Channel LED Panel With Circadian Impact". In: *IEEE Access* 8 (2020). Conference Name: IEEE Access, pp. 136498–136511. ISSN: 2169-3536. DOI: 10.1109/ACCESS.2020.3010339.

[161] Li-Li Zheng et al. "Spectral optimization of three-primary LEDs by considering the circadian action factor". In: *IEEE Photonics Journal* 8.6 (2016), pp. 1–9.

[162] Sérgio MC Nascimento and Osamu Masuda. "Psychophysical optimization of lighting spectra for naturalness, preference, and chromatic diversity". In: *Journal of the Optical Society of America A* 29.2 (2012), A144–A151.

[163] Mika Flinkman and Shigeki Nakauchi. “Illuminations that improve color discrimination ability of people with red-green color vision deficiency”. EN. In: *JOSA A* 34.10 (Oct. 2017). Publisher: Optica Publishing Group, pp. 1914–1923. ISSN: 1520-8532. DOI: 10.1364/JOSAA.34.001914.

[164] Yehoshua Almog and Arie Nemet. “The Correlation Between Visual Acuity and Color Vision as an Indicator of the Cause of Visual Loss”. en. In: *American Journal of Ophthalmology* 149.6 (June 2010), pp. 1000–1004. ISSN: 0002-9394. DOI: 10.1016/j.ajo.2010.01.011.

[165] Jasleen K. Jolly et al. “The Effect of Cataract on Color Vision Measurement with the Low-Vision Cambridge Colour Test: Providing an Adjustment Factor for Clinical Trials”. In: *Ophthalmology Science* 2.2 (June 2022), p. 100153. ISSN: 2666-9145. DOI: 10.1016/j.xops.2022.100153.

[166] Barbara Acheson Cooper et al. “The use of the Lanthony New Color Test in determining the effects of aging on color vision”. In: *Journal of Gerontology* 46.6 (1991), P320–P324.

[167] Pichayada Katemake et al. “Influence of LED-based assistive lighting solutions on the autonomous mobility of low vision people”. In: *Building and Environment* 157 (2019), pp. 172–184.

[168] James S Wolffsohn et al. “Effect of light-emitting diode colour temperature on magnifier reading performance of the visually impaired”. In: *Clinical and Experimental Optometry* 95.5 (2012), pp. 510–514.

[169] Deepa V. Ramane and Arvind D. Shaligram. “Design of multispectral reading light for individuals with low vision”. In: *Journal of Biomedical Optics* 17.1 (Jan. 2012). Publisher: SPIE, p. 018002. ISSN: 1083-3668, 1560-2281. DOI: 10.1117/1.JBO.17.1.018002.

[170] Linna Yang et al. “A multichannel LED-based lighting approach to improve color discrimination for low vision people”. In: *Electronic Imaging* 35.10 (2023), pp. 253-1–253-1. DOI: 10.2352/EI.2023.35.10.HVEI-253.

[171] M Wei et al. “Perceptual responses to LED illumination with colour rendering indices of 85 and 97”. In: *Lighting Research & Technology* 47.7 (2015), pp. 810–827. DOI: 10.1177/1477153514548089.

[172] R Srividya and Ciji Pearl Kurian. “White light source towards spectrum tunable lighting - A review”. In: *2014 International Conference on Advances in Energy Conversion Technologies (ICAECT)*. 2014, pp. 203–208. DOI: 10.1109/ICAECT.2014.6757088.

[173] Elodie Mahler, Jean-Jacques Ezrati, and Françoise Viénot. “Testing LED lighting for colour discrimination and colour rendering”. In: *Color Research & Application* 34.1 (2009), pp. 8–17. DOI: https://doi.org/10.1002/col.20459.

[174] Chi-Yuang Yu, Yen-Hui Lin, and Chih-Yong Chen. “Elucidating the effect of yellow illumination on color confusion in the semiconductor-related manufacturing industry”. In: *Human Factors and Ergonomics in Manufacturing & Service Industries* 21.5 (2011), pp. 456–463. DOI: https://doi.org/10.1002/hfm.20240.

[175] M. Delacre, D. Lakens, and C. Leys. "Why psychologists should by default use Welch's t-test instead of student's t-test". English. In: *International Review of Social Psychology* 30.1 (Apr. 2017), pp. 92–101. ISSN: 2397-8570. DOI: 10.5334/irsp.82.

[176] Graham Finlayson et al. "On calculating metamer sets for spectrally tunable LED illuminators". In: *JOSA A* 31.7 (July 2014), pp. 1577–1587. DOI: 10.1364/JOSAA.31.001577.

[177] Rade D. Paravina et al. "Color Difference Thresholds in Dentistry". In: *Journal of Esthetic and Restorative Dentistry* 27.S1 (2015), S1–S9. DOI: https://doi.org/10.1111/jerd.12149.

[178] Ming Ronnier Luo, Guihua Cui, and Brian Rigg. "The development of the CIE 2000 colour-difference formula: CIEDE2000". In: *Color Research & Application* 26.5 (2001), pp. 340–350. DOI: 10.1002/col.1049.

[179] Commission Internationale de l'Éclairage. *Colorimetry, 3rd edition*. CIE Technical Report 15:2004. Vienna, Austria: CIE Central Bureau, 2004. ISBN: 978-3-901906-33-6.

[180] Manuel Melgosa, Rafael Huertas, and Roy S. Berns. "Relative significance of the terms in the CIEDE2000 and CIE94 color-difference formulas". In: *J. Opt. Soc. Am. A* 21.12 (Dec. 2004), pp. 2269–2275. DOI: 10.1364/JOSAA.21.002269.

[181] Ming Ronnier Luo et al. "Verification of CIEDE2000 using industrial data". In: *Color and Paints: Interim Meeting of the International Color Association*. 2004, pp. 97–102.

[182] Philipp Urban et al. "Embedding non-Euclidean color spaces into Euclidean color spaces with minimal isometric disagreement". In: *Journal of the Optical Society of America A* 24.6 (2007), pp. 1516–1528. DOI: 10.1364/JOSAA.24.001516.

[183] Lorenzo Ridolfi, Marcelo Gattass, and Hélio Lopes. "Investigating Euclidean Mappings for CIEDE2000 Color Difference Formula". In: *18th Color and Imaging Conference*. Society for Imaging Science and Technology. 2010, pp. 327–333. DOI: 10.2352/SIC.2010.18.327.

[184] Philippe Colantoni, Jean-Baptiste Thomas, and Alain Trémeau. "Sampling CIELAB color space with perceptual metrics". In: *International Journal of Imaging and Robotics* 16.3 (2016), pp. 1–22.

[185] Ján Morovic. "Color Reproduction Data Flows". In: *Color Gamut Mapping*. John Wiley & Sons, Ltd, 2008. Chap. 4, pp. 73–90. ISBN: 9780470758922. DOI: https://doi.org/10.1002/9780470758922.ch4.

[186] Nawar Fdhal et al. "Color Space Transformation from RGB to CIELAB Using Neural Networks". In: *Advances in Multimedia Information Processing - PCM 2009*. Ed. by Paisarn Muneesawang et al. Berlin, Heidelberg: Springer Berlin Heidelberg, 2009, pp. 1011–1017. ISBN: 978-3-642-10467-1.

[187] Xinyue Bao, Wangan Song, and Sheng Liu. "Research on Color Space Conversion Model from CMYK to CIE-LAB Based on GRNN". In: *Image and Video Technology: 8th Pacific-Rim Symposium, PSIVT 2017, Wuhan, China, November 20-24, 2017, Revised Selected Papers*. Wuhan, China: Springer-Verlag, 2017, pp. 252–261. ISBN: 978-3-319-75785-8. DOI: 10.1007/978-3-319-75786-5_21.

[188] International Color Consortium. *Image Technology Colour Management - Architecture, Profile Format, and Data Structure*. Tech. rep. ICC.1:2022. Profile version 4.4.0.0. International Color Consortium, May 2022.

[189] International Color Consortium. *Image Technology Colour Management - Extensions to Architecture, Profile Format, and Data Structure*. Tech. rep. ICC.2:2023. iccMAX. International Color Consortium, Oct. 2023.

[190] Philippe Colantoni et al. "High-end colorimetric display characterization using an adaptive training set". In: *Journal of the Society for Information Display* 19.8 (2011), pp. 520–530. DOI: 10.1889/JSID19.8.520.

[191] T Hales. "Cannonballs and honeycombs". In: *Notices of the American Mathematical Society* 47 (Jan. 2000), pp. 440–449.

[192] Peter Morovic and Ján Morovic. "Atomic color: From points to probability distributions". In: *International Workshop on Computational Color Imaging*. Springer. 2024, pp. 3–21.

Acronyms

- WHO : World Health Organization
- LIDAR : Light Detection And Ranging
- MR : Mixed Reality
- AR : Advanced Reality
- VR : Virtual Reality
- LED : Light-Emitting Diode
- CIE : Commission Internationale de l'Eclairage
- AMD : Age-related Macular Degeneration
- EMR : Electromagnetic Radiation
- UV : Ultraviolet
- SPD : Spectral Power Distribution
- CCT : Correlated Color Temperature
- UCS : Uniform Color Space
- MCS : Munsell Color System
- NCS : Natural Color System
- CRI : Color Rendering Index
- CQS : Color Quality Scale
- GAI : Gamut Area Index
- MAE : Mean Absolute Error
- VA : Visual Acuity
- MAR : Minimal Angle of Resolution

- ETDRS : Early Treatment Diabetic Retinopathy Study
- HRR : Hardy, Rand and Rittler
- FM100 : Farnsworth-Munsell 100 hue test
- CCTV : Closed-Circuit Television
- UWB : Ultra-Wideband
- RFID : Radio Frequency Identification
- BLE : Bluetooth Low Energy
- HUD : Head-Up Display
- VLM : Vision Language Model
- LER : Luminous Efficacy of Radiation
- MELR : Melanopic Efficacy of Luminous Radiation
- COI : Cyanosis Observation Index
- TES : Total Error Score
- ETES : Extended Total Error Score
- ANOVA : Analysis Of Variance

Appendix A

Spatial measures

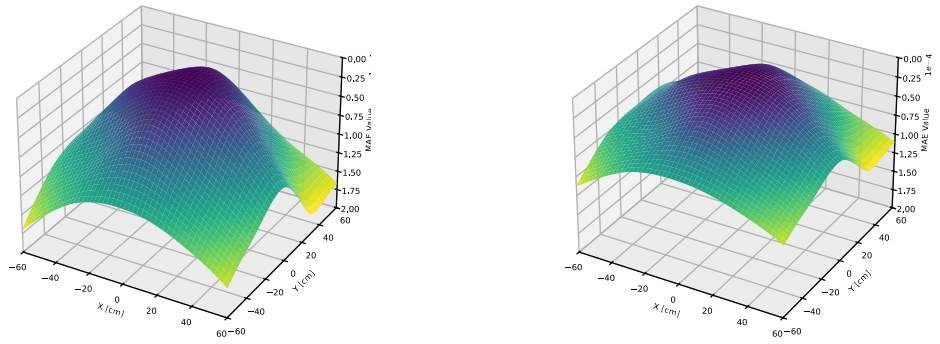

(a) Channel 1.

(b) Channel 2.

Figure A.1: Mean Average Error of the SPD compared to the center of the booth for channel 1 and 2.

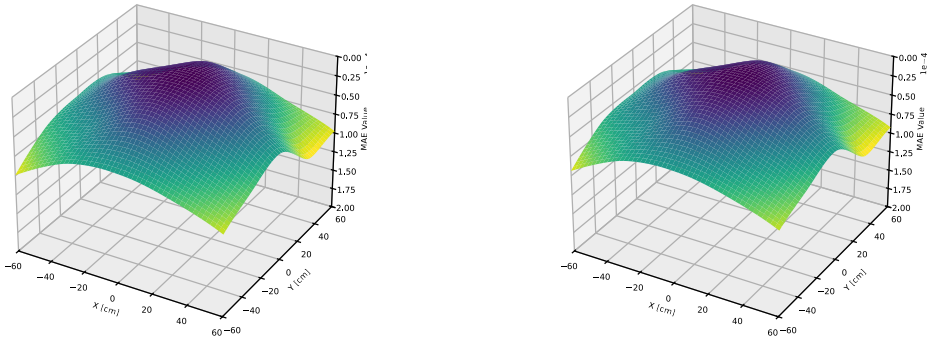

(a) Channel 3.

(b) Channel 4.

Figure A.2: Mean Average Error of the SPD compared to the center of the booth for channel 3 and 4.

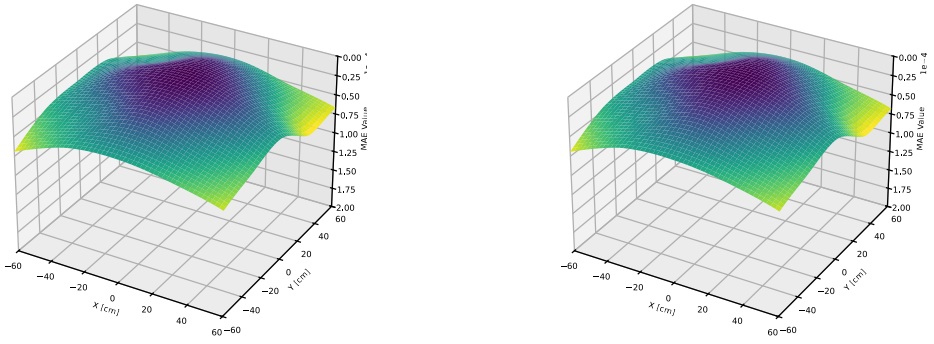

(a) Channel 5.

(b) Channel 6.

Figure A.3: Mean Average Error of the SPD compared to the center of the booth for channel 5 and 6.

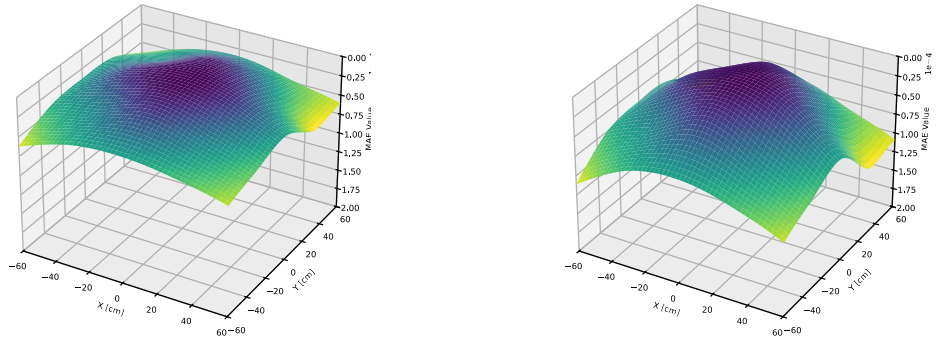

(a) Channel 7. (b) Channel 8.

Figure A.4: Mean Average Error of the SPD compared to the center of the booth for channel 7 and 8.

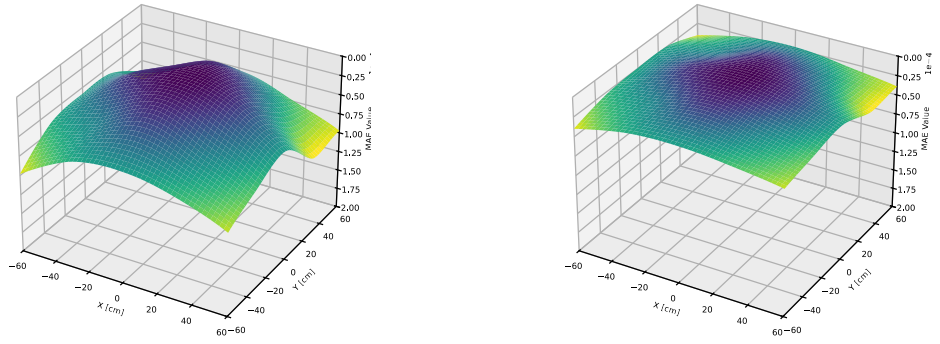

(a) Channel 9. (b) Channel 10.

Figure A.5: Mean Average Error of the SPD compared to the center of the booth for channel 9 and 10.

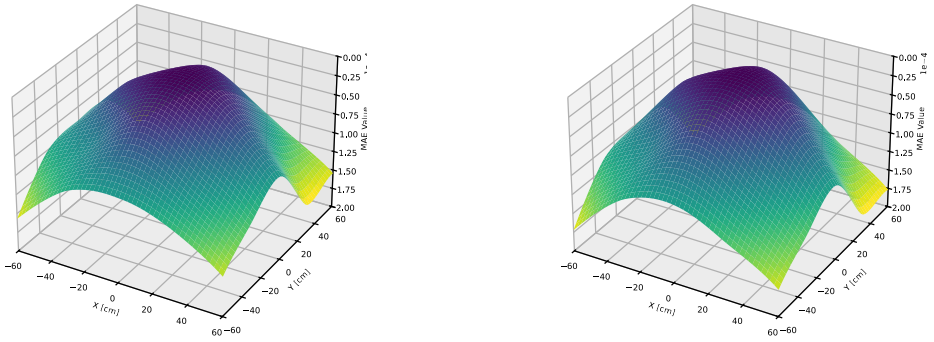

(a) Channel 11.

(b) Channel 12.

Figure A.6: Mean Average Error of the SPD compared to the center of the booth for channel 11 and 12.

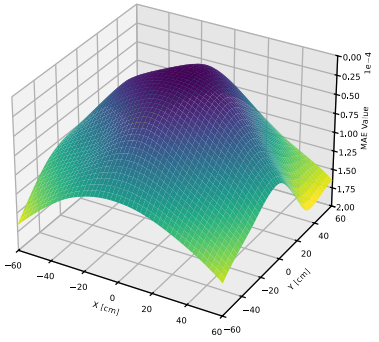

(a) Channel 13.

Figure A.7: Mean Average Error of the SPD compared to the center of the booth for channel 13.

is

Appendix B

Standard Illuminants

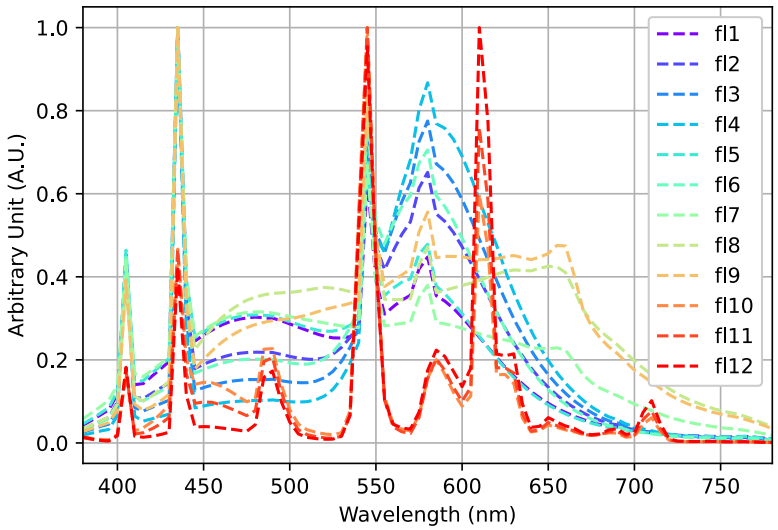

Figure B.1: SPD of CIE standard illuminants FL1-12.

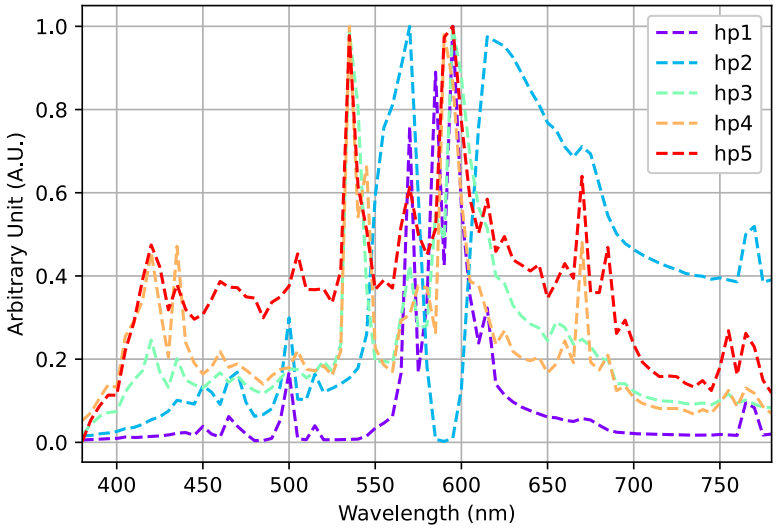

Figure B.2: SPD of CIE standard illuminants HP1-5.

Appendix C

CIEDE2000

$$\Delta L' = L^*_2 - L^*_1$$
$$\Delta C' = C'_2 - C'_1$$
$$C'_i = \sqrt{a'^2_i + b^{*2}_i}, \quad i = 1, 2$$
$$a'_i = (1 + G)a^*_i, \quad i = 1, 2$$
$$G = 0.5\left(1 - \sqrt{\frac{\bar{C}^{*7}_{ab}}{\bar{C}^{*7}_{ab} + 25^7}}\right)$$
$$\bar{C}^*_{ab} = \frac{C^*_{1,ab} + C^*_{2,ab}}{2}$$
$$C^*_{i,ab} = \sqrt{(a^*_i)^2 + (b^*_i)^2} \quad i = 1, 2$$
$$\Delta H' = 2\sqrt{C'_1 C'_2}\sin\left(\frac{\Delta h'}{2}\right)$$
$$\Delta h' = \begin{cases} h'_2 - h'_1 & |h'_2 - h'_1| \le 180^\circ \\ h'_2 - h'_1 + 360^\circ & h'_2 - h'_1 < -180^\circ \\ h'_2 - h'_1 - 360^\circ & h'_2 - h'_1 > 180^\circ \\ 0 & C'_1 C'_2 = 0 \end{cases}$$
$$h'_i = \begin{cases} 0 & \text{if } b^*_i = 0 \text{ and } a'_i = 0 \\ \tan^{-1}\left(\frac{b^*_i}{a'_i}\right) & \text{otherwise} \end{cases} \qquad i = 1, 2$$
$$R_T = -\sin(2\Delta\theta)R_C$$
$$R_C = 2\sqrt{\frac{\bar{C}'^7}{\bar{C}'^7 + 25^7}}$$
$$S_L = 1 + \frac{0.015(\bar{L}' - 50)^2}{\sqrt{20 + (\bar{L}' - 50)^2}}$$
$$S_C = 1 + 0.045\bar{C}'$$
$$S_H = 1 + 0.015\bar{C}'T$$
$$\bar{L}' = \frac{L^*_1 + L^*_2}{2}$$
$$\bar{C}' = \frac{C'_1 + C'_2}{2}$$

$$
\begin{aligned}
T &= 1 - 0.17\cos(\bar{h}' - 30^\circ) + 0.24\cos(2\bar{h}') \\
&\quad + 0.32\cos(3\bar{h}' + 6^\circ) - 0.20\cos(4\bar{h}' - 63^\circ) \\
\Delta\theta &= 30\exp\left(-\left(\frac{\bar{h}' - 275^\circ}{25}\right)^2\right) \\
\bar{h}' &= \begin{cases} \frac{h'_1 + h'_2}{2} & |h'_1 - h'_2| \le 180^\circ \\ \frac{h'_1 + h'_2 + 360^\circ}{2} & |h'_1 - h'_2| > 180^\circ \text{ and } h'_1 + h'_2 < 360^\circ \\ \frac{h'_1 + h'_2 - 360^\circ}{2} & |h'_1 - h'_2| > 180^\circ \text{ and } h'_1 + h'_2 \ge 360^\circ \\ 0 & C'_1 C'_2 = 0 \end{cases}
\end{aligned}
$$

Appendix D

SPD Selection for the Pilot Experiment

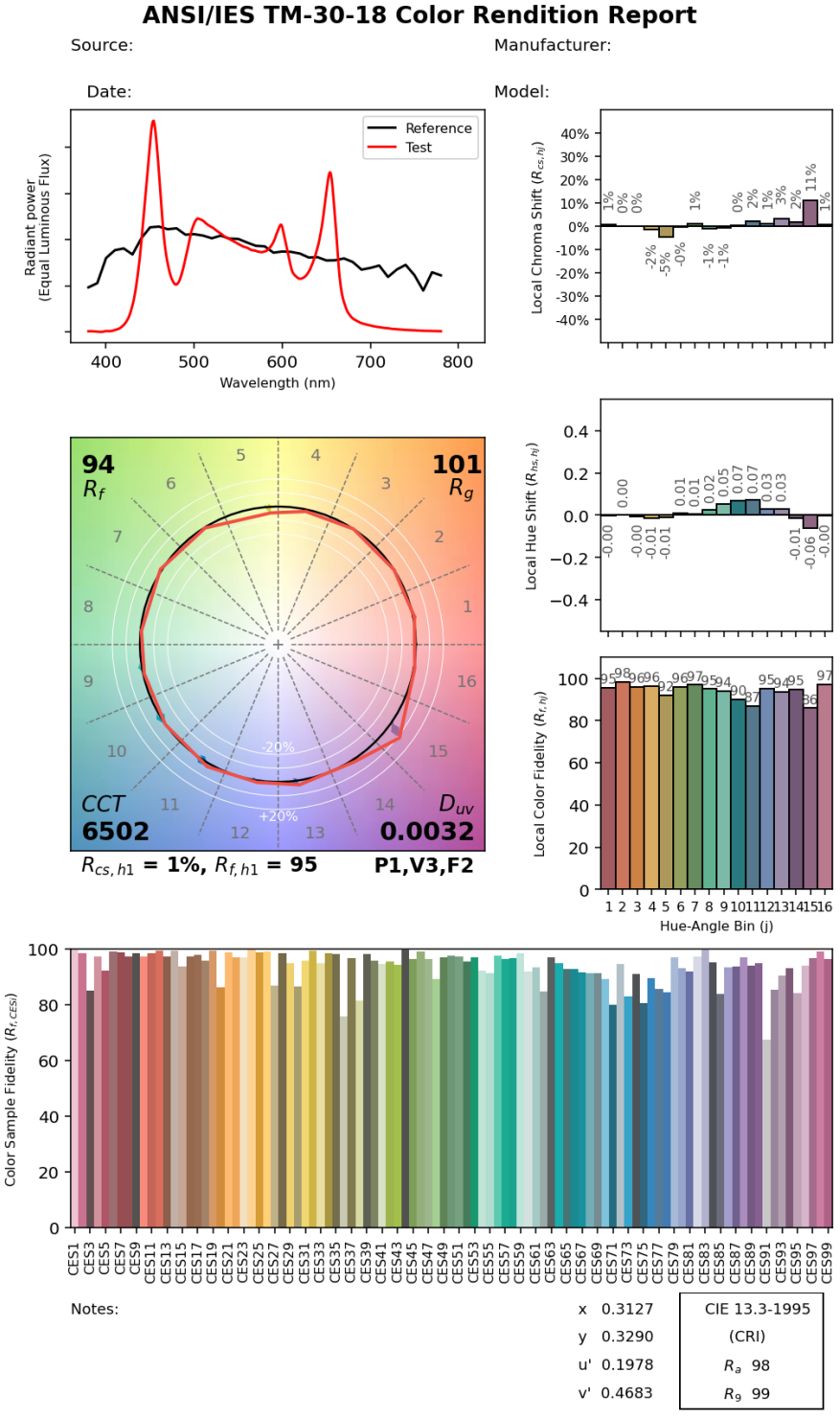

Figure D.1: TM30 report for Light 1.

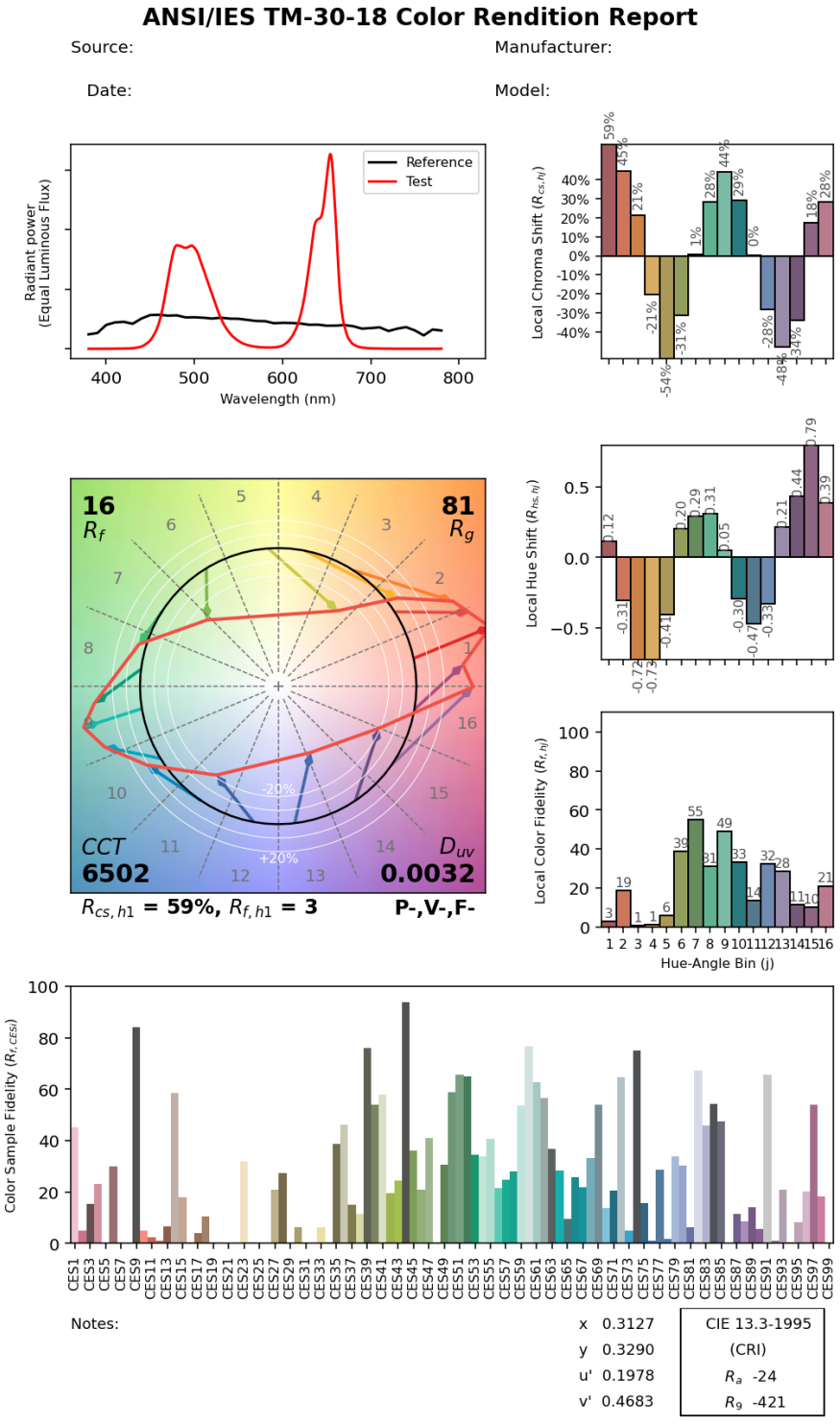

Figure D.2: TM30 report for Light 2.

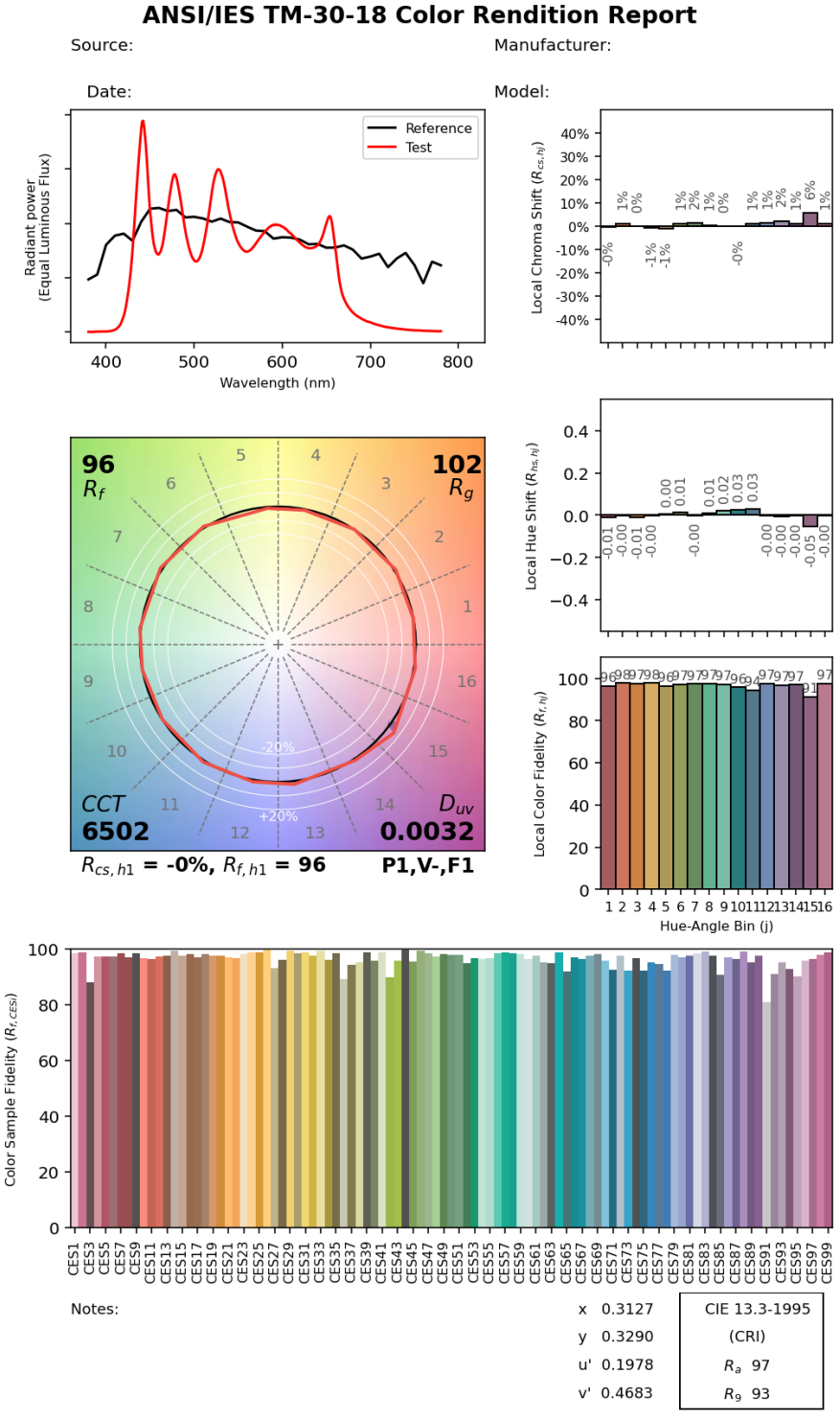

Figure D.3: TM30 report for light 3.

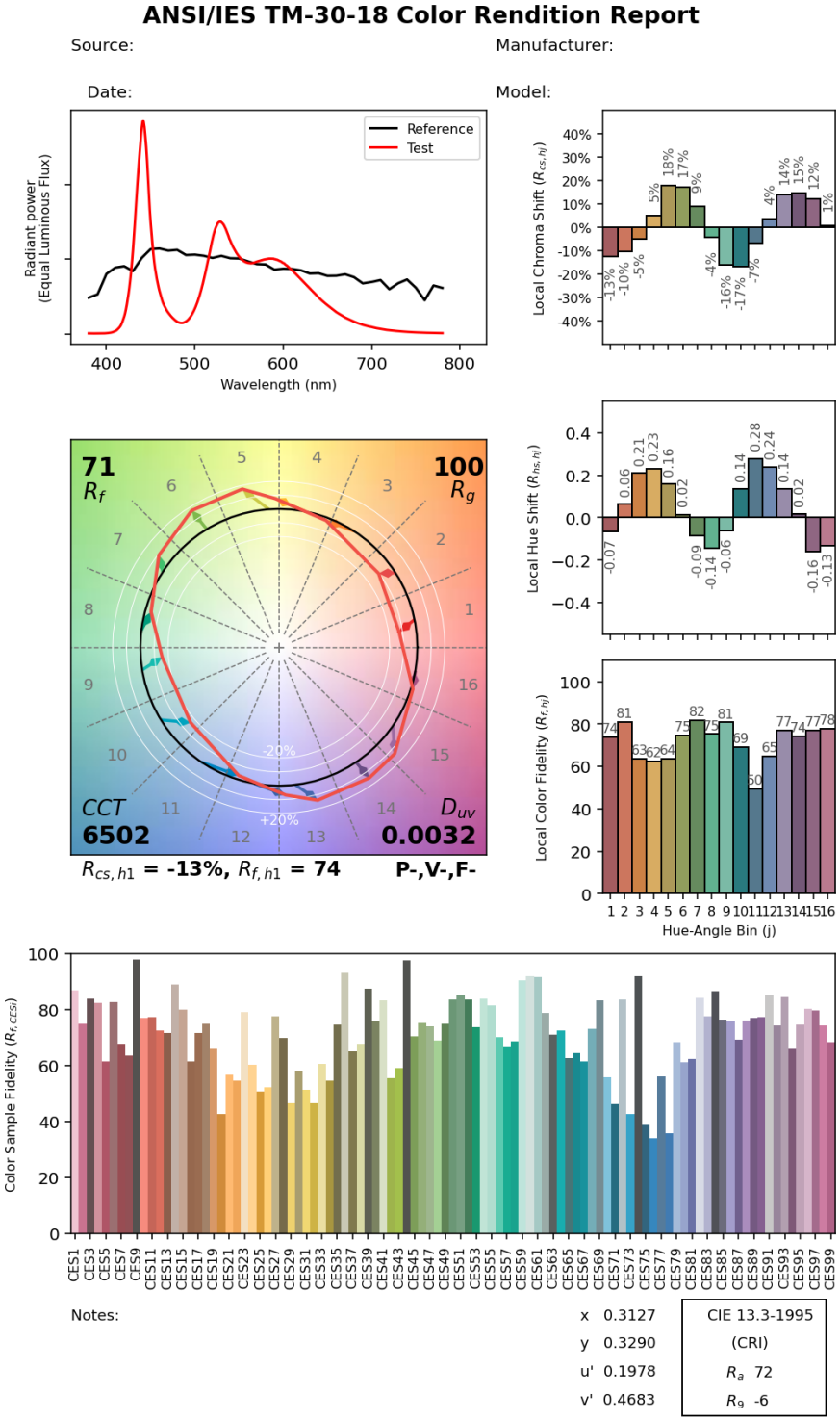

Figure D.4: TM30 report for light 4.

Appendix E

SPD selection for the experiment under white light conditions

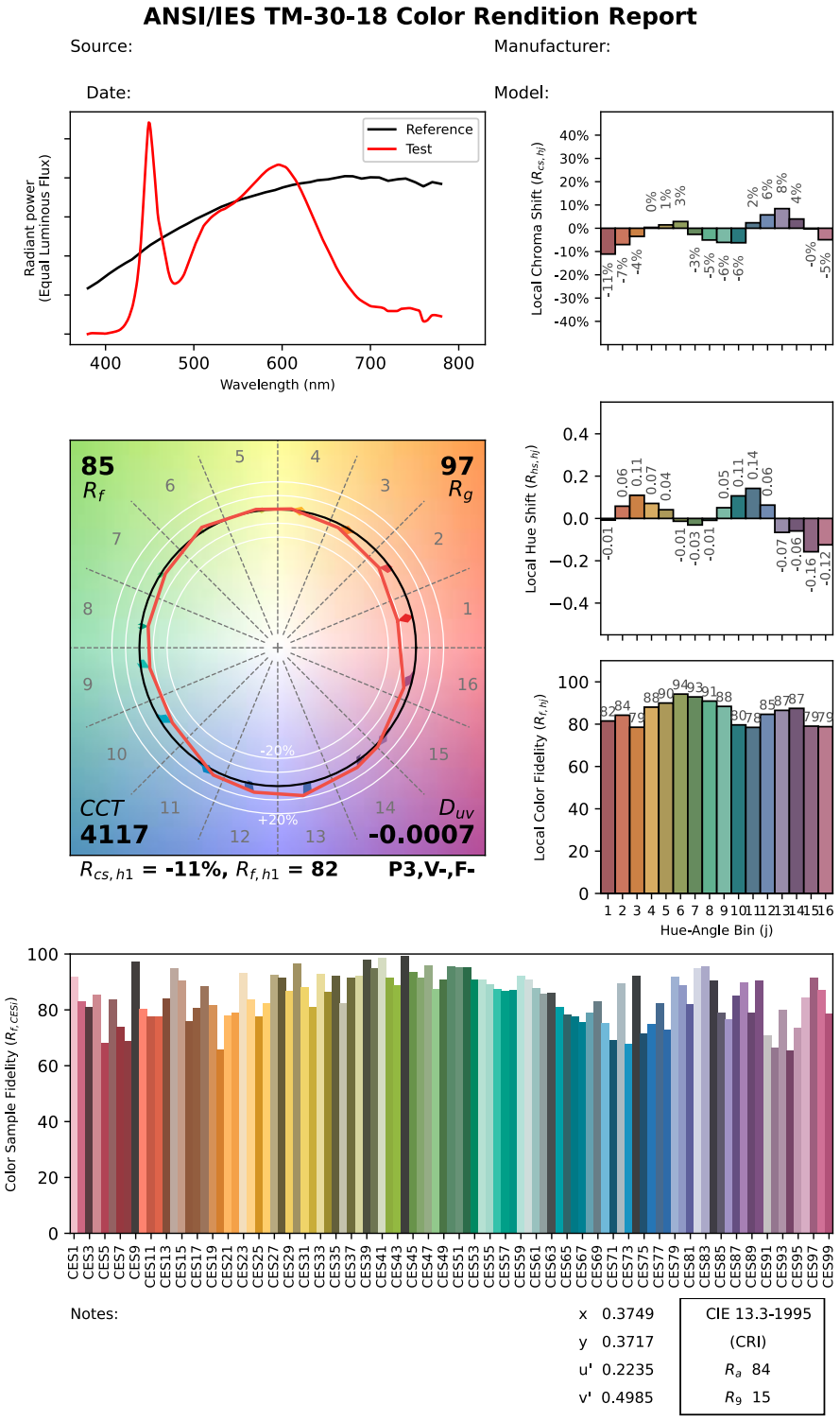

Figure E.1: TM30 report for Light 1.

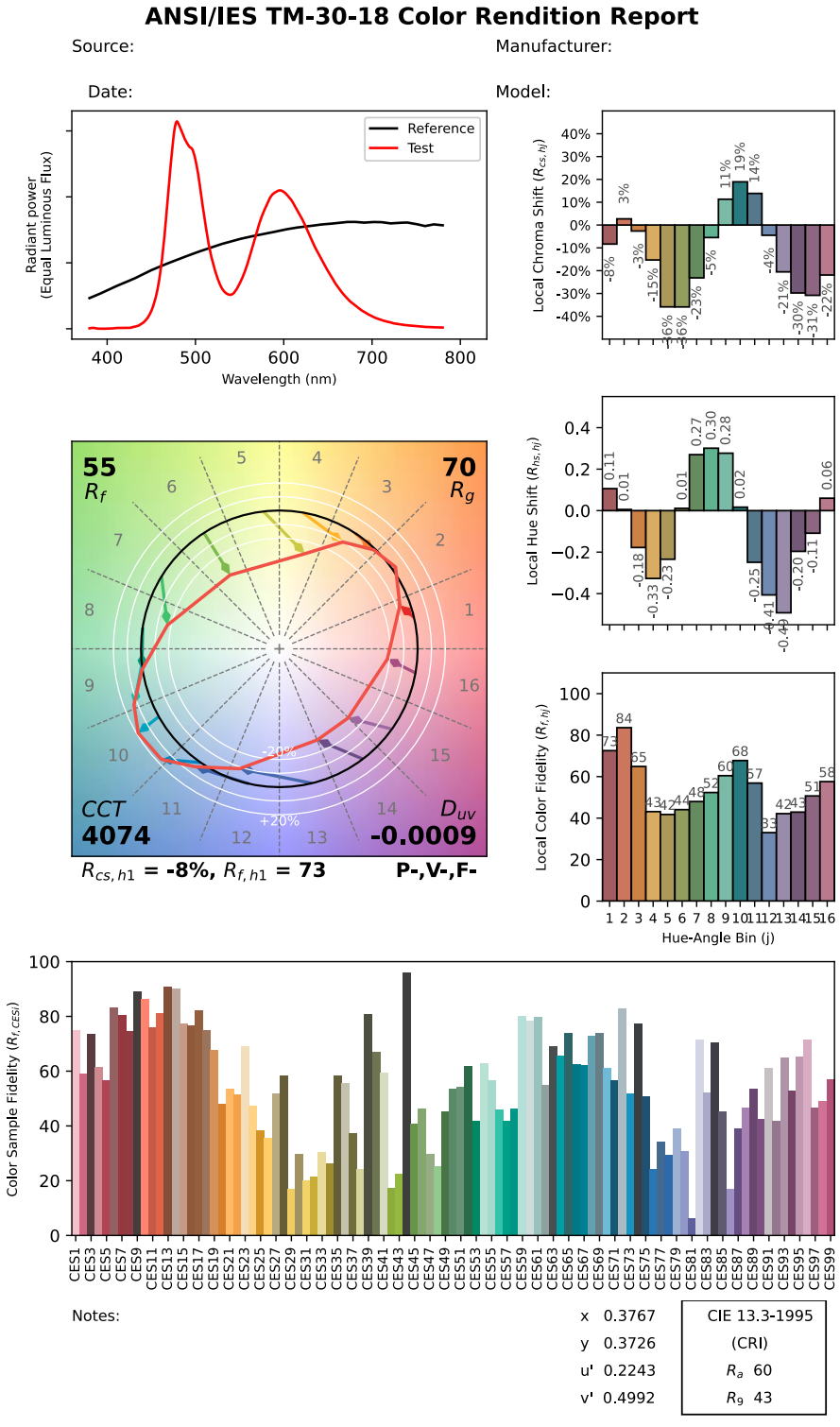

Figure E.2: TM30 report for Light 2.

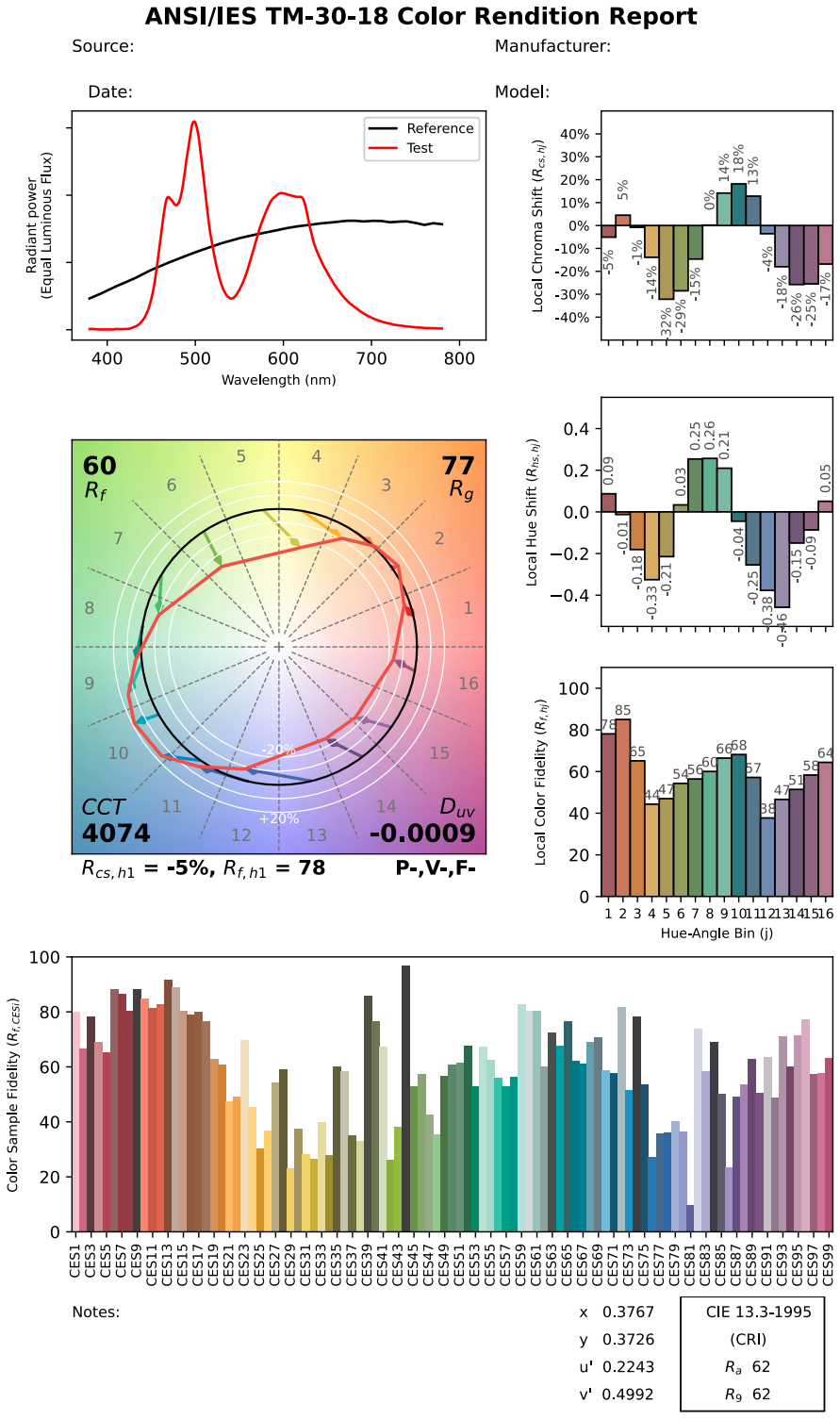

Figure E.3: TM30 report for light 3.